AN OBSERVATIONALLY COMPATIBLE MODEL FOR JUPITER'S IO-RELATED DECAMETRIC EMISSION

By

WAN-XIAN WANG

A DISSERTATION PRESENTED TO THE GRADUATE SCHOOL OF
THE UNIVERSITY OF FLORIDA
IN PARTIAL FULFILLMENT OF THE REQUIREMENTS FOR THE
DEGREE OF DOCTOR OF PHILOSOPHY

UNIVERSITY OF FLORIDA

1985

To my wife Na-na

ACKNOWLEDGEMENTS

I wish to express my heartfelt thanks to Dr. Thomas D. Carr, my research advisor, for his considerate guidance and his patience in reading and correcting the manuscript. I have benefited in many ways as his student.

I am also grateful to Drs. George R. Lebo, Alex G. Smith, Kwan-yu Chen, Thomas L. Bailey, and Heinrich K. Eichhorn for having served as members of my supervisory committee. Likewise, my deep appreciation goes to Mr. Paul P. Gombola for his technical assistance in photography and drawings.

The manuscript in final form was typed by Mrs. Adele Koehler. I admire her attention to detail and devotion to her craft.

Financial support for this research has been provided primarily by grants from the National Aeronautics and Space Administration. The project has also benefited from the support of low frequency planetary radio astronomy research by the National Science Foundation at the University of Florida. Support in the form of research assistantship by the Space Astronomy Laboratory of the University of Florida is also acknowledged.

TABLE OF CONTENTS

Page

ACKNOWLEDGEMENTS iii

ABSTRACT vi

CHAPTERS

I AN OVERVIEW 1

1. Brief Description of Jupiter's Decametric Radiation 1
2. Development of Our Knowledge on Jupiter's Magnetic Field and Magnetosphere 4
3. Early Evidence for Radiation Beaming and Some Emission Mechanism Theories 6
4. A Preliminary Statement of the Problem 9

II A FIVE-DIPOLE REPRESENTATION OF THE JOVIAN O_4 MAGNETIC FIELD MODEL 12

1. Introduction 12
2. Development of the Five-Dipole Model 13
3. Applications of the Five-Dipole Model 18
4. Derivation of Expressions for the S Bursts Frequency Drift Rates as Functions of Io Longitude and Frequencies 20

III THE EMISSION MODEL 38

1. Introduction 38
2. The Electron Beam, High-Frequency Branch Wave, and Right-Hand Cutoff Frequency 40
3. Growth Rate for the Upper-Hybrid Wave 44
4. Three-Wave Interactions 45
5. Conical Emission Pattern 48
6. Specification of Beam Pattern 52
7. Numerical Adjustment of the Model 54
8. Refraction Effect 56
9. Conclusion 62

APPENDICES

A RADIAL VECTOR, MAGNETIC FIELD, AND MAGNETIC SCALAR POTENTIAL FOR SINGLE DIPOLE 83

Page

B 24 EQUATIONS OBTAINED BY EQUATING MAGNETIC SCALAR POTENTIALS. 91

C RELATIONS AMONG THE ASSOCIATED LEGENDRE POLYNOMIALS 119

D MAGNETIC POTENTIAL AND MAGNETIC FIELD OF O_4 MODEL. 122

E SIGN TREATMENT FOR PARAMETERS OF FIVE-DIPOLE IN THE COMPUTATION 127

F EQUATIONS OF MAGNETIC FIELD LINE FOR SINGLE DIPOLE 128

G ISOCONTOUR OF MAGNETIC FIELD STRENGTH. 132

H DERIVATION FOR DRIFT RATE OF S BURST 141

I D_E LIMITS AND BOUNDARIES OF IO PHASE AND CML FOR SOURCES A AND B. 145

REFERENCES 146

BIOGRAPHICAL SKETCH 148

Abstract of Dissertation Presented to the Graduate School of
the University of Florida in Partial Fulfillment of the Requirements
for the Degree of Doctor of Philosophy

AN OBSERVATIONALLY COMPATIBLE MODEL FOR JUPITER'S IO-RELATED DECAMETRIC EMISSION

By

Wan-xian Wang

May 1985

Chairman: Thomas D. Carr
Cochairman: George R. Lebo
Major Department: Astronomy

A model for Jupiter's Io-related decametric radiation has been adjusted to provide a close fit to observed contours of emission occurrence probability on the plane of Io phase vs. the central meridian longitude for frequencies between 35 and 36 MHz. These observations were reported by Wilson, Warwick, and Libby in 1968. A nonlinear indirect emission mechanism was assumed in which Io-excited Alfvén waves produce an electron beam, which in turn, after intermediate steps, results in the emission of fast extraordinary mode electromagnetic waves. This radiation is emitted into a hollow-cone beam attached to the Io flux tube at a point where the wave frequency is slightly higher than the electron cyclotron frequency. A five-dipole representation of Jupiter's magnetic field was developed and used in this model; it closely matches the O_4 field model and has the advantage of greater computational flexibility. The Voyager-determined distribution of electron number density vs. height above the cloud-top level was used. Appropriate adjustments were made to account for the Alfvén wave propagation time between Io and the

emission point. The opening angle of the hollow-cone emission beam as a function of sub-Io longitude was the only adjustable parameter of the beam pattern used in fitting the observed decametric emission data. The angular thickness of the wall of the hollow cone was derived as a function of the conical angle from the theory of the above-mentioned emission mechanism. A first approximation in which refraction was assumed to be negligible resulted in an excellent fit to source B but a poorer one to source A. The required range of the adjusted conical angle was relatively small, 69.4° to 76.4° Refraction calculations indicated that corrections are indeed unnecessary for source B, and that they greatly improved the fit to source A.

CHAPTER I

AN OVERVIEW

1. Brief Description of Jupiter's Decametric Radiation

The discovery of Jupiter's decametric radiation, or DAM, by Burke and Franklin [1955] can be considered an introduction to the age of exploration of the solar system. We now know that Jupiter's radio emissions span over 24 octaves of the radio spectrum, from about 0.01 MHz to 300,000 MHz. Its radio emissions can be divided into three types. Thermal emission from the atmosphere accounts for mostly all the radiation at the high frequency end. Synchrotron emission from the trapped high-energy particle belt within the inner magnetosphere is the dominant spectrum from 4000 MHz down to 40 MHz. The third radio emission consists of several distinct sporadic low frequency components below 40 MHz, which are induced by plasma instabilities in the inner magnetosphere at frequencies that presumably are slightly above the local electron cyclotron frequency.

The distribution of Jovian storms in time represents a well-organized non-stochastic process. When we plot the observed probability of occurrence of activity in the vicinity of 20 MHz vs the central meridian longitude (CML) of the planet disc, a three-peaked distribution generally appears. This has been done in Figure I-1; the three peaks are designated sources B, A, and C, in order of increasing longitude. The use of the term "sources" in referring to these three active regions does not necessarily mean that their radiations originate from different locations on Jupiter. The number, widths, and locations of the peaks may vary with the frequency and the Jovicentric declination of Earth, D_E.

The longitude system derived from the radio emission patterns is designated System III (1965), it is based on a sidereal rotation rate of 870.536°/day (rotation period 9 hr 55 min 29.71 sec).

The high degree of circular polarization of Jupiter's sporadic decametric bursts was first observed by Franklin and Burke [1956]. Later observational results confirmed that the polarization sense of radiation from sources A and B at the higher frequencies is predominantly right-hand (RH), but as the frequency is decreased below about 20 MHz, progressively more left-hand (LH) polarization becomes apparent outside the A-B longitude region [Carr and Desch, 1976].

One of the most distinctive characteristics of the DAM concerns the repeatability of both coarse and fine emission features within the dynamic spectra, as was discussed by Warwick [1964] and Dulk [1965]. Dynamic spectra are representations of the instantaneous intensity of the radiation as a function of the two independent variables, frequency and time. Sometimes the features are so stable over long periods of time that comparison of landmark events separated by a Jovian year (∼11.9 years) may be used to determine the Jovian rotation period with considerable precision [Alexander, 1975]. (However, the highest-precision DAM rotation period measurements are made by comparing single-frequency occurrence probability histograms obtained about one Jovian year apart.)

This "permanent" dynamic spectrum is apparent on two time scales. On a scale of tens of minutes to hours each source has a characteristic emission envelope. On a time scale of minutes, the so-called spectral arcs are observed with shapes characteristic of their longitude regions. These arcs are either concave or convex, like the two types of parentheses, i.e., ")" or "(".

Another fundamental discovery came in 1964 with the announcement by Bigg [1964] that some of the Jovian emission was directly influenced by the Galilean satellite Io. When the same data used for Figure 1-1 are replotted as occurrence probability contours on the Io phase (Io departure from superior geocentric conjunction) vs CML plane, characteristic activity regions are obtained as shown in Figure 1-2. This figure indicates that the most notable features of DAM are controlled by Io. Source Io-A, which is related to Io, appears in the source A longitude region (CML $\sim 230^\circ$) when Io is at an orbital phase of $\sim 240^\circ$ from Superior Geocentric Conjunction. Source Io-B is at a phase of Io $\sim 90^\circ$, and CML $\sim 150^\circ$. An additional Io-dependent source, Io-C, appears at Io $\sim 240^\circ$, and CML $\sim 300^\circ$. Other radio components A, B, and C independent of Io orbital phase are presumably unrelated to Io.

Frequency-time dynamic spectra of Jovian emission are extremely complex. We refer to the intense structures on a 1 to 5 sec time scale as L (long) bursts, that on a millisecond time scale as S (short) bursts. The fundamental difference between the two types of emission is that the L burst modulation envelope originates largely in the solar wind, while the S burst modulation is intrinsic to the source or to its immediate surroundings. It must be especially pointed out that the S bursts always reveal a rapid negative frequency drift rate ranging from -5 to -45 MHz/sec [Carr, Desch, and Alexander, 1983].

Terrestrial observations of Jupiter's decametric radiation had shown that the emission is very intense and is elliptically or circularly polarized, sometimes in the left-hand sense but more commonly right-hand. The radiation was also received sporadically, exhibiting large intensity fluctuations on seconds to tens of seconds time scale. This is in sharp contrast to the smoothly and only slightly varying decimetric emission (DIM) due to the synchrotron emission from trapped relativistic electrons. In addition, it was noted that DAM was invariably confined to frequencies below 40 MHz. A lower frequency cutoff for ground-based observations was due to the opacity of the Earth's ionosphere. Voyager 1 and Voyager 2 provided a tremendous increase in our knowledge of Jupiter's magnetospheric phenomena, including the decametric, hectometric, and kilometric radio emissions. Furthermore, because the Voyager observations were free of scintillation effects due to the Earth's ionosphere and were of sufficient sensitivity and frequency resolution, another level of structure became apparent in the frequency-time dynamic spectra. It was the Voyager observations that led to the discovery of the dynamic spectral arcs.

2. Development of Our Knowledge on Jupiter's Magnetic Field and Magnetosphere

In the solar system, Mercury, Earth, Jupiter, Saturn, and probably Uranus are now known to have magnetic fields, that of Mercury is very weak.

The circular polarization of Jupiter's decametric bursts mentioned in Section 1 and the discovery of the Jovian nonthermal DIM component--the synchrotron radiation [Sloanaker, 1959, McClain and

Slysaker, 1959], provided the first evidence for Jupiter's magnetic field. The 40 MHz cutoff frequency of the DAM suggested a surface field strength of about 14 Gauss, based on the assumption that the DAM is emitted close to the local electron cyclotron frequency.

Several of the parameters of the synchrotron radiation vary systematically as the planet rotates. These effects are attributable to a predominantly dipolar configuration of Jupiter's magnetic field, the dipole axis being tipped about 10° with respect to the planetary spin axis.

The best trajectory for planetary magnetic field studies was that provided by Pioneer 11. This was a high latitude retrograde flyby with a closest Jovicentric approach distance 1.6 R_J. Although Pioneer 10 and Voyager 1 approached the planet to within 2.85 R_J and 4.9 R_J, respectively, their prograde trajectories remained close to the equatorial plane. Voyager 2 came only to within 10 R_J and thus did not contribute significant data for studies of the planetary field.

On the basis of the Pioneer 10 and 11 measurements, several models of Jupiter's magnetic field were proposed. Two principal models have emerged as "best," representing the planetary field in terms of spherical harmonics: the O_4 model of Acuña and Ness [1976] and the P 11(3,2)A model of Davis, Jones, and Smith [1975].

The best available measurement of the low-energy electron density in the plasma of the Jovian ionosphere as a function of height can be seen in Figure 1 of Hashimoto and Goldstein [1983]. It was determined from the data obtained by Pioneer 10 and Voyager 1. The Pioneer 11 plasma instrument also provided values for the low-energy proton density ranging from 10 to $100/cm^3$, and a temperature of the order of 100 eV in the inner magnetosphere.

The measurements made during the Voyager 1 and 2 encounters have altered our view of the basic Io interaction. The plasma environment of Io is quite different from what had been assumed earlier; the great Io torus affects significantly the interaction of Io with the Jovian magnetosphere. Because of the existence of the Io plasma torus, the induced current between Io and the Jovian ionosphere is in fact carried by large amplitude Alfvén waves. It has been suggested by many authors (Gurnett and Goertz, 1981, Goldstein, Sharma, Ben-Ari, Eviatar, and Papadopoulos, 1983) that the strong parallel electric field in these "kinetic" Alfvén waves is the origin of the KeV electrons that generate DAM.

3. Early Evidence for Radiation Beaming and Some Emission Mechanism Theories

One of the earliest theories of the origin of the Jovian DAM was proposed by Warwick (1961), based on the production of radiation by electrons precipitated into the Jovian ionosphere from the Van Allen belt. The discovery of the Io control of DAM indicated that the DAM emission occurs near the foot of the Io flux tube.

Dulk (1967) and Piddington (1967) independently developed geometrical models for the beaming of source B and the Io-related part of source A. Their models were similar. Dulk assumed (as did Piddington) a somewhat distorted dipole field, with the north pole tipped 10° toward Jupiter's 200° meridian. Once each 13 hours, when Io is near the 200° meridian (but only then), radiation is beamed into a conical sheet of half-angle of 79°. The cone axis lies along the field direction near the foot of the Io flux tube. Source B is observed when the leading limb of the conical sheet sweeps across the Earth, and the Io-related source A appears when the opposite limb sweeps past. The slight discrepancies between the CML values of these sources and the observed ones are attributed to the field distortion and to the stimulation of emission from an extensive region rather than from a point. Although the model appeared to have merit, it was crude at best and did not account for other observed phenomena.

A more complete model was proposed by Goldreich and Lynden-Bell [1969]. They assumed that Jupiter is enclosed successively by a corotating electrically insulating atmosphere, an ionosphere, and a low-density collisionless magnetosphere. In a reference frame rotating with the planet, there is an induced voltage across Io of 6.7×10^5 V, which causes a current to flow through Io, down along one side of the outer surface of the Io flux tube to the Jovian ionosphere, across the foot of the flux tube inside the ionosphere, and back up the opposite surface of the flux tube to Io, completing the circuit. This happens in both the northern and southern arms of the flux tube. The total direct current along the Io flux tube is about 1.1×10^6 A. They suggested that the instability responsible for the DAM results in radiation propagating nearly at a right angle to the magnetic field lines. They found that the radiation is confined to a conical sheet, which according to the relativistic correction of $\left(\frac{\pi}{2} - \frac{v_{\parallel}}{c}\right)$, has the approximate value of 79° opening angle, similar to Dulk's emission cone. The direct-current unipolar inductor theory of Goldreich and Lynden-Bell met with widespread acceptance at first, but has since been abandoned in the light of new developments.

Instead of the steady direct currents in the Io flux tube, Drell, Foley, and Ruderman [1965] suggested that the Io-induced current propagates in the form of a relatively slow Alfvén wave--so slow that Io has moved outside the flux tube before the Alfven wave can complete the circuit. This assumption was made necessary by the discovery of the Io plasma torus. Gurnett and Goertz [1981] applied this Alfvén current system to the generation of discrete decametric arcs; they attempted to explain the repetition of these arcs as due to multiple reflections of the Alfven wave between the Io torus boundaries and the Jovian ionosphere

The most widely accepted theories of the DAM today are based on nonlinear indirect emission processes resulting from beam-driven plasma instabilities. Goldstein and Thieman [1981] presented a theory of the decametric dynamic spectral arcs which was based on hollow-cone emission beams attached to the Io flux tube. They assumed that the emission conical angle varies with the frequency so that it is relatively small at both high and low frequencies, but is approximately 80° at intermediate frequencies. In order to explain the longitude asymmetry in the occurrence probability distribution for Io-related DAM, Thieman and Smith [1979] found it necessary to assume a displacement of the Io flux tube 20° ahead of the sub-Io longitude. Goldreich and Lynden-Bell [1969] had reached a somewhat similar conclusion much earlier. Hashimoto and Goldstein [1983] offered as an explanation for this displacement the suggestion that Io generates stronger Alfven waves toward the south when it is in the northern part of Io torus, and this wave then generates DAM in the northern ionosphere after it reflects from the southern ionosphere. For the mechanism itself, Goldstein, Sharma, Ben-Ari, Eviatar, and Papadopoulos [1983] presented a more complete indirect nonlinear theory that is based on the existence of beams of energetic electrons in the inner Jovian magnetosphere. This beam-like distribution tends to be unstable to the growth of both upper-hybrid and lower-hybrid electrostatic waves, which subsequently are up-converted to fast extraordinary (fast X) mode electromagnetic radiation

4. A Preliminary Statement of the Problem

In Chapter III a model for Jupiter's decametric radio emission has been developed, consisting of a continuously emitted hollow cone of radiation from the vicinity of the northern foot of the Io flux tube, each emitted frequency being slightly above the local electron cyclotron frequency. A nonlinear indirect emission mechanism is assumed in which Alfvén waves excited by Io produce an electron beam that in turn drives plasma instabilities, resulting plasma waves are up-converted to produce electromagnetic radiation beamed into a hollow cone. The parameters of the model are adjusted to fit previously published data on emission occurrence probability on the plane of Io phase vs Jovian CML in the 35-36 MHz frequency range

Chapter II describes the evolution, development, and testing of a five-dipole model of Jupiter's magnetic field to be used in the radio emission model development

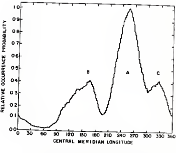

Figure 1-1. Variation of Relative Probability of Occurrence of DAM as a Function of Central Meridian Longitude. The three peaks are customarily referred to as sources B, A, and C. The data were compiled by Thieman [1977] from observations at 18, 20, and 22 MHz between 1957 and 1975 at the University of Florida and University of Texas radio observatories.

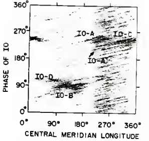

Figure I-2. Two-Dimensional Dependence of DAM Activity on CML and Io Phase at about 20 MHz. The Io-related sources are labeled.

CHAPTER II

A FIVE-DIPOLE REPRESENTATION OF THE JOVIAN O_4 MAGNETIC FIELD MODEL

1. Introduction

The first step taken toward the development of a model for the Jovian emission mechanism was to reformulate the standard O_4 multipole model of the magnetic field to provide greater flexibility in its use in computer calculations. It was found that the O_4 magnetic field could be closely matched by the sum of the fields from a particular set of 5 magnetic dipoles of different magnetic moments which are tilted from the planetary spin axis and offset from the center of the planet by different amounts. With this new formulation, one is always working with dipole field components in the computer modeling of Jupiter's magnetospheric processes. This represents a simplification over the computation algorithm required when the O_4 magnetic field formula, involving dipole, quadrupole, and octupole components, is used. As will be demonstrated, there is no appreciable loss in accuracy in using the five-dipole formula.

The mathematical evolution of the five-dipole model is illustrated in Appendix A and Appendix B. The remainder of this chapter is epitomized by a brief description of the five-dipole model. Also included is a set of curves calculated from the five-dipole model depicting several aspects of Jupiter's magnetic field in the inner magnetosphere. These curves are potentially useful not only to the modeling of Jupiter's radio emission mechanisms, but also in that of other magnetospheric processes as well

2. Development of the Five-Dipole Model

The Jovian O_4 magnetic field [Acuña and Ness, 1976, Acuña, Behannon, and Connerney, 1983] is widely used in modeling plasma interactions within the inner magnetosphere of the planet. In this field model, the magnetic potential $V(r,\theta,\phi)$ is expressed as a multipole series expansion which is truncated after the octupole ($n = 3$) term, as follows (see Appendix B, equation (B-52))

$$V(r,\theta,\phi) = \sum_{n=1}^{3} \left(\frac{1}{r}\right)^{n+1} \sum_{m=0}^{n} \left(g_n^m \cos m\phi + h_n^m \sin m\phi\right) \overline{P_n^m}(\cos\theta) \qquad \text{(II-1)}$$

where r is the Jovicentric distance to the given point P in Jupiter radii, $P_n(\cos\theta)$ is a Schmidt-normalized associated Legendre polynomial, and the values of the 15 Schmidt coefficients g_n^m and h_n^m can be found in Acuña, Behannon, and Connerney [1983]. For convenience, $\overline{P_n^m}(\cos\theta)$, g_n^m, and h_n^m are listed in Appendix B; Schmidt-normalization of associated Legendre polynomials is also discussed in this Appendix

The magnetic field $\vec{B}$ is then obtained from the relation

$$\vec{B}(r,\theta,\phi) = -\nabla V(r,\theta,\phi) \qquad \text{(II-2)}$$

Because of its simplicity, a single offset tilted dipole field is often employed instead of the O_4 model in inner magnetospheric regions beyond $r = 2R_J$ or $r = 3R_J$, in cases where the resulting loss in accuracy can be tolerated. Closer to the planetary surface, however, the quadrupole and octupole terms become increasingly important, and no single dipole model can adequately represent the field there. We have developed an alternative expression for the O_4 magnetic potential that is considerably simpler to use than (II-1) and is much more accurate than the single offset dipole expression.

The five-dipole model is produced by a particular set of 5 offset tilted dipoles for which the magnetic scalar potential $V(r,\theta,\phi)$ is very nearly the same as that for the O_4 model throughout the region where the O_4 model is applicable. One member of the set of 5, which we call the "main dipole" (despite the fact that it is not the strongest), has been chosen to be identical with the single offset dipole derived from the O_4 model; this dipole is specified by the 6 parameters in Table 1.3 of Acuña, Behannon, and Connerney [1983]. Three of these parameters specify the magnetic moment vector, and the other 3 the vector offset from the Jovicentric origin. Each of the remaining 4 dipoles in the set is represented by 6 arbitrary parameters, giving us 24 adjustable parameters to manipulate in synthesizing an acceptably accurate approximation to the O_4 field.

In (II-1), $n = 3$ for Schmidt-normalized associated Legendre polynomials of highest degree. We found it necessary in the derivation that follows to consider that (II-1) also includes $\overline{P_n^m}(\cos\theta)$ terms of degree $n = 4$, the coefficients g_n^m and h_n^m of which are all zeros. $V(r,\theta,\phi)$ due to the set of 5 dipoles was also expanded as a multipole series containing $\overline{P_n^m}(\cos\theta)\cos m\phi$ and $\overline{P_n^m}(\cos\theta)\sin m\phi$ (Tesseral Harmonics of nth degree and mth order) up to $n = 4$. The 24 adjustable parameters (together with the 6 fixed parameters of the "main dipole") then appeared in various combinations of the coefficients for this latter series. We next equated the coefficients of the corresponding Tesseral Harmonics of nth degree and mth order for these two series, obtaining the 24 equations (B-53a)-(B-53x) in Appendix B. These equations were subsequently solved for the 24 adjustable parameters, completing the specification of the set of 5 dipoles. The sign convention followed in specifying these parameters is explained in Appendix E. The 30 parameters are listed in Table II-1

The magnetic scalar potential $V(r,\theta,\phi)$ at the point P in the spherical coordinate system as given by the five-dipole model is (see Appendix G, equations (G-11)-(G-12))

$$V(r,\theta,\phi) = \sum_{i=1}^{5} V_i(r,\theta,\phi) = \sum_{i=1}^{5} \frac{M}{r^2} \frac{(F - \frac{r_o}{r} C)}{K(r)^{3/2}} \qquad \text{(II-3)}$$

Where

$$K(r) = 1 - 2\frac{r_o}{r}\cdot x + (\frac{r_o}{r})^2$$

$$x = \sin\delta\cos\theta + \cos\delta\sin\theta\cos(\phi - \phi_o + \lambda_o) \qquad \text{(see Appendix A, equation (A-22))}$$

$$F = \cos\theta\cos\theta_o + \sin\theta\sin\theta_o\cos(\phi + \lambda_o) \qquad \text{(see Appendix A, equation (A-4c))}$$

$$C = \sin\delta\cos\theta_o + \cos\delta\sin\theta_o\cos\phi_o \qquad \text{(see Appendix A, equation (A-2c)}$$

In these expressions, we have omitted the subscript i for r_o, M, and the parameters contained in terms x, F, and C

The notation is as follows (refer to Figure A-1)

θ is the colatitude of the point P,

ϕ is the longitude of the point P as measured eastward from the meridian $\lambda_{III}(1965) = 0°$,

M is the magnitude of the magnetic moment vector $\vec{M}$ of each dipole,

θ_0 is the tilt of $\vec{M}$ of each dipole from the planetary spin axis,

λ_0 is the System III longitude toward which $\vec{M}$ of each dipole is tilted,

r_0 is the offset distance of each dipole in Jupiter radii,

δ is the latitude of offset of each dipole,

ϕ_0 is the longitude of offset of each dipole as measured eastward from the direction toward which $\vec{M}$ is tilted

The components of the magnetic field $\vec{B}$ are found from $V(r,\theta,\phi)$ by

$$B_r = -\frac{\partial V}{\partial r} \qquad \text{(II-4a)}$$

$$B_\theta = -\frac{1}{r}\frac{\partial V}{\partial \theta} \qquad \text{(II-4b)}$$

$$B_\phi = -\frac{1}{r\sin\theta}\frac{\partial V}{\partial \phi} \qquad \text{(II-4c)}$$

After performing the indicated differentiations we obtain (see Appendix C, equations (C-13)-(C-15b))

$$B_r = \sum_{i=1}^{5} \frac{V_i}{r}\left[2 - \frac{\frac{r_0}{r}\,C}{F - \frac{r_0}{r}\cdot C} + 3\,\frac{\frac{r_0}{r}\cdot x - \left(\frac{r_0}{r}\right)^2}{K(r)}\right] \qquad \text{(II-5a)}$$

$$B_\theta = \sum_{i=1}^{5} \frac{V_i}{r}\left[\frac{-U}{F - \frac{r_0}{r}\cdot C} - 3\,\frac{\frac{r_0}{r}\cdot y}{K(r)}\right] \qquad \text{(II-5b)}$$

$$B_\phi = \sum_{i=1}^{5} \frac{V_i}{r} \left[\frac{-W}{F - \frac{r_o}{r} \cdot C} - 3 \frac{\frac{r_o}{r} z}{K(r)} \right] \qquad \text{(II-5c)}$$

where

$$U = -\sin\theta\cos\theta_o + \cos\theta\sin\theta_o\cos(\phi+\lambda_o)$$

$$y = -\sin\theta\sin\theta + \cos\theta\cos\theta\cos(\phi-\phi_o+\lambda_o)$$

$$W = -\sin\theta_o\sin(\phi+\lambda_o)$$

$$z = -\cos\theta\sin(\phi-\phi_o+\lambda_o)$$

As shown in Appendix G, the $(r_o/r)^2$ terms in the components B_r, B_θ, and B_ϕ can be neglected without significant loss of accuracy even in Jupiter's near field. The field components then become (see Appendix G, equations (G-16)-(G-18))

$$B_r = \sum_{i=1}^{5} \frac{M}{r^3} \left[\frac{2F - \frac{r_o}{r} (3C + F \cdot x)}{K(r)^{5/2}} \right] \qquad \text{(II-6a)}$$

$$B_\theta = \sum_{i=1}^{5} \frac{M}{r^3} \left[\frac{-U + \frac{r_o}{r} (2U \cdot x - 3F \cdot y)}{K(r)^{5/2}} \right] \qquad \text{(II-6b)}$$

$$B_\phi = \sum_{i=1}^{5} \frac{M}{r^3} \left[\frac{-W + \frac{r_o}{r} (2W \cdot x - 3F \cdot z)}{K(r)^{5/2}} \right] \qquad \text{(II-6c)}$$

When r is greater than about 2.0 R_J, equations (II-6a)-(II-6c) reduce to the much simpler approximate forms

$$B_r = \frac{1}{r^3} \sum_{i=1}^{5} M \cdot F \qquad \text{(II-7a)}$$

$$B_\theta = \frac{1}{r^3} \sum_{i=1}^{5} (-M \cdot U) \qquad \text{(II-7b)}$$

$$B_\phi = \frac{1}{r^3} \sum_{i=1}^{5} (-M \cdot W) \qquad \text{(II-7c)}$$

Tables II-2 and II-3 and Figure II-1 illustrate the accuracy of representation of the O_4 field by the five-dipole model. Table II-2 gives the magnetic field strength in Gauss at the planetary surface as a function of System III longitude and Jovigraphic latitude. There are two entries for each longitude and latitude. The upper number in each pair denotes the field as computed from the O_4 multipole expansion and the lower one that computed from the five-dipole model. The differences in the pairs of field strength values are less than 3% in every case, and in most cases less than 1%. Even these small differences rapidly become smaller when r is increased beyond 1 R_J, as can be seen from Table II-3. The test provided by Figure II-1 is discussed in the next section.

3. Applications of the Five-Dipole Model

Although the magnetic field equations (II-5a)-(II-5c) derived from the five-dipole model may not appear to be appreciably simpler than those of the O_4 model (see Appendix D, equations (D-2a)-(D-2c)), they are much easier to manipulate, particularly in iterative computations. In some calculations, such as those necessary for the plotting of isocontours of magnetic field strength, it is most expeditious to make successive approximations to the final values. In the first approximation, the exact equations in (F-10a)-(F-10c) are used for the "main dipole" alone, preserving its tilt but assuming no offset from the origin (see Appendix G, equations (G-1a)-(G-1c)); corrections for obtaining the second approximation are next computed by restoring the offset of the "main dipole." Then corrections for the final isocontour values are determined from the field of the five-dipole model by using the Taylor expansion with the first order derivatives. We have employed such procedures in the computation (see Appendix G) and also have plotted a variety of field-related quantities from the five-dipole model in Figure II-1 through Figure II-7.

Figure II-1 is a latitude vs. longitude plot of a series of magnetic field lines that cross the Jovian equator at $r = 5.91\ R_J$, i.e., at Io's orbit. These lines were traced by using equation (G-20) in Appendix G, which is derived from the five-dipole model. The plots were found to be indistinguishable from a series made by Garnavich [1983] from the O_4 multipole expansion. From Table II-2, Table II-3, and Figure II-1, it is apparent that there is no appreciable sacrifice in accuracy when the equations based on the five-dipole model instead of O_4 multipole model are used for determining the magnetic field at any point in Jupiter's inner magnetosphere.

The curves in Figure II-2 through Figure II-7 were also computed from the five-dipole model. Figure II-2 and Figure II-3 are northern and southern hemisphere latitude vs. longitude plots of isocontours of magnetic field strength on the surface generated by the midline of the Io flux tube, the field lines of Figures II-2 and II-3 are the same as those shown in Figure II-1. Figure II-4 and Figure II-5 indicate the heights above the cloud-top level of the loci of points of magnetic field strength that are plotted in Figure II-2 and Figure II-3. Each curve in Figure II-6 and Figure II-7 indicates the electron cyclotron frequency gradient along the Io flux tube at the points on the flux tube having the value of the electron cyclotron frequency given in parentheses.

These figures and others that can be plotted with the aid of the five-dipole model will undoubtedly be useful in the modeling of various types of Jupiter's magnetospheric phenomena, including the decametric radiation. Figure II-6 and Figure II-7 will be of particular value in the study of Jovian S bursts. The measured drift rate of the electron cyclotron frequency of a given S burst, $\frac{df_c}{dt}$, divided by the electron cyclotron frequency gradient $\frac{df_c}{ds}$ along the Io flux tube should yield the approximate velocity of the S burst emission source along the Io flux tube. The value of $\frac{df_c}{ds}$ can be found from Figure II-6 or Figure II-7; it is the ordinate for which the abscissa is the known System III longitude of Io at the time of observation (a longitude correction having first been made to account for the finite Alfvén wave velocity between Io and the radio emission source).

4. Derivation of Expressions for the S Burst Frequency Drift Rates as Functions of Io Longitude and Frequencies

Jupiter's decametric S bursts are always "Io-related," and always drift from higher to lower frequencies at rates that are usually from -5 to -45 MHz·sec^{-1} [Carr, Desch, and Alexander, 1983]. They presumably originate near the foot of the Io flux tube. It is generally assumed that the frequency of emission of an S burst (and also of an L burst) is close to the electron cyclotron frequency at its source. The negative frequency drift rate is believed to result from the motion of the source upward along the Io flux tube. Thus the frequency drift rate is proportional to the negative of the product of the source velocity along the Io flux tube and the field strength gradient along it. It is apparent from Figure II-6 and Figure II-7 that the electron cyclotron frequency gradients at any particular value of frequency do not vary appreciably with the longitudes at which the field lines intersect Io's orbit. It follows that the drift rates of S bursts at any particular frequency should also be nearly independent of Io's longitude at the time they are emitted. This point will be discussed further at the end of this section. In the derivation which follows, a simple expression for the drift rate of S bursts as a function of longitude and their frequencies is obtained. From equations (B-53a)-(B-53c) in Appendix B, we find that the vector sum of the magnetic moments of the 5 dipoles can be replaced by the single vector moment of the "main dipole" (see Appendix H, equation (H-8)); that is, the vector sum of the magnetic moments of dipoles 2 through 5 is zero. (It does not follow that the vector sum of their contributions to $\vec{B}$ is zero because they have different offsets from the origin.) The offset of each dipole is so small compared with the Jovicentric distance to a point on the Io flux tube that in this case it can be neglected. Therefore, the following Jovicentric relation for the magnetic potential at a point on the Io flux tube can be used (see Appendix H, equation (H-9c))

$$V = \frac{\hat{r}\cdot\vec{M}_1}{r^2} \qquad \text{(II-8)}$$

where M_1 is the magnitude of the magnetic moment vector of the "main dipole."

The magnetic field strength gradient along the Io flux tube is then (see Appendix H, equation (H-13))

$$\frac{dB}{ds} = -\frac{9}{\sqrt{3}r}\sqrt{B^2 - \left(\frac{M_1}{r^3}\right)^2} + \frac{4}{\sqrt{3}B^2 r}\left[B^2 - \left(\frac{M_1}{r^3}\right)^2\right]^{3/2} \qquad \text{(II-9)}$$

By making use of the equations (G-1a) and (G-1c) in Appendix G, in the single "main dipole" approximation we have

$$r = L(D^2 + E^2) \qquad \text{(II-10a)}$$

$$B = \frac{M_1}{r^3}\sqrt{4 - 3(D^2 + E^2)} \qquad \text{(II-10b)}$$

where

$D = \cos\theta\sin\theta_o - \sin\theta\cos\theta_o\cos\phi$

$E = \sin\theta\sin\phi$

L is the shell number, defined in equation (F-7) of Appendix F.

This means that

$$r = \frac{L}{3}\left(4 - \frac{B^2 r^6}{M_1^2}\right) \qquad \text{(II-11)}$$

The magnetic field strength B is constant on its isocontour. This implies that r is constant, too, in the light of equation (II-11), therefore, the value of $\frac{dB}{d\phi}$ becomes a negative constant on the basis of equation (II-9). Thus the electron cyclotron frequency gradient at a fixed frequency is, to within the accuracy of the approximations made, independent of the longitude of the field line intersecting Io's orbit. (This result is apparent from Figure II-6 and Figure II-7, the calculations for which were more rigorous than the above approximate derivation.) This theoretical prediction can easily be tested observationally, probably using already published data. For example, one need only compare the mean frequency drift rates of S bursts obtained at a frequency of, say, 18 MHz for CML sources A and B, for which the sub-Io longitudes are quite different.

The drift rate of the electron cyclotron frequency of S burst is (see Appendix H, equation (H-14))

$$\frac{df_c}{dt} = 2.8 \frac{dB}{d\phi} v_{\|} \qquad \text{(II-12)}$$

where

f_c is the electron cyclotron frequency,

$v_{\|}$ is the velocity of the source along the Io flux tube.

If the velocity of the source along the field is constant, then it follows that the S burst frequency drift rate at a given frequency is a negative constant, i.e., is independent of Io's longitude.

Furthermore, in the first approximation, upon substituting r for r_s and M_1 for M in equation (F-2) of Appendix F, we obtain

$$B = \frac{M_1}{r^3}\sqrt{4 - 3\sin^2\theta^*} \qquad \text{(II-13)}$$

But since

$$(4 - 3\sin^2\theta^*) \geq 4 - 3 \times 1^2 = 1$$

we have

$$B \geq \frac{M_1}{r^3} \qquad \text{(II-14)}$$

Usually, for the not very far field of Jupiter, this inequality becomes

$$B \gg \frac{M_1}{r^3} \qquad \text{(II-15)}$$

Based on equation (II-15), we can simplify equations (II-9) and (II-12) to

$$\frac{dB}{ds} = -\frac{5}{\sqrt{3}}\frac{B}{r} \qquad \text{(II-16a)}$$

A check has been made indicating that the difference between the value of $\frac{dB}{ds}$ here and that computed without approximations (shown in Figures II-6 and II-7) is negligible

$$\frac{df_c}{dt} = -\frac{5}{\sqrt{3}}\frac{f_c}{r}v_{\parallel} \qquad \text{(II-16b)}$$

If the velocity of the S burst source along the Io flux tube is constant, then it is obvious that

$$\frac{df_c}{dt} = -f_c/\tau \qquad \text{(II-17)}$$

Since τ is nearly constant for different values of f_c near the foot of the Io flux tube, then we have the following relation

$$\frac{df_c}{dt} \propto -f_c \qquad \text{(II-18)}$$

Thus the theory derived here predicts that the drift rate of the electron cyclotron frequency of S bursts having the same source velocity along the flux tube should be proportional to the negative of their frequencies. Has such a proportionality actually been observed? It remains to be confirmed. Ample published data are available from which this predicted proportionality can be tested. If it is indeed found to be true, the result will tend to verify the theory itself and at the same time to attest to the constancy of the source velocities of S bursts along the Io flux tube. If on the other hand the predicted proportionality is found not to be true, it may simply mean that the velocities are not necessarily the same for different frequencies.

It is instructive to calculate the B-parallel source velocities of S bursts corresponding to a particular observed S burst drift rate, using the foregoing equations (II-16a) and (II-16b) (or more simply, Figure II-6 or Figure II-7). Flagg and Desch [1979] observed S bursts at 33 MHz with drift rates of about -41 MHz sec^{-1}. The magnetic field strength corresponding to this frequency is B = 33/2.8 = 11.8 Gauss. The radial distance as calculated from equation (II-11) is about 0.94 R_J. This is about the same as for the Jovian "surface" (it is < R_J because of polar flattening) and is consistent with the assumption that the emission must come from just above the Jovian ionosphere. Thus the theoretical electron cyclotron frequency gradient of this S burst along the Io flux tube is

$$\frac{df_c}{ds} = -\frac{14B}{\sqrt{3}r} = -\frac{14\times 11.8}{\sqrt{3}\times 0.94} = -101.5\ \mathrm{MHz}/R_J = -1.42\times 10^{-3}\ \mathrm{MHz/km}$$

Then the B-parallel source velocity of S burst is given by

$$V_{||} = \frac{df_c/dt}{df_c/ds} = \frac{-41}{-1.42\times 10^{-3}} \approx 28{,}850\ \mathrm{km/sec} \cong 0.096\ c$$

where

c is the speed of light.

Electrons of this velocity have a kinetic energy of

$$E = 511\left(\frac{1}{\sqrt{1-\left(\frac{V_{||}}{c}\right)^2}} - 1\right) = 511\left(\frac{1}{\sqrt{1-0.096^2}} - 1\right) = 2.37\ \mathrm{KeV}$$

These electrons were presumably accelerated by some process in the Jovian ionosphere [Flagg and Desch, 1979].

Table II-1. Parameters of the Five-Dipole Field Model

i (Dipole No.)	M (Gauss R_J^3)	θ_0 (deg.)	λ_0 (deg.)	r_0 (R_J)	δ (deg.)	ϕ_0 (deg.)
1	4.278	9.6	201.7	0.131	-8.0	53.1
2	7.008	94.7	104.7	0.127	-58.3	89.5
3	6.457	140.7	328.9	0.142	38.8	50.4
4	5.957	49.2	242.5	0.144	10.9	132.6
5	1.833	-23.8	118.3	0.144	51.6	307.8

Table II-2, Comparison of the O_4 and Five-Dipole Models at Jovian Surface (upper number denotes O_4, lower one five-dipole), The numbers are magnetic field strengths in Gauss

Latitude	360	340	320	300	280	260	240	220	200	180	160	140	120	100	80	60	40	20	0
90	[illegible]	[illegible]	[illegible]	[illegible]	[illegible]	[illegible]	[illegible]	[illegible]	[illegible]	[illegible]	[illegible]	[illegible]	[illegible]	[illegible]	[illegible]	[illegible]	[illegible]	[illegible]	[illegible]
80	[illegible]	[illegible]	[illegible]	[illegible]	[illegible]	[illegible]	[illegible]	[illegible]	[illegible]	[illegible]	[illegible]	[illegible]	[illegible]	[illegible]	[illegible]	[illegible]	[illegible]	[illegible]	[illegible]
70	[illegible]	[illegible]	[illegible]	[illegible]	[illegible]	[illegible]	[illegible]	[illegible]	[illegible]	[illegible]	[illegible]	[illegible]	[illegible]	[illegible]	[illegible]	[illegible]	[illegible]	[illegible]	[illegible]
60	[illegible]	[illegible]	[illegible]	[illegible]	[illegible]	[illegible]	[illegible]	[illegible]	[illegible]	[illegible]	[illegible]	[illegible]	[illegible]	[illegible]	[illegible]	[illegible]	[illegible]	[illegible]	[illegible]
50	[illegible]	[illegible]	[illegible]	[illegible]	[illegible]	[illegible]	[illegible]	[illegible]	[illegible]	[illegible]	[illegible]	[illegible]	[illegible]	[illegible]	[illegible]	[illegible]	[illegible]	[illegible]	[illegible]
40	[illegible]	[illegible]	[illegible]	[illegible]	[illegible]	[illegible]	[illegible]	[illegible]	[illegible]	[illegible]	[illegible]	[illegible]	[illegible]	[illegible]	[illegible]	[illegible]	[illegible]	[illegible]	[illegible]
30	[illegible]	[illegible]	[illegible]	[illegible]	[illegible]	[illegible]	[illegible]	[illegible]	[illegible]	[illegible]	[illegible]	[illegible]	[illegible]	[illegible]	[illegible]	[illegible]	[illegible]	[illegible]	[illegible]
20	[illegible]	[illegible]	[illegible]	[illegible]	[illegible]	[illegible]	[illegible]	[illegible]	[illegible]	[illegible]	[illegible]	[illegible]	[illegible]	[illegible]	[illegible]	[illegible]	[illegible]	[illegible]	[illegible]
10	[illegible]	[illegible]	[illegible]	[illegible]	[illegible]	[illegible]	[illegible]	[illegible]	[illegible]	[illegible]	[illegible]	[illegible]	[illegible]	[illegible]	[illegible]	[illegible]	[illegible]	[illegible]	[illegible]
0	[illegible]	[illegible]	[illegible]	[illegible]	[illegible]	[illegible]	[illegible]	[illegible]	[illegible]	[illegible]	[illegible]	[illegible]	[illegible]	[illegible]	[illegible]	[illegible]	[illegible]	[illegible]	[illegible]
-10	[illegible]	[illegible]	[illegible]	[illegible]	[illegible]	[illegible]	[illegible]	[illegible]	[illegible]	[illegible]	[illegible]	[illegible]	[illegible]	[illegible]	[illegible]	[illegible]	[illegible]	[illegible]	[illegible]
-20	[illegible]	[illegible]	[illegible]	[illegible]	[illegible]	[illegible]	[illegible]	[illegible]	[illegible]	[illegible]	[illegible]	[illegible]	[illegible]	[illegible]	[illegible]	[illegible]	[illegible]	[illegible]	[illegible]
-30	[illegible]	[illegible]	[illegible]	[illegible]	[illegible]	[illegible]	[illegible]	[illegible]	[illegible]	[illegible]	[illegible]	[illegible]	[illegible]	[illegible]	[illegible]	[illegible]	[illegible]	[illegible]	[illegible]
-40	[illegible]	[illegible]	[illegible]	[illegible]	[illegible]	[illegible]	[illegible]	[illegible]	[illegible]	[illegible]	[illegible]	[illegible]	[illegible]	[illegible]	[illegible]	[illegible]	[illegible]	[illegible]	[illegible]
-50	[illegible]	[illegible]	[illegible]	[illegible]	[illegible]	[illegible]	[illegible]	[illegible]	[illegible]	[illegible]	[illegible]	[illegible]	[illegible]	[illegible]	[illegible]	[illegible]	[illegible]	[illegible]	[illegible]
-60	[illegible]	[illegible]	[illegible]	[illegible]	[illegible]	[illegible]	[illegible]	[illegible]	[illegible]	[illegible]	[illegible]	[illegible]	[illegible]	[illegible]	[illegible]	[illegible]	[illegible]	[illegible]	[illegible]
-70	[illegible]	[illegible]	[illegible]	[illegible]	[illegible]	[illegible]	[illegible]	[illegible]	[illegible]	[illegible]	[illegible]	[illegible]	[illegible]	[illegible]	[illegible]	[illegible]	[illegible]	[illegible]	[illegible]
-80	[illegible]	[illegible]	[illegible]	[illegible]	[illegible]	[illegible]	[illegible]	[illegible]	[illegible]	[illegible]	[illegible]	[illegible]	[illegible]	[illegible]	[illegible]	[illegible]	[illegible]	[illegible]	[illegible]
-90	[illegible]	[illegible]	[illegible]	[illegible]	[illegible]	[illegible]	[illegible]	[illegible]	[illegible]	[illegible]	[illegible]	[illegible]	[illegible]	[illegible]	[illegible]	[illegible]	[illegible]	[illegible]	[illegible]

Table II-3. Comparison of B Values Obtained from the Five-Dipole and the O_4 Model

r (R_J)	Maximum Percentage Difference (%)
=1 (surface)	3
1.2	1
1.5	0.6
1.8	<0.001

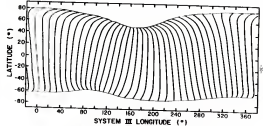

Figure II-1. Latitude vs. Longitude Plot of Magnetic Field Lines that Intersect Io's Orbit, as Calculated from the Five-Dipole Field Model. The upper and lower envelopes of these curves represent the foot-track of the Io flux tube.

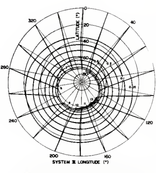

Figure II-2. Northern Hemisphere Latitude vs. Longitude Plot of Magnetic Field Parameters on the Surface Formed by the Aggregate of the Field Lines through Io's Orbit, as Calculated from the Five-Dipole Model. Isocontours of magnetic field strength on this surface are shown, indicated strengths are in Gauss. Representative field lines lying on the surface are also plotted, these are the same as the northern hemisphere parts of the field lines in Figure II-1

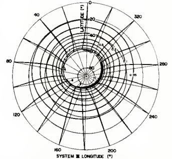

Figure II-3: Southern Hemisphere Latitude vs. Longitude Plot of Magnetic Field Parameters on the Surface Formed by the Aggregate of the Field Lines through Io's Orbit, Corresponding to Figure II-2.

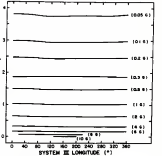

Figure II-4. Plot of Height above Cloud-Top Level vs. Longitude for Isocontours of Magnetic Field Strength in Figure II-2 (northern hemisphere).

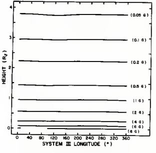

Figure II-5. Plot of Height above Cloud-Top Level vs. Longitude for Isocontours of Magnetic Field Strength in Figure II-3 (southern hemisphere).

Figure II-6 Northern Hemisphere Plot of the Electron Cyclotron Frequency Gradient along the Io Flux Tube ($\Delta f_c/\Delta s$) vs. the Longitude of Io for Points on the Flux Tube Having the Indicated Values of the Electron Cyclotron Frequency.

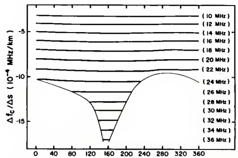
Δf_c/ΔS (10⁻⁴ MHz/km)
-5
-10
-15
0
40
80
120
160
200
240
280
320
360
SYSTEM III LONGITUDE OF IO (°)
(10 MHz)
(12 MHz)
(14 MHz)
(16 MHz)
(18 MHz)
(20 MHz)
(22 MHz)
(24 MHz)
(26 MHz)
(28 MHz)
(30 MHz)
(32 MHz)
(34 MHz)
(36 MHz)

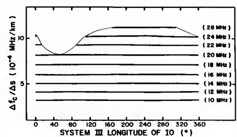

Figure II-7. Southern Hemisphere Plot Corresponding to Figure II-6.

CHAPTER III

THE EMISSION MODEL

1. Introduction

In this chapter, one of a number of possible types of decametric radio emission (DAM) mechanisms radiating near the local electron cyclotron frequency into a hollow-cone beam with its axis tangent to the Io flux tube (as discussed in Chapter 1) is assumed. The emission mechanism selected for the model is of the type classified by Goldstein and Goertz [1983] as nonlinear and indirect. Parameters of the model are adjusted to provide a close fit to the contours of observed emission probability on the Io phase-CML plane, which were made with the University of Colorado radio spectrograph for a narrow frequency range, 35-36 MHz, between 1960 and June 1966 [Wilson, Warwick, and Libby, 1968]. This contour plot is reproduced in Figure III-1. The frequency band used is sufficiently close to the 39.5 MHz cutoff of the decametric radiation that the emission must have occurred from within a very limited magnetospheric region where the magnetic field strength is relatively strong. Presumably, 35-36 MHz emission occurs only when the Io flux tube penetrates this region; when it does occur, it may or may not be beamed toward Earth (or Voyager).

As is usual with hollow-cone models of the Jovian decametric radiation, it is assumed that activity is observed only when rays between the inner and outer surfaces of the hollow cone can reach Earth (or Voyager). Such a simple beam model may have three adjustable parameters: the conical angle, the angular thickness of the wall of the hollow-cone beam (i.e., the difference between the half-angular openings of the inner and outer conical surfaces), and the amount by which the Io flux tube, at the point of emission, leads Io in longitude.

In the present modeling, the first of these three beam parameters was allowed to vary and is the one that was adjusted to fit the observed data. The second was derived from the first using the theory of the indirect emission model, and the third was taken from the theory of Bagenal [1983] for the propagation of Alfvén waves in the Io flux tube.

In the review of decametric emission mechanism theories by Goldstein and Goertz [1983], a distinction is made between direct and indirect theories. In direct mechanisms the radiation is generated by energetic electrons without intermediate steps. In indirect mechanisms, Io, through the excitation of Alfvén waves, can create a "beamlike" velocity distribution near the foot of Io flux tube, thus the free energy contained in an electron beam distribution is transformed into electrostatic waves which then combine to produce the electromagnetic radiation. In the indirect mechanism assumed in this paper the energetic electrons first excite electrostatic waves, then beam-driven instabilities in the plasma generate both upper-hybrid and lower-hybrid waves which in turn couple in some manner to produce the beam of electromagnetic waves. The terrestrial kilometric radiation (TKR) is believed to be emitted by a somewhat similar mechanism.

A konwledge of the magnetic field vector and of the electron number density as functions of position throughout the Jovian upper ionosphere were required in making the computations based on the assumed emission model. The field information was of course provided by the five-dipole model. The electron densities were obtained from the distribution function derived from Voyager measurements, found in Hashimoto and Goldstein [1983]. It was shown that in the present model corrections for refraction in the Jovian ionosphere were necessary for the source A contour but not for source B.

2. The Electron Beam, High Frequency Branch Wave, and Right-hand Cutoff Frequency

The chain of events in the assumed emission mechanism culminating in the production of the beamed electromagnetic radiation is discussed in the sections that follow. The electron beam in the Io flux tube will be considered first. The motion of magnetospheric plasma past Io due to the Jovian rotation continually excites shear Alfvén waves which are guided along the Io flux tube. The Alfvén wave intensity is controlled by the mean electron density over at least several Alfvén wavelengths adjacent to Io's location. When Io is in the northernmost part of the torus, Io sees a denser plasma in the south and a dilute plasma in the north. In this situation a stronger Alfvén wave is generated southward, and the northward directed wave is too weak to stimulate the DAM radiation when it reaches the northern ionosphere. However, the intense southward directed wave will, after reflection in the southern ionosphere, propagate to the northern foot of the same flux tube (which has moved past Io by this time), where it generates the DAM radiation [Hashimoto and Goldstein, 1983]. At the leading and trailing edges of the Io-generated Alfvén wave packet, parallel electric fields respectively accelerate and decelerate the electrons, producing a beam distribution of electron velocities parallel to $\vec{B}$. The distribution of $V_{\parallel}$ (B-parallel velocity) for the electrons in the beam is thus distinct from that for the undisturbed ambient cold-plasma electrons.

Both distributions are assumed to be Maxwellian, that is, for the ambient electron distribution function

$$f_e(V_{\parallel}) = \frac{1}{\sqrt{2\pi}V_e} \exp\left[-\frac{V_{\parallel}^2}{2V_e^2}\right] \qquad \text{(III-1a)}$$

and for the electron beam distribution function

$$f_b(V_{\parallel}) = \frac{1}{\sqrt{2\pi}V_b} \exp\left[-\frac{(V_{\parallel} - u)^2}{2V_b^2}\right] \qquad \text{(III-1b)}$$

where

V_e is the thermal velocity of electrons,

V_b is the thermal spread of the beam, and

u is the beam speed.

The formulas in this section are from Harris [1968] and from Goldstein and Goertz [1983].

The electron beam excites electrostatic waves, instabilities in which generate the upper-hybrid and lower-hybrid waves. Their phase velocities can be calculated from the real part of the cold-plasma dielectric function

$$\varepsilon = 1 - \omega_{pe}^2 \left(\frac{\sin^2\theta}{\omega^2 - \omega_{ce}^2} + \frac{\cos^2\theta}{\omega^2}\right) - \frac{\omega_{pi}^2 \sin^2\theta}{\omega_{ci}^2} \qquad \text{(III-2)}$$

where

ω_{pe} is the electron plasma frequency, $\omega_{pe}^2 = 4\pi n_e e^2/m_e$,

ω_{pi} is the ion plasma frequency, $\omega_{pi}^2 = 4\pi n_e e^2/M_i$,

ω_{ce} is the electron cyclotron frequency, $\omega_{ce} = eB/m_e c$,

ω_{ci} is the ion cyclotron frequency, $\omega_{ci} = eB/M_i c$,

m_e is the mass of electron,

M_i is the mass of ion,

c is the speed of light, and

θ is the angle between the wave vector $\vec{K}$ and the magnetic field $\vec{B}$.

We may ignore the ion term in (III-2) for all angles of propagation of eigenmode waves. This leads to

$$\varepsilon = 1 - \omega_{pe}^2 \left(\frac{\sin^2\theta}{\omega^2 - \omega_{ce}^2} + \frac{\cos^2\theta}{\omega^2}\right) \qquad \text{(III-3)}$$

The solution for the high frequency branch (between the electron cyclotron frequency and the upper-hybrid frequency) can be obtained from the dispersion relation

$$\omega^2 = \frac{1}{2}\left[\omega_{UHR}^2 + (\omega_{UHR}^4 - 4\omega_{ce}^2\omega_{pe}^2 \cdot \cos^2\theta)^{\frac{1}{2}}\right] \qquad \text{(III-4)}$$

where ω_{UHR} is the upper-hybrid right-hand frequency, and

$$\omega_{UHR}^2 = \omega_{pe}^2 + \omega_{ce}^2$$

The right-hand cutoff frequency is

$$\omega_R = \frac{1}{2}\,\omega_{ce}\,\{1 + [1 + 4(\omega_{ce}\omega_{ci} + \omega_{pe}^2)/\omega_{ce}^2]^{\frac{1}{2}}\} \qquad \text{(III-5)}$$

It is obvious that $\omega_{ci} \ll \omega_{ce}$. In the Jovian ionosphere, a typical value of the electron number density, n_e, is about 3×10^5 cm^{-3} [Hashimoto and Goldstein, 1983], hence the ratio of the electron plasma frequency to the electron cyclotron frequency for the frequency range 35-36 MHz is

$$\frac{\omega_{pe}}{\omega_{ce}} = \frac{9 \times 10^{-3}\,\sqrt{n_e}}{2.8B} = \frac{9 \times 10^{-3}\,\sqrt{3 \times 10^5}}{2.8 \times 12} \approx 0.14 \qquad \text{(III-6)}$$

Based on the above relation, we can simplify the expression (III-5) to

$$\omega_R = \frac{1}{2}\omega_{ce}\left\{1+\left[1+4\left(\frac{\omega_{pe}}{\omega_{ce}}\right)^2\right]^{\frac{1}{2}}\right\} = \frac{1}{2}\omega_{ce}\left[1+1+2\left(\frac{\omega_{pe}}{\omega_{ce}}\right)^2\right] = \omega_{ce}\left[1+\left(\frac{\omega_{pe}}{\omega_{ce}}\right)^2\right] \qquad \text{(III-7)}$$

Substituting (III-6) into (III-7), we have for the right-hand cutoff frequency

$$\omega_R \approx 1.02\,\omega_{ce} \qquad \text{(III-8)}$$

3. Growth Rate for the Upper-Hybrid Wave

The wave frequency of the high branch in (III-4) can be simplified to

$$\omega^2 = \frac{1}{2}\omega_{ce}^2\left[1+\left(\frac{\omega_{pe}}{\omega_{ce}}\right)^2+\sqrt{1+2\left(\frac{\omega_{pe}}{\omega_{ce}}\right)^2+\left(\frac{\omega_{pe}}{\omega_{ce}}\right)^4-4\left(\frac{\omega_{pe}}{\omega_{ce}}\right)^2\cdot\cos^2\theta}\right] \qquad \text{(III-9a)}$$

Then neglecting the $\left(\frac{\omega_{pe}}{\omega_{ce}}\right)^4$ term, and using the binomial theorem, we have

$$\omega^2 = \frac{1}{2}\omega_{ce}^2\left[1+\left(\frac{\omega_{pe}}{\omega_{ce}}\right)^2+1-\left(\frac{\omega_{pe}}{\omega_{ce}}\right)^2\cdot\cos 2\theta\right] = \omega_{ce}^2\left[1+\left(\frac{\omega_{pe}}{\omega_{ce}}\right)^2\cdot\sin^2\theta\right] \qquad \text{(III-9b)}$$

Then

$$\omega = \omega_{ce}\left[1+\frac{1}{2}\left(\frac{\omega_{pe}}{\omega_{ce}}\right)^2\cdot\sin^2\theta\right] \qquad \text{(III-9c)}$$

Comparing (III-9c) with (III-7) and (III-8), we can get the following relation

$$\omega_{ce} < \omega < \omega_R = 1.02\ \omega_{ce} \qquad \text{(III-10)}$$

The upper-hybrid wave is excited through the beam-driven Landau resonance. The rate of increase in its amplitude is represented by the quantity γ, called the growth rate. In the first approximation we confine our attention to the case for which $\omega \gg \omega_{ce}$. Under this circumstance, the growth rate is given by [Goldstein and Goertz, 1983]

$$\gamma = \sqrt{\frac{\pi}{2}}\,\frac{n_b}{n_e}\,\frac{\omega_{ce}}{2}\left(\frac{\omega_{pe}}{\omega_{ce}}\right)^4\left(\frac{n}{V_b}\right)^2\cdot\cos^2\theta\sin^2\theta\,\left(\frac{u}{V_b}-\frac{\omega_{ce}}{KV_b\cos\theta}\right)$$

$$\exp\left[-\frac{1}{2}\left(\frac{u}{V_b}-\frac{\omega_{ce}}{KV_b\cos\theta}\right)^2\right] \qquad \text{(III-11)}$$

where

K is the wave number and

n_b is the electron beam density

Here, in considering only Landau resonance, we are neglecting a term for thermal damping by cyclotron absorption [Goldstein et al., 1983].

4. Three-Wave Interactions

If the intensity of the upper-hybrid wave grows to a large amplitude, it can decay into two other waves, one electrostatic wave with very low frequency (subscript 1), and one electromagnetic wave (subscript 2), this process can be denoted by

$$\omega \to \omega_1 + \omega_2 \qquad \text{(III-12)}$$

This notation implies that two resonance conditions must be satisfied, one requiring momentum conservation

$$\vec{K} = \vec{K}_1 + \vec{K}_2 \qquad \text{(III-12a)}$$

and a second ensuring energy conservation (frequency matching)

$$\omega = \omega_1 + \omega_2 \qquad \text{(III-12b)}$$

Since for the upper-hybrid wave $\omega < \omega_R$, we have $\omega_2 < \omega < \omega_R$. This means that the electromagnetic wave cannot propagate out

Alternatively, the upper-hybrid wave can combine with a second electrostatic wave to produce an electromagnetic wave. This is known as up-conversion, which we can denote as

$$\sigma + \sigma_1 \rightarrow \sigma_2 \qquad \text{(III-13)}$$

The resonance conditions are

$$\vec{k} + \vec{k}_1 = \vec{k}_2 \qquad \text{(III-13a)}$$

$$\omega + \omega_1 = \omega_2 \qquad \text{(III-13b)}$$

Since $\omega_2 > \omega$, there may exist a product wave of frequency $\omega_2 > \omega_R$, which can freely escape from the Jovian ionosphere and magnetosphere

In the present DAM emission model, the up-conversion process represented by equation (III-13) is assumed Here a fast extraordinary (fast X) mode electromagnetic wave is the result of the beating of the large-amplitude upper-hybrid wave with a very low frequency electrostatic wave. The latter wave, however, could itself have been produced by the decay process denoted by equation (III-12) In such a case a large-amplitude upper-hybrid wave is assumed to have decayed at a nearby place into the required low frequency electrostatic wave together with an electromagnetic wave which cannot escape.

The schematic view of a three-wave interaction is shown in Figure III-2.

The wave number of the electromagnetic wave is small, that is,

$$|\vec{k}_2| << |\vec{k}_1| \text{ or } |\vec{k}| \qquad \text{(III-14)}$$

The three-wave resonance for up-conversion requires that $\vec{k} \approx -\vec{k}_1$, consequently, the upper-hybrid and second electrostatic waves must propagate in opposite directions for up-conversion (frequency addition) to take place.

By equating the B-parallel components of equation (III-13a), we obtain

$$K \cos\theta - K_1 \cos\theta \approx K_2 \cos\theta_2 \qquad \text{(III-15)}$$

where θ_2 is the angle between the wave vector of the electromagnetic wave, $\vec{k}_2$, and $\vec{B}$, the so-called conical angle.

It follows that

$$\cos\theta_2 = \frac{K - K_1}{K_2} \cos\theta \qquad \text{(III-16)}$$

The following limitations are a guide in approximating the relation between θ_2 and θ (Goldstein and Geerts, 1983): (1) the upper boundary condition $\theta < 88^\circ$, imposed by the requirement that the up-conversion frequency must exceed the right-hand cutoff frequency, and (2) the lower boundary condition $\theta_2 > 55°$, imposed by the inequality

$$K_{2\parallel} << K_{2\perp} = K_2 \sin\theta_2 \tag{III-17}$$

Considering these conditions, we have the approximate ratio of θ_2/θ from 0.7 to 1.5.

For the sake of simplicity, we choose $\theta_2 = \theta$ for the DAM modeling in the frequency range 35-36 MHz. This assumption is made plausible by the above limits.

This selection assures that the up-conversion process is capable of generating fast X mode radiation into a hollow conical emission pattern.

5. Conical Emission Pattern

Because of the uncertainty of many of the parameters, such as ω_b, ω_e, υ, V_e, and V_b, it is difficult to directly evaluate the conical angle θ_2 from the equation (III-11) by maximizing the growth rate, even if we have made the simplification that $\theta_2 = \theta$. Assuming that the growth rate of the upper-hybrid wave is near its theoretical maximum and using the following relations

$$\theta_2 = \theta \tag{III-18a}$$

$$\Delta\theta_2 = \Delta\theta \tag{III-18b}$$

the relationship between the conical angle θ_2 and the angular thickness $\Delta\theta_2$ would be established. Next, with the help of the five-dipole magnetic field model, we could geometrically calculate the value of θ_2 for the boundaries of the contour plots for sources A and B; then using the derived relation between θ_2 and $\Delta\theta_2$, we might fit the observed data. This procedure was indeed followed and proved to be very successful.

Following is the derivation of the relation between the conical angle θ_2 and the angular thickness $\Delta\theta_2$.

Figure III-3 is a plot of growth rate as a function of the angle between the upper-hybrid wave vector and the magnetic field, as given by equation (III-11).

The angle at which the peak value γ_0 occurs is designated θ_0, thus,

$$\gamma_0 = \max \gamma = \gamma(\theta_0) \qquad \text{(III-19a)}$$

We assume that within the angular thickness range $\theta_0 \pm \Delta\theta$, the growth rate is high enough to excite oblique propagation of the upper-hybrid wave. For a given value of $\Delta\theta$, the drop rate of γ is defined as

$$d_r = \frac{\gamma(\theta_0 \pm \Delta\theta)}{\gamma_0} = \frac{\gamma_0 - \Delta\gamma}{\gamma_0} \qquad \text{(III-19b)}$$

Again we assume that d_r is constant; that is, the excitation of the upper-hybrid wave is uniform everywhere within the emission region

In the first approximation, $\omega \approx \omega_{ce}$, also, we fix the parameters n_b, n_e, u, V_b, ω_{ce}, and ω_{pe}, i.e., assume that

$$\sqrt{\frac{\pi}{2}}\,\frac{n_b}{n_e}\,\frac{\omega_{ce}}{2}\left(\frac{\omega_{pe}}{\omega_{ce}}\right)^4\left(\frac{u}{V_b}\right)^2 = \text{constant} = C \qquad \text{(III-20a)}$$

Since d_r is constant, it implies that

$$\frac{\Delta\gamma}{\gamma_0} = \text{constant} = D \qquad \text{(III-20b)}$$

By taking the logarithms on both sides of equation (III-11) at $\theta = \theta_0$, it becomes

$$\ln \gamma_0 = \ln C + 2\ln(\sin\theta_0\cos\theta_0) + \ln\left[\frac{u}{V_b} - \frac{\omega_{ce}}{KV_b\cos\theta_0}\right]$$

$$- \frac{1}{2}\left\{\frac{u}{V_b} - \frac{\omega_{ce}}{KV_b\cos\theta_0}\right\}^2 \qquad \text{(III-21)}$$

Suppose

$$\frac{u}{V_b} = A \qquad \text{(III-22a)}$$

$$\frac{\omega_{ce}}{KV_b} = B \qquad \text{(III-22b)}$$

Differentiating (III-21) and inserting (III-20b) into it, we have

$$0 = f(\theta_0)\Delta\theta \qquad \text{(III-23a)}$$

and

$$f(\theta_o) = \frac{2(\cos^2\theta_o - \sin^2\theta_o)}{\sin\theta_o \cos\theta_o}$$

$$+ \frac{B\sin\theta_o}{\cos^2\theta_o}\left[\left(A - \frac{B}{\cos\theta_o}\right) - \frac{1}{\left(A - \frac{B}{\cos\theta_o}\right)}\right] \qquad \text{(III-23b)}$$

Hence

$$\Delta\theta = \frac{D}{f(\theta_o)} \qquad \text{(III-24)}$$

By making use of equations (III-18a) and (III-18b), we can get a similar relation

$$\Delta\theta_2 = \frac{D}{f(\theta_2)} \qquad \text{(III-25)}$$

where we have selected the angle θ_2 to be equivalent to the angle θ_o.

There is too much uncertainty to permit a plausible estimate to be made of A and B directly. Each assumed pair of values for these constants establishes a certain relationship between θ_2 and $\Delta\theta_2$. It was found, however, that a particular pair of values optimized the fitting of the observed occurrence probability contours by adjusting θ_2. The optimum values were found to be A = 3.257 and B = 0.268. The angle $\Delta\theta_2$ as a function of θ_2 is listed in Table III-1. It must be pointed out that the values of $\Delta\theta_2$ are very sensitive to the selection of parameters A and B.

6. Specification of Beam Pattern

The longitude of the foot of the Io flux tube leads Io in longitude by the amount [Hashimoto and Goldstein, 1983]

$$\Delta\lambda = 17.18^\circ + 3.74^\circ \sin\lambda \tag{III-26}$$

where

$$\lambda = \lambda_{Io} - 112^\circ$$

The terms λ_{Io} and $\lambda_{Io} + \Delta\lambda$ are both sub-Io longitudes (System III), the former referring to the time at which the Alfvén waves began propagating in the Alfvén current tube and the latter to the time radiation was actually emitted The geometry is shown in Figure III-4, where we have ignored the distortion of Alfvén current tube away from the Io flux tube within Jupiter's near field

The relationship between CML, $\Delta\lambda$, γ_{Io} (Io departure from Superior Geocentric Conjunction), and λ_{Io} can be obtained from Figure III-5

$$\text{CML} = \lambda_{Io} + \gamma_{Io} + \Delta\lambda - 180^\circ \tag{III-27}$$

We now utilize the five-dipole magnetic field model to calculate the conical angle θ_2 (with respect to the magnetic field $\vec{B}$), and the conical angle β (with respect to the radial vector)

In Figure III-6, let the X axis be in the direction of System III longitude λ_{III} (1965) = 0°, the Y axis be perpendicular to the X axis, and the Z axis be in the planetary spin axis. The X, Y, and Z axes form a left-hand coordinate system.

The unit vector in the direction of magnetic field $\vec{B}$ is

$$\hat{a} = \frac{\vec{B}}{B} = \frac{1}{B}\{[(B_r\sin\theta + B_\theta\cos\theta)\cos\lambda + B_\phi\sin\lambda]\hat{i}$$

$$+ [(B_r\sin\theta + B_\theta\cos\theta)\sin\lambda - B_\phi\cos\lambda]\hat{j}$$

$$+ (B_r\cos\theta - B_\theta\sin\theta)\hat{k}\} \qquad \text{(III-28)}$$

where B_r, B_θ, and B_ϕ are the components of $\vec{B}$ in a spherical coordinate system, θ and λ are the colatitude and System III longitude of source P, respectively.

The unit directional vector of source P toward Earth is

$$\bar{J}_E = \cos\lambda_{III}\cos D_E\,\hat{i} + \sin\lambda_{III}\cos D_E\,\hat{j} + \sin D_E\,\hat{k} \qquad \text{(III-29)}$$

where λ_{III} is the CML of Jupiter, D_E is the declination of Earth with respect to Jovicentric system.

The conical angle Φ_2 (relative to an observer on Earth) can be obtained from

$$\cos\Phi_2 = \hat{a}\cdot\hat{J}_E$$

$$= \frac{1}{B}\{[(B_r\sin\theta + B_\theta\cos\theta)\cos\lambda + B_\phi\sin\lambda]\cos\lambda_{III}\cos D_E$$

$$+ [(B_r \sin\theta + B_\theta \cos\theta)\sin\lambda - B_\phi \cos\lambda] \sin\lambda_{III} \cos D_E$$

$$+ (B_r \cos\theta - B_\theta \sin\theta)\sin D_E\} \qquad \text{(III-30)}$$

The unit vector in the radial direction $\hat{r}$ is

$$\hat{r} = \sin\theta\cos\lambda\ \hat{i} + \sin\theta\sin\lambda\ \hat{j} + \cos\theta\ \hat{k} \qquad \text{(III-31)}$$

The conical angle ξ (relative to an observer on Earth) can be obtained from

$$\cos\xi = \hat{r}\cdot\hat{j}_E$$

$$= \sin\theta\cos\lambda\cos\lambda_{III}\cos D_E$$

$$+ \sin\theta\sin\lambda\sin\lambda_{III}\cos D_E + \cos\theta\sin D_E \qquad \text{(III-32)}$$

This angle will be discussed in the next section

7. Numerical Adjustment of the Model

The next step is to adjust the emission model so that it agrees numerically with the outer contours of the plot of observed probability of occurrence of activity in the frequency range 33-36 MHz, as shown in Figure III-1. It was considered to be necessary to make the calculation only within the range of the sub-Io longitude λ_{Io} from 134° to 232°. The upper bound of this λ_{Io} range is based on the magnetic field strength, beyond it the strength is too low for us to receive the DAM radiation in the frequency range 35-36 MHz. The lower bound is considered to be the critical longitude at which the denser plasma in the southern part of Io torus is just strong enough to generate the Alfvén wave toward the south. The reason for the assumption that the Alfvén wave that excites radio emission in the northern hemisphere propagates first southward from Io, and then is reflected northward, is given in Section 2 of this chapter.

The emission region is bounded by the above-mentioned sub-Io longitudes, by the Jovigraphic latitude planes 48.7° and 55.2°, and by the constant-altitude surfaces (above the cloud-top level) at 400 km and 4000 km

The final result of the development and fitting of the radio emission model can be summarized by Figure III-7 and Figure III-8. As stated previously, the arbitrary parameter that was adjusted to give a fit to the observationally determined contours was the conical angle θ_2 with respect to the tangent to the magnetic field at the emission point, expressed as a function of the sub-Io longitude λ_{Io} at the time of excitation of the corresponding Alfvén wave by Io. The angular thickness $\Delta\theta_2$ of the hollow cone of emitted rays was computed for each value of θ_2, using the relation derived from the assumed emission model. The resulting fit is shown in Figure III-8, the dot-dashed contours representing the observationally determined data and the solid line contours representing the model fit. Thus far, it has been assumed that refraction in the Jovian ionosphere at 35-36 MHz is negligible insofar as the present model is concerned. As will be shown in the next section, this assumption was valid for source B, but was not true for source A except for the left-hand part. It is apparent that the fit for source B was essentially perfect without refraction corrections. It would perhaps have been more gratifying if a constant cone angle θ_2 instead of the variable cone angle in Figure III-7 had yielded the excellent fit in Figure III-8. This, however, would have probably been unrealistic; one could not expect such a high degree of magnetospheric uniformity to exist as this would have implied. The required variation in θ_2, from 69.4° to 76.4°, is after all relatively small and does not seem unlikely.

Table III-2 is a listing of the values from which the curve in Figure III-7 was plotted.

Table III-3 lists the emission events for sources A and B in the frequency range 35-36 MHz during the period from 1960 to June 1966, as obtained from the catalog by Warwick, Dulk, and Riddle [1975].

The upper and lower limits of D_E and the boundaries of Io phase and CML, as used in the computation of outer contours for sources A and B, respectively, are illustrated in Appendix 1. For the sake of convenience, we also depict the signs of D_E for the above-mentioned limits in Figure III-1.

8. Refraction Effect

It was not feasible to incorporate the effect of refraction in the Jovian ionosphere into the emission model. One reason for this is that the height of the source region above the cloud-top level where the fast X mode electromagnetic emission occurs is difficult to determine, another reason is the resulting increase in computational complexity. In obtaining the plots of Figure III-8 it was therefore assumed that refraction can be neglected. As is apparent from the figure, an excellent fit was obtained to source B without the refraction correction, but the fit to source A was poor except at its left-hand end. In this section, calculations are made to determine the parts of the model contour plots in Figure III-8 for which the omission of a refraction correction was probably justified, and the parts which are in serious error as a result of the omission. These calculations are based on the model Jovian ionosphere previously assumed [Hashimoto and Goldstein, 1983].

In the Jovian ionosphere, the refractive index n for fast X mode electromagnetic waves is expressed by the Appleton-Hartree equation as

$$n^2 = 1 - \frac{2\omega_{pe}^2\left(1 - \frac{\omega_{pe}^2}{\omega^2}\right)}{2(\omega^2-\omega_{pe}^2)-\omega_{ce}^2\sin^2\theta_2-\omega_{ce}\left[\omega_{ce}^2\sin^4\theta_2+4(\omega^2-\omega_{pe}^2)\cos^2\theta_2\right]^{\frac{1}{2}}}$$

(III-33a)

Since the ratio of $\omega_{pe}/\omega_{ce} = 0.14 << 1$ near the emission region in ionosphere, thus equation (III-33a) can be reduced to

$$n^2 = 1 - \frac{\omega_{pe}^2}{\omega^2 - \frac{1}{2}\,\omega_{ce}^2\sin^2\theta_2-\omega_{ce}\left[\frac{1}{4}\,\omega_{ce}^2\sin^4\theta_2+\omega^2\cos^2\theta_2\right]^{\frac{1}{2}}}$$

(III-33b)

which becomes

$$n^2 = 1 - \frac{\left(\frac{\omega_{pe}}{\omega}\right)^2}{1 - \frac{1}{2}\left(\frac{\omega_{ce}}{\omega}\right)^2 \sin^2\theta_2 - \left(\frac{\omega_{ce}}{\omega}\right)\left[\frac{1}{4}\left(\frac{\omega_{ce}}{\omega}\right)^2 \sin^4\theta_2 + \cos^2\theta_2\right]^{\frac{1}{2}}} \qquad \text{(III-33c)}$$

For the DAM emission $\omega > \omega_{ce}$, so n always < 1

We make the assumption that the Jovian spherically stratified ionosphere can be regarded as plane-stratified because the thickness of the ionospheric layer is negligible compared with the Jupiter radius. It follows from Snell's Law that the product ($n \sin\beta$) is a constant for a given ray path, where n is the refractive index and β the angle between the ray tangent and the ionospheric normal at any point on the ray. Thus in Figure III-9, if n and β refer to the point at which the radiation is emitted and the corresponding angle β' refers to a point on the ray path in the empty space outside the ionosphere (where $n = 1$), then

$$n \sin\beta = \sin\beta' \qquad \text{(III-34a)}$$

Its derivative gives

$$n \cos\beta\Delta\beta = \cos\beta'\Delta\beta' \qquad \text{(III-34b)}$$

where

β is the angle for the mid-ray of the incident beam with respect to the ionospheric normal;

β' is the angle for the mid-ray of the emergent beam;

$\Delta\beta$ is the angular thickness of the incident beam, and

$\Delta\beta'$ is the angular thickness of the emergent beam.

Although the present emission model is based on the assumption of no ionospheric refraction, some refraction does of course occur. It is of no consequence, however, as long as the total angle of deflection due to refraction is small compared with the sum of the hollow-cone beam wall thicknesses before and after refraction. In such a case, rays that reach Earth without refraction having been accounted for also reach Earth when the refraction correction is made, and those that do not reach Earth in the one case also do not in the other. It is apparent from Figure III-9 that the total refractive deflection angle is $\beta - \beta'$, and that the sum of the beam wall thickness before and after refraction is $\Delta\beta + \Delta\beta'$. We will assume that the condition under which refraction can be neglected is

$$\beta - \beta' \leq \Delta\beta + \Delta\beta' \qquad \text{(III-34c)}$$

The following relations can be obtained from equations (III-34a)-(III-34c)

$$\Delta\beta' = \frac{n \cos\beta}{\cos\beta'} \Delta\beta \qquad \text{(III-35a)}$$

$$\beta - \sin^{-1}(n \sin\beta) \leq \Delta\beta \left[1 + \frac{n \cos\beta}{(1 - n^2 \sin^2\beta)^{\frac{1}{2}}}\right] \qquad \text{(III-35b)}$$

The first equation indicates the reduction of the angular thickness of the emission cone wall after refraction, the second one the change of the direction of the mid-ray of the cone wall.

Both $\Delta\theta$ and $\Delta\Theta_2$ represent the angular thickness of the same cone wall before refraction, so it is obvious that

$$\Delta\theta = \Delta\Theta_2 \tag{III-36a}$$

The same is also true for the angular thickness after refraction, it leads to

$$\Delta\theta' = \Delta\Theta_2' \tag{III-36b}$$

where $\Delta\Theta_2'$ is the angular thickness after refraction.

If we take the ratio of wave frequency to right-hand cutoff frequency, $\omega/\omega_R = 1.08$, then the ratios of ω_{ce}/ω and ω_{pe}/ω can be evaluated from the following relations

$$\frac{\omega_{ce}}{\omega} = \frac{\omega_R}{\omega}\frac{\omega_{ce}}{\omega_R} = \frac{\omega_R}{\omega}\left[1 + \left(\frac{\omega_{pe}}{\omega_{ce}}\right)^2\right]^{-1} = \frac{1}{1.08} \times [1+0.14^2]^{-1} = 0.908 \tag{III-37a}$$

and

$$\frac{\omega_{pe}}{\omega} = \frac{\omega_R}{\omega}\frac{\omega_{pe}}{\omega_{ce}}\frac{\omega_{ce}}{\omega_R} = \frac{\omega_R}{\omega}\frac{\omega_{pe}}{\omega_{ce}}\left[1 + \left(\frac{\omega_{pe}}{\omega_{ce}}\right)^2\right]^{-1} = \frac{1}{1.08} \times 0.14 \times [1+0.14^2]^{-1}$$

$$= 0.127 \tag{III-37b}$$

Substituting (III-37a) and (III-37b) into (III-33c), and taking the average of the conical angle, $\Theta_2 = 75.3°$ for the right-hand end region in source A, we have

$$s = 0.95 \tag{III-38}$$

The average of the angular thickness of the wall of the hollow cone, $\Delta\beta$ (same value as $\Delta\theta_2$), is about 5.7° from Table III-1. Substituting this value of $\Delta\beta$ and the refractive index in (III-38) into (III-35b), we obtain the value of β for which the deflection due to refraction is equal to $(\Delta\beta + \beta')$, this value is designated β_1. It is approximately

$$\beta_1 \doteq 76.4^\circ \tag{III-39}$$

It was found that $\beta < \beta_1$, for all of the modeled contour of source B, and also for that part of the source A to the left of the dashed line in Figure III-8. Therefore, only the part of the source A contour to the right of the dashed line needs to be corrected for refraction.

The cone axis (which is tangent to the magnetic field) is tilted in such a way that β is larger for the right-hand part of source A than for the left-hand part of source A and any part of source B. The effect of refraction in the Jovian ionosphere is to bend the source A beam toward lower longitude (CML), and to bend its trailing-edge boundary more than its leading-edge one. Thus, as a result of refraction, source A is compressed in longitude and is displaced toward lower longitudes, the compression being more in the higher-longitude part. The ratio of the decrease in CML to that for β is $\frac{dCML}{d\beta}$; this quantity is about 3.3°-6.6° for β values between 81°-84° in source A, as obtained from Figure III-10. The values of the bending angle (i.e., the total refractive deflection angle $\beta-\beta'$) for different values of β are listed in Table III-4, as calculated from the left-hand side of (III-35b). The amounts by which different parts of source A are shifted to the left by refraction can now be evaluated. For example, the bending angle for that part having β values between about 81° and 84° is approximately 12°. The corresponding decrease in CML will be between about 40° and 80°, enough to move this part of source A leftward across the dashed line (but not enough to move it past the extreme left-hand boundary of source A in the figure). For the other values of β which are greater than 78.4°, the same is true. If the value of β is less than 78.4°, there will be considerably less change of CML, especially for the region near the left-hand boundary, only about 5°-8°. The effect of refraction for such values of β is to move the left-hand boundary a relatively small amount to the left, but not enough to appreciably degrade the fit of this part of source A to the observed contour. It is apparent from the foregoing argument that when the entire modeled source A contour is corrected for refraction (using the assumed model Jovian ionosphere), the corrected contour will fit the observed one nearly as well as does that for source B (for which such a correction was unnecessary).

9. Conclusion

The success of the Jovian decametric emission model developed in this chapter was due in no small part to the limiting of the observational data used as its basis to a quite high frequency range, 35 to 36 MHz, which is the highest range of the available data sets. Since the emitted frequency is presumably only slightly above the local electron cyclotron frequency, the possible source locations in the Jovian ionosphere are confined to the relatively small area within which the Jovian magnetic field is near its highest value. As a result, only the source A and B CML regions were present (source C not occurring at such high frequencies), and they were much more concentrated in the Io phase-CML plane than they are at lower frequencies. In fact, the diagonal line representing the path along which the sub-Io longitude is 167° on the Io phase-CML plot in Figure III-1 neatly separates the source A and source B contour systems. At lower frequencies, sources A and B overlap badly when occurrence probability is plotted vs. sub-Io longitude, greatly complicating modeling problems.

Another consequence of the use of the highest feasible frequency range was that Jupiter's ionospheric refraction effects were minimized. In Section B, rough estimates have been made of the extent to which an assumed model Jovian ionosphere would alter the emission model. It was fortunate indeed that the refraction of source B rays turned out to be relatively small, and that only the source A contour seemed to need correction. At a lower frequency, the refraction of source B rays would probably not be negligible, greatly multiplying the uncertainties in the model.

It will not be difficult to replot the source A contour completely, taking into account the ray refraction by the assumed model Jovian ionosphere. Then, as has already been shown, the new modeled source A contour will fit the observed one nearly as well as does that for source B. There is also a possibility that after the refraction corrections for source A are applied, a slight readjustment of the assumed values of θ_2 in Figure III-7 can be made that will reduce the range of variation for sub-Io longitude.

The present successful modeling of Jupiter's decametric emission mechanism opens up several avenues for further modeling. Perhaps the next step is to attempt the modeling of sources A and B at a lower frequency range, and to see whether or not source C also makes an appearance. Another thing that needs to be done is to attempt to reconcile the three types of hollow-cone emission models that have been used to account for quite different Jovian phenomena: the present model for occurrence probability on the Io phase-CML plane, the hollow-cone model of Goldstein and Thieman [1981] for dynamic spectral arcs, and the hollow-cone model of Maeda and Carr [1984, 1985] to account for the results of simultaneous observations of Jovian activity at 22 MHz obtained from the two Voyager spacecraft and from ground stations.

Finally, the outcome of the emission model creates a new need for additional Jovian decametric observations, particularly at frequencies above 25 MHz. Continuous monitoring of Jupiter activity throughout the approaching years for the sunspot minimum is needed. Such monitoring should include bands between 35 and 36 MHz, and, say, 31 and 32 MHz. New data in the 35-36 MHz band would be invaluable for testing and extending the present model and that in the 31-32 MHz band would be used for modeling at a lower frequency. The methods developed in the present model will also open up new possibilities for the interpretation of the Jovian polarization measurements and S burst observations.

Table III-1 The Angular Thickness $\Delta\theta_2$ as a Function of the Conical Angle θ_2 (both in degrees)

θ_2	$\Delta\theta_2$	θ_2	$\Delta\theta_2$
68.10	1.10	73.10	1.99
68.20	1.10	73.20	2.05
68.30	1.10	73.30	2.11
68.40	1.10	73.40	2.18
68.50	1.11	73.50	2.26
68.60	1.11	73.60	2.34
68.70	1.11	73.70	2.43
68.80	1.11	73.80	2.52
68.90	1.12	73.90	2.62
69.00	1.12	74.00	2.74
69.10	1.13	74.10	2.86
69.20	1.13	74.20	2.99
69.30	1.14	74.30	3.14
69.40	1.14	74.40	3.30
69.50	1.15	74.50	3.48
69.60	1.16	74.60	3.67
69.70	1.16	74.70	3.88
69.80	1.17	74.80	4.12
69.90	1.18	74.90	4.38
70.00	1.19	75.00	4.67
70.10	1.20	75.10	5.00
70.20	1.21	75.20	5.36
70.30	1.22	75.30	5.76
70.40	1.23	75.40	6.20
70.50	1.24	75.50	6.69
70.60	1.26	75.60	7.24
70.70	1.27	75.70	7.83
70.80	1.28	75.80	8.47
70.90	1.30	75.90	9.15
71.00	1.31	76.00	9.85
71.10	1.33	76.10	10.56
71.20	1.35	76.20	11.21
71.30	1.37	76.30	11.78
71.40	1.39	76.40	12.20
71.50	1.41	76.50	12.41
71.60	1.43	76.60	12.37
71.70	1.45	76.70	12.07
71.80	1.48	76.80	11.52
71.90	1.50	76.90	10.77
72.00	1.53	77.00	9.89
72.10	1.56	77.10	8.94
72.20	1.59	77.20	7.99
72.30	1.63	77.30	7.08
72.40	1.66	77.40	6.23
72.50	1.70	77.50	5.46
72.60	1.74	77.60	4.78
72.70	1.78	77.70	4.18
72.80	1.83	77.80	3.66
72.90	1.88	77.90	3.21
73.00	1.93	78.00	2.82

Table III-2 The Conical Angle Φ_2 as a Function of Io Longitude λ_{Io}. λ and θ are the System III longitude and the colatitude of the northern foot of the Io flux tube (all in degrees)

λ_{Io}	λ	θ	Φ_2	λ_{Io}	λ	θ	Φ_2
134	150.56	38.00	71.65	184	174.92	41.18	75.46
135	151.06	38.16	71.55	185	175.37	41.15	75.47
136	151.59	38.28	71.45	186	175.84	41.12	75.50
137	152.08	38.40	71.35	187	176.33	41.08	75.49
138	152.57	38.50	71.15	188	176.85	41.04	75.48
139	153.08	38.72	71.00	189	177.39	41.00	75.45
140	153.59	38.84	70.85	190	177.73	40.92	75.42
141	154.09	39.00	70.60	191	178.33	40.88	75.44
142	154.59	39.12	70.50	192	178.70	40.80	75.47
143	155.08	39.24	70.40	193	179.11	40.72	75.50
144	155.58	39.36	70.20	194	179.79	40.68	75.52
145	156.08	39.48	70.00	195	180.25	40.60	75.56
146	156.58	39.60	69.80	196	180.74	40.52	75.60
147	157.08	39.72	69.60	197	181.26	40.44	75.61
148	157.54	39.80	69.40	198	181.73	40.32	75.62
149	158.05	39.92	70.30	199	182.10	40.24	75.63
150	158.51	40.00	70.70	200	182.72	40.16	75.64
151	159.04	40.12	71.00	201	183.07	40.04	75.64
152	159.51	40.20	71.20	202	183.75	39.96	75.65
153	159.97	40.28	71.40	203	184.17	39.84	75.67
154	160.45	40.36	71.60	204	184.62	39.72	75.69
155	160.93	40.44	71.70	205	185.10	39.60	75.71
156	161.41	40.52	71.80	206	185.62	39.48	75.75
157	161.91	40.60	71.80	207	186.18	39.36	75.82
158	162.41	40.68	71.80	208	186.44	39.20	75.86
159	162.92	40.76	72.00	209	187.08	39.08	76.05
160	163.34	40.80	72.20	210	187.74	38.96	76.10
161	163.88	40.88	73.50	211	188.12	38.80	76.25
162	164.31	40.92	73.60	212	188.63	38.64	76.37
163	164.87	41.00	73.70	213	189.14	38.48	76.40
164	165.33	41.04	73.75	214	189.50	38.36	76.43
165	165.79	41.08	73.80	215	189.98	38.16	76.44
166	166.27	41.12	73.85	216	190.55	38.00	76.44
167	166.76	41.16	74.20	217	191.16	37.84	76.43
168	167.26	41.20	75.35	218	191.81	37.68	76.42
169	167.78	41.22	75.34	219	192.14	37.48	76.40
170	168.16	41.24	75.30	220	192.68	37.52	76.36
171	168.71	41.26	75.28	221	193.29	37.12	76.30
172	169.12	41.28	75.33	222	193.74	36.92	76.25
173	169.70	41.30	75.35	223	194.24	36.72	76.25
174	170.14	41.32	75.36	224	194.78	36.52	76.18
175	170.59	41.32	75.36	225	195.36	36.32	76.10
176	171.06	41.32	75.36	226	195.98	36.12	76.08
177	171.54	41.32	75.36	227	196.65	35.92	76.04
178	172.05	41.32	75.38	228	196.98	35.68	76.00
179	172.57	41.30	75.41	229	197.74	35.48	76.00
180	172.93	41.28	75.43	230	198.15	35.24	75.60
181	173.49	41.26	75.44	231	198.99	35.04	74.80
182	173.88	41.24	75.44	232	199.50	34.80	74.00
183	174.48	41.21	75.46				

Table III-3. Emission Events at Frequency Range 35-36 MHz

1. Io-A source

Date yr.mon.day	Emission Start hr min	Emission End hr min	Intensity	Burstness	Frequency Range (MHz)	Longitude (1965.0) (deg.)	Io Phase (from S.G.C.) (deg.)	Declination of Earth (deg.)
1961 6 16	1153	1323	3	strong	22-35	204.8-259.2	227.1-239.8	-0.61°
1961 7 18	0741	1024	3	strong	13-35	196.0-292.5	226.7-249.7	-0.62°
1961 8 12	0357	0547	3	strong	14-35	225.0-291.5	245.5-261.0	-0.66°
1961 10 31	0001	0006	2	moderate	23-37	240.5-243.5	291.1-291.8	-0.66°
1962 1 30	1933	2021	2	smooth	23-35	225.8-254.8	235.5-242.3	-0.12°
1962 7 7	0850	1113	3	strong	11-35	204.6-291.1	231.7-251.9	+1.38°
1962 8 1	0415	0554	2	strong	12-36	204.5-264.3	241.7-255.7	+1.45°
1962 8 8	0446	0743	3	moderate	13-36	197.9-304.9	231.3-256.4	+1.45°
1963 2 27	1625	1803	1	smooth	23-35	199.4-258.6	226.2-240.0	+1.57°
1963 7 3	1112	1214	1	moderate	14-35	236.5-273.9	236.3-245.0	+2.69°
1963 7 28	0559	0914	2	weak	13-35	210.6-328.5	237.6-265.2	+2.85°
1963 9 10	1122	1358	2	weak	17-38	193.5-287.8	238.7-260.7	+3.00°
1963 9 17	1206	1412	3	moderate	14-37	196.8-271.0	230.1-247.9	+2.99°
1963 9 26	0445	1020	2	strong	9-35	204.3-406.8	200.2-247.6	+2.98°
1963 10 12	0708	1008	2	strong	13-35	181.5-290.4	238.4-263.8	+2.92°
1963 10 19	0748	1158	3	weak	14-35	180.3-331.5	229.3-264.7	+2.88°
1963 11 20	0439	0623	1	weak	17-35	205.0-267.8	237.2-251.9	+2.68°
1963 11 27	0542	0648	2	moderate	15-35	216.7-256.6	230.7-240.0	+2.64°
1965 4 28	2136	2221	1	weak	22-35	231.3-258.5	239.5-245.8	+2.77°
1965 9 26	1057	1150	2	strong	13-36	231.7-263.7	248.4-255.9	+2.46°
1965 10 3	1134	1220	1	moderate	17-35	228.0-255.8	237.6-244.1	+2.46°
1965 10 10	1230	1259	1	weak	22-35	235.8-253.3	229.7-233.8	+2.45°
1965 11 4	0728	0858	2	weak	12-35	218.5-272.9	234.9-247.6	+2.44°
1965 12 6	0259	0502	2	moderate	13-35	197.4-271.8	231.6-249.0	+2.44°
1966 1 26	0854	1037	3	moderate	12-35	174.1-236.4	225.2-239.8	+2.37°
1966 2 20	0447	0707	2	strong	13-36	187.1-271.7	237.6-257.4	+2.30°

Table III-3 continued

2. Io-B source

Date yr mon day	Emission Start hr min	 End hr.min	Intensity	Burstness	Frequency Range (MHz)	Longitude (1965.0) (deg.)	Io Phase (from S.G.C.) (deg.)	Declination of Earth (deg.)
1961 2 13	1520	1525	1	smooth	34-38	178.1-181.1	77.9- 78.6	-1.32°
1961 5 11	1044	1152	3	strong	14-37	141.0-182.1	90.7-100.3	-0.72°
1961 6 12	0629	0733	1	smooth	18-36	126.4-165.1	87.0- 96.0	-0.61°
1961 8 27	0732	0849	3	strong	10-38	94.0-140.5	89.6-100.5	-0.69°
1961 9 28	0406	0520	2	strong	13-38	105.8-150.6	93.1-103.6	-0.72°
1961 10 5	0453	0620	3	strong	15-39	107.3-159.9	83.9- 96.2	-0.71°
1961 10 30	0031	0125	2	weak	16-36	108.6-141.3	91.9- 99.6	-0.66°
1961 10 30	0205	0208	1	weak	35-37	165.5-167.3	105.2-105.6	-0.66°
1961 10 30	0230	0232	1	weak	34-35	180.6-181.8	108.7-109.0	-0.66°
1961 11 6	0135	0429	3	strong	12-38	119.6-224.8	84.5-109.0	-0.65°
1962 4 30	1033	1113	3	strong	16-36	111.1-135.3	93.9- 99.5	+0.86°
1962 5 7	1147	1322	3	strong	19-35	129.0-186.4	87.7-101.1	+0.93°
1962 6 8	0802	1001	2	moderate	13-36	128.8-200.7	84.2-101.0	+1.21°
1962 7 15	1230	1329	2	moderate	14-37	102.6-138.3	91.0- 99.4	+1.41°
1962 8 16	0855	0925	1	strong	11-37	113.9-132.1	95.3- 99.5	+1.44°
1962 9 17	0423	0534	3	weak	12-39	90.7-133.6	92.6-102.7	+1.33°
1962 9 26	0506	0742	1	moderate	13-38	91.1-185.4	84.0-106.0	+1.30°
1962 10 1	0632	0833	1	strong	10-36	117.2-190.3	81.1- 98.2	+1.26°
1962 10 26	0123	0350	3	moderate	10-39	93.7-182.5	85.8-106.5	+1.14°
1962 11 2	0230	0500	2	moderate	12-38	119.6-198.2	82.4-100.7	+1.13°
1962 12 3	2334	2432	2	strong	16-36	133.8-168.7	83.9- 92.1	+1.10°
1963 2 4	0005	0041	3	weak	22-37	104.8-132.4	91.6- 98.1	+1.39°
1963 2 11	0113	0155	1	moderate	22-36	123.6-149.0	85.4- 91.3	+1.44°
1963 3 7	2002	2245	3	smooth	22-38	92.9-191.4	82.9-105.9	+1.61°
1963 4 1	1603	1651	2	moderate	19-38	105.8-134.8	90.5- 97.3	+1.87°
1963 4 8	1730	1855	3	smooth	20-36	130.5-181.9	85.6- 97.6	+1.93°

Table III-3. continued

2. Io-B source

Date	Emission		Intensity	Burstness	Frequency Range	Longitude (1965.0)	Io Phase (from S.G.C.)	Declination of Earth
yr.mon.day	Start hr.min.	End hr.min.			(MHz)	(deg.)	(deg.)	(deg.)
1963 5 3	1238	1440	1	smooth	23-39	112.4-186.2	78.1- 96.7	+2.17°
1963 6 4	0946	1121	2	strong	11-36	141.1-198.5	86.9-100.3	+2.45°
1963 8 5	0827	1016	2	moderate	11-38	64.8-130.7	86.4-101.8	+2.89°
1963 8 12	0957	1305	2	strong	15-36	93.3-207.0	83.5-110.1	+2.92°
1963 8 19	1115	1320	2	strong	15-35	114.8-190.3	79.3- 97.0	+2.95°
1963 9 6	0519	0607	2	weak	14-37	91.3-120.4	93.0- 99.8	+2.99°
1963 9 13	0536	0738	2	weak	10-37	76.2-150.0	80.6- 97.8	+3.00°
1963 9 20	0709	0904	3	strong	11-37	107.2-176.8	78.9- 95.2	+2.99°
1963 10 15	0130	0325	3	moderate	14-39	69.2-138.7	81.4- 97.7	+2.90°
1963 10 15	0418	0453	1	weak	15-35	170.8-191.9	103.2-110.1	+2.90°
1963 10 22	0256	0539	3	weak	14-38	93.7-194.2	78.9-101.9	+2.87°
1963 11 23	-0005	0145	2	moderate	20-37	124.9-191.4	87.5-103.0	+2.66°
1964 1 6	0401	0626	2	moderate	10-37	52.5-140.2	73.7- 94.2	+2.49°
1964 2 7	0216	0401	2	moderate	9-36	119.2-182.7	83.7-100.3	+2.50°
1964 4 28	1329	1433	1	weak	16-37	98.6-137.3	83.2- 94.3	+2.80°
1964 5 5	1531	1610	1	smooth	19-35	144.5-168.1	85.3- 90.8	+2.83°
1964 5 10	2343	2413	2	smooth	22-35	113.5-131.4	91.0- 95.3	+2.86°
1964 5 30	1118	1221	2	weak	14-35	149.7-187.8	91.0- 99.9	+2.94°
1964 6 7	1122	1342	1	moderate	18-39	90.6-175.2	80.4-100.1	+3.19°
1964 9 1	0713	0805	2	moderate	12-35	103.3-134.7	90.7- 98.1	+3.26°
1964 9 8	0807	1021	3	moderate	10-36	110.0-191.0	82.5-101.5	+3.29°
1964 10 3	0253	0404	2	strong	12-36	85.7-128.6	86.2- 96.3	+3.34°
1964 10 10	0416	0641	3	moderate	13-36	110.4-198.0	82.9-103.4	+3.35°
1964 11 23	0956	1034	2	moderate	12-36	106.8-128.6	90.1- 95.2	+3.27°
1964 11 30	1110	1146	1	moderate	12-36	124.8-146.6	85.5- 90.6	+3.21°
1965 1 1	0614	0903	2	weak	12-38	84.0-186.2	77.5-101.3	+3.06°

Table III-3. continued

2. Io-B source

Date	Emission		Intensity	Burstness	Frequency Range	Longitude (1965.0)	Io Phase (from S.G.C.)	Declination of Earth
yr.mon.day	Start hr.min	End hr.min			(MHz)	(deg.)	(deg.)	(deg.)
1965 1 26	0235	0333	2	weak	12-35	113.0-148.1	93.1-101.3	+2.95°
1965 2 2	0330	0529	1	weak	13-35	119.0-190.9	84.7-101.5	+2.93°
1965 2 26	2304	2400	2	strong	20-38	117.0-150.7	91.2- 99.1	+2.86°
1965 3 6	-0038	0145	2	strong	18-35	100.1-186.3	77.1- 97.3	+2.84°
1965 3 30	1858	2136	3	strong	21-36	97.8-193.3	82.3-104.6	+2.81°
1965 4 24	1500	1609	3	weak	20-38	110.8-151.9	90.6-100.2	+2.77°
1965 5 1	1643	1732	2	smooth	20-35	145.1-174.7	88.0- 94.9	+2.76°
1965 5 7	0054	0137	3	smooth	20-36	112.9-138.9	93.6- 99.7	+2.76°
1965 5 26	1224	1321	1	smooth	28-35	145.6-180.0	93.0-101.1	+2.73°
1965 6 7	2103	2314	3	smooth	24-37	102.9-182.1	85.4-103.9	+2.72°
1965 7 9	1809	1921	2	moderate	23-36	128.2-171.8	85.4- 95.6	+2.65°
1965 8 3	1333	1500	2	strong	17-37	120.9-173.5	88.8-101.1	+2.58°
1965 8 21	0754	0817	2	moderate	27-36	103.6-117.5	100.8-104.1	+2.54°
1965 8 28	0813	0953	3	strong	11-40	88.1-148.6	87.0-101.1	+2.52°
1965 9 4	0925	1128	3	strong	12-35	105.0-179.3	80.6- 96.0	+2.51°
1965 9 9	1832	1903	3	strong	20-36	108.1-126.8	94.8- 99.1	+2.50°
1965 9 16	1851	2032	1	moderate	22-37	93.0-154.1	81.2- 95.5	+2.49°
1965 10 11	1503	1533	3	moderate	20-37	118.8-136.9	94.8- 99.1	+2.45°
1965 10 18	1543	1723	1	weak	23-37	117.1-177.5	84.9- 99.0	+2.44°
1965 11 7	0230	0513	2	strong	10-35	130.3-228.8	83.4-106.4	+2.44°
1965 11 12	1001	1149	3	weak	11-36	76.2-141.5	84.9-100.2	+2.44°
1965 11 19	1145	1347	3	moderate	8-36	113.8-187.6	84.7-101.9	+2.44°
1965 12 14	0637	0740	3	weak	11-35	94.6-132.7	91.4-100.3	+2.43°
1965 12 21	0724	1005	3	moderate	11-35	97.6-194.9	93.4-106.2	+2.43°

Table III-3. continued

2. Io-B source

Date	Emission		Intensity	Burstness	Frequency Range	Longitude (1965.0)	Io Phase (from S.G.C.)	Declination of Earth
yr mon day	Start hr min.	End hr min			(MHz)	(deg.)	(deg.)	(deg.)
1966 1 22	0341	0606	3	strong	12-36	102.7-190.4	86.8-107.3	+2.39°
1966 2 15	2303	2347	3	strong	19-37	97.5-124.1	95.2-101.4	+2.32°
1966 2 23	0010	0201	3	strong	20-37	111.0-178.1	88.8-104.6	+2.29°

Table III-4. Total Refractive Deflection Angle $\beta-\beta'$ as a Function of Angle β. β is the angle between a mid-ray of the emitted hollow-cone beam and the ionospheric normal, β' is the corresponding angle after refraction has taken place. Both are in degrees

β	$\beta-\beta'$
75.00	8.42
76.00	8.81
77.00	9.23
78.00	9.68
79.00	10.16
80.00	10.68
81.00	11.23
82.00	11.82
83.00	12.45
84.00	13.13
85.00	13.85
86.00	14.61
87.00	15.43
88.00	16.30
89.00	17.22
90.00	18.19

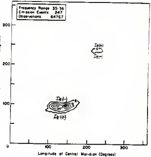

Figure III-1. Probability of DAM Activity for the Frequency Range 35-36 MHz in the Io Phase-CML Plane. Occurrence probability contours are labeled in percentages, signs of the declination of Earth (D_E) are also marked. The lower emission region is referred to as source Io-B; the smaller one at the upper right is source Io-A. SGC denotes Superior Geocentric Conjunction. This figure is after Wilson, Warwick, and Libby [1968].

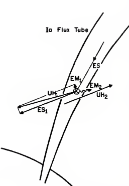

Figure III-2 A Schematic View of a Three-Wave interaction. An electrostatic wave ES first excites the upper-hybrid wave UH_1, then it can decay into an electrostatic wave ES_1 and an electromagnetic wave EM_1 which cannot propagate. The electrostatic wave ES_1 combines with another upper-hybrid wave UH_2 which was generated nearby, producing electromagnetic wave EM_2.

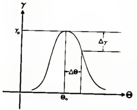

Figure III-3. The Growth Rate γ as a Function of Θ (angle between the wave vector $\vec{K}$ of the upper-hybrid wave and the magnetic field $\vec{B}$)

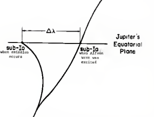

Figure III-4. Suggested Trajectory of an Io-Excited Alfven Wave That Propagates along a Given Magnetic Flux Tube First Southward, then after Reflection Travels to the Northern Hemisphere Where the DAM Radiation Is Emitted.

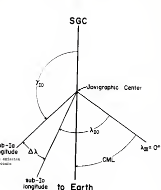

Figure III-5. Relationship between CML, $\Delta\lambda$, γ_{Io}, and λ_{Io}. SGC denotes superior geocentric conjunction with respect to Earth.

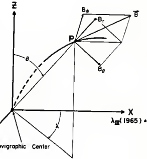

Figure III-6. The Components of the Magnetic Field in the Spherical Coordinate System.

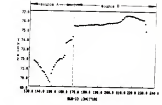

Figure III-7. Curve of the Conical Angle θ_2 vs. the Sub-Io Longitude λ_{Io}. The values of λ_{Io} from 134° to 167° correspond to source A, and the values from 167° to 232° to source B

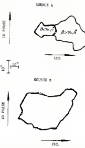

Figure III-8 Comparison of the Computational Result as Predicted by the Emission Model with the Observational Data. The solid line denotes the modeling, not accounting for refraction, the dot-dashed line the observed activity, and the dashed line within source A the boundary of the region computed from the model after suggested refraction correction. β is the conical angle with respect to the radial vector from the center of the planet. The scales for CML and Io phase are not the same in this figure. Their scale lengths are in the ratio 1:1.64.

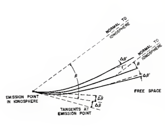

Figure III-9. Refraction of Conical Beam Propagating out of Jupiter's Ionospheric Region. β and β' are the conical angles with respect to the radial vector before and after refraction, respectively, $\Delta\beta$ and $\Delta\beta'$ are their angular wall thicknesses

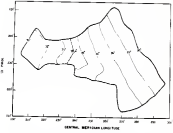

Figure III-10. Modeled Source A Region from Figure III-8, Uncorrected for Refraction, with Labeled Contours Indicating the Directions of the Emitted Rays with Respect to the Ionospheric Normal, β. The part to the right of the dashed line, which is in disagreement with the observed contour, is shown largely to disappear when ionospheric refraction is taken into account.

APPENDIX A

RADIAL VECTOR, MAGNETIC FIELD, AND MAGNETIC SCALAR POTENTIAL FOR SINGLE DIPOLE

1. Radial Vector $\vec{r}_s$

For a spherical coordinate system of Jupiter, we choose the origin to be at the center of Jupiter, Z axis to be the planetary spin axis, X axis in the direction toward which single dipole $\vec{M}$ is tilted, and Y axis such that a right-hand Jovicentric coordinate system is formed.

In Figure A-1, we introduce the following notation

M	magnitude of the magnetic moment vector $\vec{M}$ of single dipole,
r	Jovicentric distance to the given point P in Jupiter radii;
r_s	distance from center O' of dipole to the point P in Jupiter radii,
θ_s	colatitude of the point P, i.e., the angle from the planetary spin axis,
ϕ_s	longitude of the point P as measured eastward from X axis,
r_o	offset distance of dipole in Jupiter radii,
θ_o	tilt of $\vec{M}$ from the planetary spin axis,
λ_o	System III longitude toward which $\vec{M}$ is tilted,
δ	latitude of offset,
μ	System III longitude of offset,
ϕ_o	longitude of offset as measured eastward from X axis, $\phi_o = \lambda_o - \mu$.

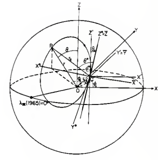

Figure A-1. Transformation among Single Offset Tilted Dipole Coordinate Systems and Joviocentric Coordinate System

Let Z* axis be in the direction of the magnetic moment vector $\vec{M}$, X* axis be on the plane spanned by $\vec{r}_s$ and Z* axis, $\bar{Z}$ axis be identical with Z* axis, the plane spanned by $\bar{X}$ and $\bar{Z}$ axes be parallel to meridian $\lambda_{III} = \lambda_0$, Z' and X' axes passing through the point O' be parallel to Z and X axes, respectively, Y' axis be identical with $\bar{Y}$ axis. All X*Y*Z*, $\overline{XYZ}$, and X'Y'Z' systems are the right-hand axes.

Thus, ϕ^* is the longitude of $\vec{r}_s$ as measured eastward from $\bar{X}$ axis and θ^* is the colatitude of point P from Z* axis.

The transformation of coordinates of point P from X*Y*Z* to XYZ is

$$r\begin{pmatrix} \sin\theta_s\cos\phi_s \\ \sin\theta_s\sin\phi_s \\ \cos\theta_s \end{pmatrix} = R_2(-\theta_0)R_3(-\phi^*)\begin{pmatrix} r_s\sin\theta^* \\ 0 \\ r_s\cos\theta^* \end{pmatrix} + \begin{pmatrix} r_0\cos\theta\cos\phi_0 \\ r_0\cos\theta\sin\phi_0 \\ r_0\sin\theta \end{pmatrix}$$

$$= \begin{pmatrix} \cos\theta_0(r_s\sin\theta^*\cos\phi^*) + \sin\theta_0(r_s\cos\theta^*) + r_0\cos\theta\cos\phi_0 \\ r_s\sin\theta^*\sin\phi^* \qquad\qquad + r_0\cos\theta\sin\phi_0 \\ -\sin\theta_0(r_s\sin\theta^*\cos\phi^*) + \cos\theta_0(r_s\cos\theta^*) + r_0\sin\theta \end{pmatrix} \begin{matrix} \text{(A-1a)} \\ \text{(A-1b)} \\ \text{(A-1c)} \end{matrix}$$

where R_2 and R_3 are orthogonal rotation matrices, i.e.,

$$R_2(-\theta_0) = \begin{pmatrix} \cos\theta_0 & 0 & \sin\theta_0 \\ 0 & 1 & 0 \\ -\sin\theta_0 & 0 & \cos\theta_0 \end{pmatrix}, \quad R_3(-\phi^*) = \begin{pmatrix} \cos\phi^* & -\sin\phi^* & 0 \\ \sin\phi^* & \cos\phi^* & 0 \\ 0 & 0 & 1 \end{pmatrix}$$

Then we assume

$$A = \sin\theta\sin\theta_0 - \cos\theta\cos\theta_0\cos\phi_0 \tag{A-2a}$$

$$B = \qquad \cos\theta \quad \sin\phi_0 \tag{A-2b}$$

$$C = \sin\theta\cos\theta_0 + \cos\theta\sin\theta_0\cos\phi_0 \tag{A-2c}$$

such that

$$A^2 + B^2 + C^2 = 1 \tag{A-3}$$

and assume

$$D = \cos\theta_s \sin\theta_o - \sin\theta_s \cos\theta_o \cos\phi_s \tag{A-4a}$$

$$E = \qquad \sin\theta_s \quad \sin\phi_s \tag{A-4b}$$

$$F = \cos\theta_s \cos\theta_o + \sin\theta_s \sin\theta_o \cos\phi_s \tag{A-4c}$$

such that

$$D^2 + E^2 + F^2 = 1 \tag{A-5}$$

Multiplying (A-1a) by $\sin\theta_s$ or $\cos\theta_s$ and (A-1c) by $\cos\theta_o$ or $(-\sin\theta_s)$, respectively, and adding them we obtain the following expressions

$$r \cdot F = r_s \cos\theta^* + r_o \cdot C \tag{A-6a}$$

$$-r\,D = r_s \sin\theta^* \cos\phi^* - r_o \cdot A \tag{A-6b}$$

From (A-1b) we have

$$r \cdot E = r_s \sin\theta^* \sin\phi^* + r_o \cdot B \tag{A-6c}$$

Therefore, the relations among r_s, θ^*, and ϕ^* can be established from (A-6a) to (A-6c), as follows

$$r_s \cos\theta^* = r \cdot F - r_o \cdot C \tag{A-7a}$$

$$r_s \sin\theta^* \cos\phi^* = -r \cdot D + r_o \cdot A \tag{A-7b}$$

$$r_s \sin\theta^* \sin\phi^* = r \cdot E - r_o \cdot B \tag{A-7c}$$

With the help of (A-3), (A-5), and (A-7a)-(A-7c), it is easy to prove that

$$r_s^2 = r^2[1 - 2(\frac{r_o}{r})(A\cdot D+B\cdot E+C\cdot F) + (\frac{r_o}{r})^2] \tag{A-8a}$$

$$\sin^2\theta^* = \frac{(D^2+E^2) - 2(\frac{r_o}{r})(A\cdot D+B\cdot E) + (\frac{r_o}{r})^2(A^2+B^2)}{1 - 2(\frac{r_o}{r})(A\cdot D+B\cdot E+C\cdot F) + (\frac{r_o}{r})^2} \tag{A-8b}$$

$$\cos^2\theta^* = \frac{[F - (\frac{r_o}{r})\ C]^2}{1 - 2(\frac{r_o}{r})(A\cdot D+B\cdot E+C\cdot F) + (\frac{r_o}{r})^2} \tag{A-8c}$$

2. Magnetic Field $\vec{B}$

Magnetic field $\vec{B}$ is the curl of vector potential $\vec{A}$

$$\vec{B} = \nabla \times \vec{A} \tag{A-9}$$

Vector potential $\vec{A}$ can be expressed as

$$\vec{A} = \nabla\frac{1}{r_s} \times \vec{M} \tag{A-10}$$

Thus (A-9) leads us to

$$\vec{B} = \nabla \times (\nabla\frac{1}{r_s} \times \vec{M}) = (\vec{M}\cdot\nabla)\nabla\frac{1}{r_s} - (\nabla\cdot\nabla\frac{1}{r_s})\vec{M} - \nabla\frac{1}{r_s}\cdot\nabla\vec{M} + (\nabla\cdot\vec{M})\nabla\frac{1}{r_s} \tag{A-11}$$

But, $\nabla\cdot\nabla\frac{1}{r_s} = -4\pi\rho = 0$ if $r_s > r_o$, where ρ denotes the source density, since $\vec{M}$ is a constant vector, $\nabla\vec{M}$ (tensor) and $\nabla\cdot\vec{M}$ are all zeros. On the other hand, $\nabla\frac{1}{r_s} = -\frac{\vec{r}_s}{r_s^3}$. Thus (A-11) becomes

$$\vec{B} = -(\vec{M}\cdot\nabla)\frac{\vec{r}_e}{r_e^3} = -\vec{M}\cdot\nabla\frac{\vec{r}_e}{r_e^3} \qquad \text{(A-12)}$$

The tensor $\nabla\frac{\vec{r}_e}{r_e^3}$ can be decomposed into

$$\nabla\frac{\vec{r}_e}{r_e^3} = (\nabla\frac{1}{r_e^3})\vec{r}_e + \frac{1}{r_e^3}\nabla\vec{r}_e \qquad \text{(A-13)}$$

Since

$$\nabla\frac{1}{r_e^3} = \frac{-3}{r_e^4}(\frac{\vec{r}_e}{r_e})$$

and $\nabla\vec{r}_e = \overleftrightarrow{I}$ (unit tensor), (A-13) becomes

$$\nabla\frac{\vec{r}_e}{r_e^3} = -\frac{3}{r_e^5}(\vec{r}_e\vec{r}_e) + \frac{1}{r_e^3}\overleftrightarrow{I} \qquad \text{(A-14)}$$

What follow are the tensor identities

$$\vec{A}\cdot(\vec{B}\vec{C}) = (\vec{A}\cdot\vec{B})\vec{C} \qquad \text{(A-15a)}$$

$$\vec{M}\cdot\overleftrightarrow{I} = \overleftrightarrow{I}\cdot\vec{M} = \vec{M} \qquad \text{(A-15b)}$$

with the help of (A-14), (A-15a), and (A-15b), (A-12) can be written as

$$\vec{B} = \frac{3}{r_e^5}(\vec{M}\cdot\vec{r}_e)\vec{r}_e - \frac{1}{r_e^3}\vec{M} = \frac{3\hat{r}_e(\hat{r}_e\cdot\vec{M}) - \vec{M}}{r_e^3} \qquad \text{(A-16)}$$

where $\hat{r}_e$ is unit vector on $\vec{r}_e$.

3. Magnetic Scalar Potential V

Since $\nabla\cdot\vec{M}$ and $\nabla\times\vec{M}$ are zero terms, and

$$\nabla \times \frac{\vec{r}_s}{r_s^3} = 0$$

we can add three terms

$$-\frac{\vec{r}_s}{r_s^3}\,\nabla\cdot\vec{M}, \quad -\vec{M} \times \left(\nabla \times \frac{\vec{r}_s}{r_s^3}\right), \quad \text{and} \quad -\frac{\vec{r}_s}{r_s^3} \times (\nabla\times\vec{M})$$

to (A-12). As a result, we have

$$\vec{B} = -(\vec{M}\cdot\nabla)\frac{\vec{r}_s}{r_s^3} - \left(\frac{\vec{r}_s}{r_s^3}\cdot\nabla\right)\vec{M} - \vec{M} \times \left(\nabla \times \frac{\vec{r}_s}{r_s^3}\right) - \frac{\vec{r}_s}{r_s^3} \times (\nabla\times\vec{M}) \qquad \text{(A-17)}$$

Invoking the vector identity

$$\nabla(\vec{A}\cdot\vec{B}) = (\vec{A}\cdot\nabla)\vec{B} + (\vec{B}\cdot\nabla)\vec{A} + \vec{A} \times (\nabla\times\vec{B}) + \vec{B} \times (\nabla\times\vec{A}) \qquad \text{(A-18)}$$

we obtain

$$\vec{B} = -\nabla\left(\vec{M}\cdot\frac{\vec{r}_s}{r_s^3}\right) \qquad \text{(A-19)}$$

Comparing (A-19) with $\vec{B} = -\nabla V$, we can get

$$V = \frac{\vec{M}\cdot\vec{r}_s}{r_s^3} = \frac{\vec{M}\cdot r_s}{r_s^2} = \frac{M\cos\theta^*}{r_s^2} \qquad \text{(A-20)}$$

To substitute (A-8a) and (A-8c) into (A-20), we have

$$V = \frac{M}{r^2} \frac{(F - \frac{r_o}{r} \cdot C)}{[1 - 2(\frac{r_o}{r})(A \cdot D + B \cdot E + C \cdot F) + (\frac{r_o}{r})^2]^{3/2}} \tag{A-21}$$

Next we proceed to simplify the term $(A \cdot D+B \cdot E+C \cdot F)$ From the expressions of (A-2a)-(A-4c), it is clear that

$$\begin{aligned} x &= A \cdot D+B \cdot E+C \cdot F \\ &= (\sin\delta\sin\theta_o - \cos\delta\cos\theta_o\cos\phi_o)(\cos\theta_s\sin\theta_o - \sin\theta_s\cos\theta_o\cos\phi_s) \\ &\quad + \cos\delta\sin\phi_o\sin\theta_s\sin\phi_s \\ &\quad + (\sin\delta\cos\theta_o + \cos\delta\sin\theta_o\cos\phi_o)(\cos\theta_s\cos\theta_o + \sin\theta_s\sin\theta_o\cos\phi_s) \\ &= \sin\delta\cos\theta_s + \cos\delta\sin\theta_s\cos(\phi_s-\phi_o) \end{aligned} \tag{A-22}$$

The differential form of Coulomb expansion gives

$$\frac{(\frac{r_o}{r})}{[1 - 2(\frac{r_o}{r})x + (\frac{r_o}{r})^2]^{3/2}} = \sum_{n=0}^{\infty} (\frac{r_o}{r})^n P'_n(x) \tag{A-23}$$

With the substitution of (A-23), (A-21) becomes

$$\begin{aligned} V &= \frac{M}{r^2}(\frac{r}{r_o})(F - \frac{r_o}{r} \cdot C) \sum_{n=0}^{\infty} (\frac{r_o}{r})^n P'_n(x) \\ &= \frac{M}{r^2} (F - \frac{r_o}{r} \cdot C) \sum_{n=0}^{\infty} (\frac{r_o}{r})^{n-1} P'_n(x) \end{aligned} \tag{A-24}$$

Since $P'_o(x) = 0$, we can begin the sum from $n = 1$, thus (A-24) is

$$V = \frac{M}{r^2} (F - \frac{r_o}{r} \cdot C) \sum_{n=1}^{\infty} (\frac{r_o}{r})^{n-1} P'_n(x) \tag{A-25}$$

APPENDIX B

24 EQUATIONS OBTAINED BY EQUATING MAGNETIC SCALAR POTENTIALS

1 Expression of Magnetic Potential for Single Dipole with Legendre Polynomials

Truncating the higher order terms after $n = 4$ in (A-25), we have

$$V = \frac{M}{r^2}\left(P - \frac{r_o}{r}\ C\right) \sum_{n=1}^{4} \left(\frac{r_o}{r}\right)^{n-1} P_n'(x) \qquad \text{(B-1)}$$

where

$$P = \cos\theta_s \cos\theta_o + \sin\theta_s \sin\theta_o \cos\theta_s \qquad \text{(B-1a)}$$

$$C = \sin\delta \cos\theta_o + \cos\delta \sin\theta_o \cos\phi_o \qquad \text{(B-1b)}$$

$$x = \sin\delta \cos\theta_o + \cos\delta \sin\theta_s \cos(\phi_s - \phi_o) \qquad \text{(B-1c)}$$

the notations of θ_s, ϕ_s, r, θ_o, ϕ_o, r_o, δ, and M are the same as those in Appendix A. The differential relation of Legendre polynomials is

$$P_n'(x) - P_{n-2}'(x) = (2n-1)P_{n-1}(x) \qquad \text{(B-2)}$$

and

$$P_1'(x) = 1, \quad P_{-n}'(x) = 0 \text{ for } n = 0, \text{ and } n = 1$$

Equation (B-2) can be rewritten as

$$P_n'(x) = (2n-1)P_{n-1}(x) + P_{n-2}'(x) \qquad \text{(B-3)}$$

Substituting (B-3) into (B-1), we obtain

$$V = \frac{M}{r^2}(P - \frac{r_o}{r} \cdot C)\left\{\sum_{n=1}^{4} (\frac{r_o}{r})^{n-1}[(2n-1)P_{n-1}(x) + P'_{n-2}(x)]\right\} \qquad (B-4)$$

On the other hand, the addition theorem for Legendre polynomials gives

$$P_n(\cos\gamma) = \sum_{m=0}^{n} \frac{2}{\delta m}\frac{(n-m)!}{(n+m)!}(\cos m\phi_o \cos m\phi_s + \sin m\phi_o \sin m\phi_s)P_n^m(\sin\theta\ )P_n^m(\cos\theta_s) \qquad (B-5)$$

where

$$\delta m = \begin{cases} 2 & m = 0 \\ 1 & m \neq 0 \end{cases}$$

$$\cos\gamma = \sin\theta \cos\theta_s + \cos\theta \sin\theta_s \cos(\phi_o - \phi_s)$$

With the substitution of (B-5) and (B-1c), the Legendre polynomial $P_{n-1}(x)$ is

$$P_{n-1}(x) = \sum_{m=0}^{n-1} \frac{2}{\delta m}\frac{(n-m-1)!}{(n+m-1)!}(\cos m\phi_o \cos m\phi_s + \sin m\phi_o \sin m\phi_s)$$

$$P_{n-1}^m(\sin\theta)P_{n-1}^m(\cos\theta_s) \qquad (B-6)$$

The term P in (B-1a) can be converted into

$$P = \cos\theta_s \cos\theta_o + \sin\theta_s \sin\theta_o \cos\phi_s = P_1^0(\cos\theta_s)\cos\theta_o + P_1^1(\cos\theta_s)\sin\theta_o \cos\phi_s \qquad (B-7)$$

From now on, we omit the argument $\cos\theta_s$ in Legendre polynomials for the sake of convenience.

For a given n (in our case, $n \leq 4$), we define

$$G_n = (2n-1)P_{n-1}(x) + P'_{n-2}(x) \qquad (B-8)$$

Then, we can expand G_n in the light of (B-6)

$$G_n = (2n-1)\sum_{m=0}^{n-1} \frac{2}{\delta m} \frac{(n-m-1)!}{(n+m-1)!} (\cos m\phi_o \cos m\phi_s + \sin m\phi_o \sin m\phi_s) P_{n-1}^m (\sin\delta) P_{n-1}^m$$

$$+ P'_{n-2}(x)$$

$$= (2n-1)[P_{n-1}^0(\sin\delta)P_{n-1}^0$$

$$+ \frac{2(n-2)!}{n!}(\cos\phi_o\cos\phi_s + \sin\phi_o\sin\phi_s)P_{n-1}^1(\sin\delta)P_{n-1}^1$$

$$+ \frac{2(n-3)!}{(n+1)!}(\cos 2\phi_o \cos 2\phi_s + \sin 2\phi_o \sin 2\phi_s)P_{n-1}^2(\sin\delta)P_{n-1}^2$$

$$+ \frac{2(n-4)!}{(n+2)!}(\cos 3\phi_o \cos 3\phi_s + \sin 3\phi_o \sin 3\phi_s)P_{n-1}^3(\sin\delta)P_{n-1}^3]$$

$$+ P'_{n-2}(x) \tag{B-9}$$

From recurrence relations we have

$$(n-m+1)P_{n+1}^m - (2n+1)P_1^0 \cdot P_n^m + (n+m)P_{n-1}^m = 0 \tag{B-10a}$$

$$P_{n+1}^{m+1} - P_{n-1}^{m+1} = (2n+1)P_1^1 \cdot P_n^m \tag{B-10b}$$

Thus

$$(2n+1)(P_1^0 \cdot P_n^m) = (n-m+1)P_{n+1}^m + (n+m)P_{n-1}^m \tag{B-11a}$$

$$(2n+1)(P_1^1 \cdot P_n^m) = P_{n+1}^{m+1} - P_{n-1}^{m+1} \tag{B-11b}$$

Back to (B-4), the partial coefficient of term $\frac{M}{r^2}\left(\frac{r_o}{r}\right)^{n-1}$ is

$$(2n-1)P\cdot P_{n-1}(x) = (2n-1)(P_1^0\cos\theta_o + P_1^1\sin\theta_o\cos\phi_s)$$

$$[P^0_{n-1}(\sin\delta)P^0_{n-1} + \frac{2(n-2)!}{n!}(\cos\phi_o\cos\phi_s+\sin\phi_o\sin\phi_s)P^1_{n-1}(\sin\delta)P^1_{n-1}$$

$$+\frac{2(n-3)!}{(n+1)!}(\cos2\phi_o\cos2\phi_s+\sin2\phi_o\sin2\phi_s)P^2_{n-1}(\sin\delta)P^2_{n-1}$$

$$+\frac{2(n-4)!}{(n+2)!}(\cos3\phi_o\cos3\phi_s+\sin3\phi_o\sin3\phi_s)P^3_{n-1}(\sin\delta)P^3_{n-1}] \quad \text{(B-12)}$$

Next, we catalog the terms in (B-12) by the Tesseral Harmonics of nth degree and mth order We observe that all the labeled terms in the following (B-13)-(B-41) can be either canceled out or converted into the first terms in (B-13)-(B-17)

(1) P^0_n (for m = 0)

$$(2n-1)(P^0_1 P^0_{n-1})P^0_{n-1}(\sin\delta)\cos\theta_o = [nP^0_n + (n-1)P^0_{n-2}]P^0_{n-1}(\sin\delta)\cos\theta_o$$

$$= [nP^0_{n-1}(\sin\delta)\cos\theta_o]P^0_n + \overset{①}{[(n-1)P^0_{n-1}(\sin\delta)\cos\theta_o]}P^0_{n-2} \quad \text{(B-13)}$$

(2) $P^1_n\cos\phi_s$ (for m = 1)

$$(2n-1)[(P^1_1\cdot P^0_{n-1})P^0_{n-1}(\sin\delta)\sin\theta_o\cos\phi_s$$

$$+\frac{2(n-2)!}{n!}(P^0_1\cdot P^1_{n-1})P^1_{n-1}(\sin\delta)\cos\theta_o\cos\phi_o\cos\phi_s]$$

$$= (P^1_n - P^1_{n-2})P^0_{n-1}(\sin\delta)\sin\theta_o\cos\phi_s$$

$$+\frac{2(n-2)!}{n!}[(n-1)P^1_n + nP^1_{n-2}]P^1_{n-1}(\sin\delta)\cos\theta_o\cos\phi_o\cos\phi_s$$

$$= [P^0_{n-1}(\sin\delta)\sin\theta_o + \frac{2}{n}P^1_{n-1}(\sin\delta)\cos\theta_o\cos\phi_o]P^1_n\cos\phi_s$$

$$+\overset{②}{[-P^0_{n-1}(\sin\delta)\sin\theta_o]}P^1_{n-2}\cos\phi_s$$

③

$$+ [\frac{2}{n-1} P^1_{n-1}(\sin\delta)\cos\delta_n\cos\phi_n]P^1_{n-2}\cos\phi_s \qquad (B-14)$$

(3) $P^1_n\sin\phi_s$ (for $n = 1$)

$$(2n-1)[\frac{2(n-2)!}{n!}(P^0_1 \cdot P^1_{n-1})P^1_{n-1}(\sin\delta)\cos\delta_n\sin\phi_n\sin\phi_s$$

$$= \frac{2(n-2)!}{n!}[(n-1)P^1_n + nP^1_{n-2}]P^1_{n-1}(\sin\delta)\cos\delta_n\sin\phi_n\sin\phi_s$$

$$= [\frac{2}{n}P^1_{n-1}(\sin\delta)\cos\delta_n\sin\phi_n]P^1_n\sin\phi_s$$

④

$$+ [\frac{2}{n-1}P^1_{n-1}(\sin\delta)\cos\delta_n\sin\phi_n]P^1_{n-2}\sin\phi_s \qquad (B-15)$$

(4) $P^2_n\cos 2\phi_s$ (for $n = 2$)

$$(2n-1)[\frac{2(n-2)!}{n!}(P^1_1 \cdot P^1_{n-1})P^1_{n-1}(\sin\delta)\sin\delta_n\cos\phi_n\cos^2\phi_s$$

$$+ \frac{2(n-3)!}{(n+1)!}(P^0_1 \cdot P^2_{n-1})P^2_{n-1}(\sin\delta)\cos\delta_n\cos 2\phi_n\cos 2\phi_s]$$

$$= \frac{2(n-2)!}{n!}(P^2_n - P^2_{n-2})P^1_{n-1}(\sin\delta)\sin\delta_n\cos\phi_n\frac{(1+\cos 2\phi_s)}{2}$$

$$+ \frac{2(n-3)!}{(n+1)!}[(n-2)P^2_n + (n+1)P^2_{n-2}]P^2_{n-1}(\sin\delta)\cos\delta_n\cos 2\phi_n\cos 2\phi_s$$

$$= [\frac{1}{n(n-1)}P^1_{n-1}(\sin\delta)\sin\delta_n\cos\phi_n$$

$$+ \frac{2}{(n+1)n(n-1)}P^2_{n-1}(\sin\delta)\cos\delta_n\cos 2\phi_n]P^2_n\cos 2\phi_s$$

⑤

$$+ [\frac{2}{n(n-1)(n-2)}P^2_{n-1}(\sin\delta)\cos\delta_n\cos 2\phi_n]P^2_{n-2}\cos 2\phi_s$$

⑥

$$+ [\frac{1}{n(n-1)}P^1_{n-1}(\sin\delta)\sin\delta_n\cos\phi_n]P^2_n$$

$$+ \overset{⑦}{\left[-\frac{1}{n(n-1)} P_{n-1}^{1}(\sin\delta)\sin\theta_o\cos\phi_o\right]} P_{n-2}^{2}\cos 2\phi_s$$

$$+ \overset{⑧}{\left[-\frac{1}{n(n-1)} P_{n-1}^{1}(\sin\delta)\sin\theta_o\cos\phi_o\right]} P_{n-2}^{2} \qquad \text{(B-16)}$$

(5) $P_n^2\sin 2\phi_s$ (for $m = 2$)

$$(2n-1)\left[\frac{2(n-2)!}{n!}(P_1^1 \cdot P_{n-1}^1)P_{n-1}^1(\sin\delta)\sin\theta_o\sin\phi_o\sin\phi_s\cos\phi_s\right.$$

$$\left.+ \frac{2(n-3)!}{(n+1)!}(P_1^0 \cdot P_{n-1}^2)P_{n-1}^2(\sin\delta)\cos\theta_o\sin 2\phi_o\sin 2\phi_s\right]$$

$$= \frac{2(n-2)!}{n!}(P_n^2 - P_{n-2}^2)P_{n-1}^1(\sin\delta)\sin\theta_o\sin\phi_o\frac{\sin 2\phi_s}{2}$$

$$+ \frac{2(n-3)!}{(n+1)!}[(n-2)P_n^2 + (n+1)P_{n-2}^2]P_{n-1}^2(\sin\delta)\cos\theta_o\sin 2\phi_o\sin 2\phi_s$$

$$= \left[\frac{1}{n(n-1)} P_{n-1}^1(\sin\delta)\sin\theta_o\sin\phi_o\right.$$

$$\left.+ \frac{2}{(n+1)n(n-1)} P_{n-1}^2(\sin\delta)\cos\theta_o\sin 2\phi_o\right]P_n^2\sin 2\phi_s$$

$$+ \overset{⑨}{\left[\frac{2}{n(n-1)(n-2)} P_{n-1}^2(\sin\delta)\cos\theta_o\sin 2\phi_o\right]} P_{n-2}^2\sin 2\phi_s$$

$$+ \overset{⑩}{\left[-\frac{1}{n(n-1)} P_{n-1}^2(\sin\delta)\sin\theta_o\sin\phi_o\right]} P_{n-2}^2\sin 2\phi_s \qquad \text{(B-17)}$$

(6) $P_n^3\cos 3\phi_s$ (for $m = 3$)

$$(2n-1)\left[\frac{2(n-3)!}{(n+1)!}(P_1^1 \cdot P_{n-1}^2)P_{n-1}^2(\sin\delta)\sin\theta_o\cos 2\phi_o\cos\phi_s\cos 2\phi_s\right.$$

$$\left.+ \frac{2(n-4)!}{(n+2)!}(P_1^0 \cdot P_{n-1}^3)P_{n-1}^3(\sin\delta)\cos\theta_o\cos 3\phi_o\cos 3\phi_s\right]$$

$$= \frac{2(n-3)!}{(n+1)!}(P_n^3 - P_{n-2}^3)P_{n-1}^2(\sin\delta)\sin\theta_o\cos 2\phi_o\frac{(\cos 3\phi_s + \cos\phi_s)}{2}$$

$$+ \frac{2(n-4)!}{(n+2)!} [(n-3)P_n^3 + (n+2)P_{n-2}^3]P_{n-1}^3(\sin\theta)\cos\theta_o \cos3\phi_o \cos3\phi_s$$

$$= [\frac{1}{(n+1)n(n-1)(n-2)} P_{n-1}^2(\sin\theta)\sin\theta_o \cos2\phi_o$$

$$+ \frac{2}{(n+2)(n+1)n(n-1)(n-2)} P_{n-1}^3(\sin\theta)\cos\theta_o \cos3\phi_s]P_n^3 \cos3\phi_o$$

⑪

$$+ [\frac{1}{(n+1)n(n-1)(n-2)} P_{n-1}^2(\sin\theta)\sin\theta_o \cos2\phi_o]P_n^3 \cos\phi_s$$

where $P_{n-2}^3 = 0$ for $n \leq 4$ (B-18)

(7) $P_n^3 \sin3\phi_o$ (for $m = 3$)

$$(2n-1)[\frac{2(n-3)!}{(n+1)!} (P_1^1 \cdot P_{n-1}^2)P_{n-1}^2(\sin\theta)\sin\theta_o \sin2\phi_s \cos\phi_o \sin2\phi_s$$

$$+ \frac{2(n-4)!}{(n+2)!} (P_1^0 \cdot P_{n-1}^3)P_{n-1}^3(\sin\theta)\cos\theta_o \sin3\phi_o \sin3\phi_s]$$

$$= \frac{2(n-3)!}{(n+1)!} (P_n^3 - P_{n-2}^3)P_{n-1}^2(\sin\theta)\sin\theta_o \sin2\phi_s \frac{(\sin3\phi_o + \sin\phi_s)}{2}$$

$$+ \frac{2(n-4)!}{(n+2)!} [(n-3)P_n^3 + (n+2)P_{n-2}^3]P_{n-1}^3(\sin\theta)\cos\theta_o \sin3\phi_s \sin3\phi_s$$

$$= [\frac{1}{(n+1)n(n-1)(n-2)} P_{n-1}^2(\sin\theta)\sin\theta_o \sin2\phi_n$$

$$+ \frac{2}{(n+2)(n+1)n(n-1)(n-2)} P_{n-1}^3(\sin\theta)\cos\theta_s \sin3\phi_o]P_n^3 \sin3\phi_o$$

⑫

$$+ [\frac{1}{(n+1)n(n-1)(n-2)} P_{n-1}^2(\sin\theta)\sin\theta_s \sin2\phi_o]P_n^3 \sin\phi_o$$

where $P_{n-2}^3 = 0$ for $n \leq 4$ (B-19)

(8) $P_n^4\cos4\phi_s$ (for $n = 4$)

$$(2n-1)[\frac{2(n-4)!}{(n+2)!}(P_1^1\cdot P_{n-1}^3)P_{n-1}^3(\sin\delta)\sin\theta_o\cos3\phi_o\cos\phi_s\cos3\phi_s]$$

$$= \frac{2(n-4)!}{(n+2)!}(P_n^4 - P_{n-2}^4)P_{n-1}^3(\sin\delta)\sin\theta_o\cos3\phi_o\frac{(\cos4\phi_s+\cos2\phi_s)}{2}$$

$$= [\frac{1}{(n+2)(n+1)n(n-1)(n-2)(n-3)}P_{n-1}^3(\sin\delta)\sin\theta_o\cos3\phi_o]P_n^4\cos4\phi_s$$

⑬

$$+ [\frac{1}{(n+2)(n+1)n(n-1)(n-2)(n-3)}P_{n-1}^3(\sin\delta)\sin\theta_o\cos3\phi_o]P_n^4\cos2\phi_s$$

where $P_{n-2}^4 \equiv 0$ for $n \leq 4$ (B-20)

(9) $P_n^4\sin4\phi_s$ (for $n = 4$)

$$(2n-1)[\frac{2(n-4)!}{(n+2)!}(P_1^1\cdot P_{n-1}^3)P_{n-1}^3(\sin\delta)\sin\phi_o\sin3\phi_o\cos\phi_s\sin3\phi_s]$$

$$= \frac{2(n-4)!}{(n+2)!}(P_n^4 - P_{n-2}^4)P_{n-1}^3(\sin\delta)\sin\theta_o\sin3\phi_o\frac{(\sin4\phi_s+\sin2\phi_s)}{2}$$

$$= [\frac{1}{(n+2)(n+1)n(n-1)(n-2)(n-3)}P_{n-1}^3(\sin\delta)\sin\theta_o\sin3\phi_o]P_n^4\sin4\phi_s$$

⑭

$$+ [\frac{1}{(n+2)(n+1)n(n-1)(n-2)(n-3)}P_{n-1}^3(\sin\delta)\sin\theta_o\sin3\phi_o]P_n^4\sin2\phi_s$$

where $P_{n-2}^4 \equiv 0$ for $n \leq 4$ (B-21)

Then, the remainder of magnetic scalar potential V for $\frac{M}{r^2}(\frac{r_o}{r})^{n-1}$ in (B-4) is

$$P\cdot P'_{n-2}(x) - C[(2n-3)P_{n-2}(x) + P'_{n-3}(x)] = P\cdot P'_{n-2}(x) - C\cdot P'_{n-1}(x) \quad \text{(B-22)}$$

From recurrence relations, there are

$$P'_{n-2}(x) = (2n-5)P_{n-3}(x) + P'_{n-4}(x) = (2n-5)P_{n-3}(x) \text{ for } n \leq 4 \quad \text{(B-23a)}$$

$$P'_{n-1}(x) = (2n-3)P_{n-2}(x) + P'_{n-3}(x) = (2n-3)P_{n-2}(x)$$

$$+ (2n-7)P_{n-4}(x) + P'_{n-5}(x)$$

$$= (2n-3)P_{n-2}(x) + (2n-7)P_{n-4}(x) \qquad \text{for } n \leq 4 \qquad \text{(B-23b)}$$

With the substitution of (B-23a), the first term in (B-22) becomes

$$F \cdot P'_{n-2}(x) = (P_1^0\cos\theta_m + P_1^1\sin\theta_o\cos\phi_o)(2n-5)P_{n-3}(x)$$

$$= (2n-5)(P_1^0\cos\theta_m + P_1^1\sin\theta_o\cos\phi_m)$$

$$\left[\sum_{m=0}^{n-3}\frac{2}{\epsilon_m}\frac{(n-m-3)!}{(n+m-3)!}P_{n-3}^m(\sin\delta)P_{n-3}^m(\cos m\phi_m\cos m\phi_o + \sin m\phi_o\sin m\phi_m)\right] \qquad \text{(B-24)}$$

By doing the same procedure in (B-24) as before, we get the following catalogs named by the first term

(10) P_{n-2}^0 (for $m = 0$)

$$(2n-5)[(P_1^0 P_{n-3}^0)P_{n-3}^0(\sin\delta)\cos\theta_o]$$

$$= [(n-2)P_{n-2}^0 + (n-3)P_{n-4}^0]P_{n-3}^0(\sin\delta)\cos\theta_m$$

$$= \overset{⑮}{[(n-2)P_{n-3}^0(\sin\delta)\cos\theta_o]}P_{n-2}^0 + \overset{⑯}{[(n-3)P_{n-3}^0(\sin\delta)\cos\theta_m]}P_{n-4}^0 \qquad \text{(B-25)}$$

(11) $P_{n-2}^1\cos\phi_o$ (for $m = 1$)

$$(2n-5)[(P_1^1 \cdot P_{n-3}^0)P_{n-3}^0(\sin\delta)\sin\theta_m\cos\phi_o$$

$$+ \frac{2(n-4)!}{(n-2)!}(P_1^0 P_{n-3}^1)P_{n-3}^1(\sin\delta)\cos\theta_m\cos\phi_o\cos\phi_m]$$

$$= (P_{n-2}^{1} - P_{n-4}^{1})P_{n-3}^{0}(\sin\delta)\sin\theta_s\cos\phi_s$$

$$+ \frac{2(n-4)!}{(n-2)!}[(n-3)P_{n-2}^{1} + (n-2)P_{n-4}^{1}]P_{n-3}^{1}(\sin\delta)\cos\theta_n\cos\phi_n\cos\phi_s$$

⑰

$$= [P_{n-3}^{0}(\sin\delta)\sin\theta_s]P_{n-2}^{1}\cos\phi_n$$

⑱

$$+ [\frac{2}{n-2}P_{n-3}^{1}(\sin\delta)\cos\theta_s\cos\phi_n]P_{n-2}^{1}\cos\phi_s$$

where $P_{n-4}^{1} = 0$ for $n \leq 4$ (B-26)

(12) $P_{n-2}^{1}\sin\phi_n$ (for $m = 1$)

$$(2n-5)[\frac{2(n-4)!}{(n-2)!}(P_{1}^{0}\cdot P_{n-3}^{1})P_{n-3}^{1}(\sin\delta)\cos\theta_n\sin\phi_n\sin\phi_s]$$

$$= \frac{2(n-4)!}{(n-2)!}[(n-3)P_{n-2}^{1} + (n-2)P_{n-4}^{1}]P_{n-3}^{1}(\sin\delta)\cos\theta_s\sin\phi_n\sin\phi_s$$

⑲

$$= [\frac{2}{n-2}P_{n-3}^{1}(\sin\delta)\cos\theta_s\sin\phi_s]P_{n-2}^{1}\sin\phi_n$$

where $P_{n-4}^{1} = 0$ for $n \leq 4$ (B-27)

(13) $P_{n-2}^{2}\cos 2\phi_n$ (for $m = 2$)

$$(2n-5)[\frac{2(n-4)!}{(n-2)!}(P_{1}^{1}\cdot P_{n-3}^{1})P_{n-3}^{1}(\sin\delta)\sin\theta_n\cos\phi_n\cos^2\phi_s]$$

$$= \frac{2(n-4)!}{(n-2)!}(P_{n-2}^{2} - P_{n-4}^{2})P_{n-3}^{1}(\sin\delta)\sin\theta_n\cos\phi_n\frac{(1+\cos 2\phi_n)}{2}$$

⑳

$$= [\frac{1}{(n-2)(n-3)}P_{n-3}^{1}(\sin\delta)\sin\theta_s\cos\phi_n]P_{n-2}^{2}\cos 2\phi_s$$

㉑

$$+ [\frac{1}{(n-2)(n-3)}P_{n-3}^{1}(\sin\delta)\sin\theta_s\cos\phi_n]P_{n-2}^{2}$$

where $P_{n-4}^{2} \equiv 0$ for $n \leq 4$ (B-28)

(14) $P_{n-2}^{2}\sin 2\phi_s$ (for $m = 2$)

$$(2n-5)\left[\frac{2(n-4)!}{(n-2)!}\,(P_1^1\,P_{n-3}^1)P_{n-3}^1(\sin\delta)\sin\delta_o\sin\phi_o\sin\phi_s\cos\phi_s\right]$$

$$= \frac{2(n-4)!}{(n-2)!}\,(P_{n-2}^2 - P_{n-4}^2)P_{n-3}^1(\sin\delta)\sin\delta_o\sin\phi_o\,\frac{\sin 2\phi_s}{2}$$

㉒

$$= \left[\frac{1}{(n-2)(n-3)}\,P_{n-3}^1(\sin\delta)\sin\delta_o\sin\phi_o\right]P_{n-2}^2\sin 2\phi_s$$

where $P_{n-4}^2 \equiv 0$ for $n \leq 4$ (B-29)

With the substitution of (B-23h), the second term in (B-22) becomes

$$-C\,P'_{n-1}(x) = -[P_1^0(\sin\delta)\cos\delta_o + P_1^1(\sin\delta)\sin\delta_o\cos\phi_o]$$

$$[(2n-3)P_{n-2}(x) + (2n-7)P_{n-4}(x)]$$

$$= -[P_1^0(\sin\delta)\cos\delta_o + P_1^1(\sin\delta)\sin\delta_o\cos\phi_o]$$

$$\left\{(2n-3)\left[\sum_{m=0}^{n-2}\frac{2}{\delta m}\,\frac{(n-m-2)!}{(n+m-2)!}\,P_{n-2}^m(\sin\delta)P_{n-2}^m(\cos m\phi_o\cos m\phi_s+\sin m\phi_o\sin m\phi_s)\right]\right.$$

$$+\ (2n-7)\left[\sum_{m=0}^{n-4}\frac{2}{\delta m}\,\frac{(n-m-4)!}{(n+m-4)!}\,P_{n-4}^m(\sin\delta)\ \cdot\right.$$

$$\left.\left.P_{n-4}^m(\cos m\phi_o\cos m\phi_s+\sin m\phi_o\sin m\phi_s)\right]\right\} \qquad \text{(B-30)}$$

Same as before, we have the following terms

(15) P_{n-2}^{0} (for $m = 0$)

$$-(2n-3)\left\{[P_1^1(\sin\delta)P_{n-2}^0(\sin\delta)]\sin\delta_o\cos\phi_o P_{n-2}^0\right.$$

$$\left.+\ [P_1^0(\sin\delta)P_{n-2}^0(\sin\delta)]\cos\delta_o P_{n-2}^0\right\}$$

$$= -[P^1_{n-1}(\sin\delta) - P^1_{n-3}(\sin\delta)]\sin\theta_o\cos\phi_n P^0_{n-2}$$

$$- [(n-1)P^0_{n-1}(\sin\delta) + (n-2)P^0_{n-3}(\sin\delta)]\cos\theta_o P^0_{n-2}$$

$$= \overset{\text{㉓}}{[-P^1_{n-1}(\sin\delta)\sin\theta_n\cos\phi_n]}P^0_{n-2} + \overset{\text{㉔}}{[P^1_{n-3}(\sin\delta)\sin\theta_o\cos\phi_o]}P^0_{n-2}$$

$$+ \overset{\text{㉕}}{[-(n-1)P^0_{n-1}(\sin\delta)\cos\theta_o]}P^0_{n-2}$$

$$+ \overset{\text{㉖}}{[-(n-2)P^0_{n-3}(\sin\delta)\cos\theta_n]}P^0_{n-2} \qquad \text{(B-31)}$$

(16) $P^1_{n-2}\cos\phi_o$ (for $m = 1$)

$$-(2n-3)\left\{\frac{2(n-3)!}{(n-1)!}\,[P^1_1(\sin\delta)P^1_{n-2}(\sin\delta)]\sin\theta_o\cos^2\phi_o P^1_{n-2}\cos\phi_o\right.$$

$$\left. + \frac{2(n-3)!}{(n-1)!}\,[P^0_1(\sin\delta)P^1_{n-2}(\sin\delta)]\cos\theta_o\cos\phi_n P^1_{n-2}\cos\phi_o\right\}$$

$$= -\frac{2(n-3)!}{(n-1)!}\left\{[P^2_{n-1}(\sin\delta) - P^2_{n-3}(\sin\delta)]\sin\theta_o\,\frac{(1+\cos2\phi_n)}{2}\right.$$

$$\left. + [(n-2)P^1_{n-1}(\sin\delta) + (n-1)P^1_{n-3}(\sin\delta)]\cos\theta_o\cos\phi_o\right\} P^1_{n-2}\cos\phi_n$$

$$= \overset{\text{㉗}}{[-\frac{1}{(n-1)(n-2)}\,P^2_{n-1}(\sin\delta)\sin\theta_n]}P^1_{n-2}\cos\phi_n$$

$$+ \overset{\text{㉘}}{[-\frac{1}{(n-1)(n-2)}\,P^2_{n-1}(\sin\delta)\sin\theta_o\cos2\phi_o]}P^1_{n-2}\cos\phi_n$$

$$+ \overset{\text{㉙}}{[-\frac{2}{n-1}\,P^1_{n-1}(\sin\delta)\cos\theta_o\cos\phi_o]}P^1_{n-2}\cos\phi_n$$

$$+ \overset{\text{㉚}}{[-\frac{2}{n-2}\,P^1_{n-3}(\sin\delta)\cos\theta_n\cos\phi_o]}P^1_{n-2}\cos\phi_o$$

where $P^2_{n-3}(\sin\delta) = 0$ for $n \le 4$ (B-32)

(17) $P_{n-2}^{1}\sin\phi_o$ (for m = 1)

$$= (2n-3)\left\{\frac{2(n-3)!}{(n-1)!}\,[P_1^1(\sin\delta)P_{n-2}^1(\sin\delta)]\sin\theta_o\sin\phi_o\cos\phi_o P_{n-2}^1\sin\phi_o\right.$$

$$\left.+\frac{2(n-3)!}{(n-1)!}\,[P_1^0(\sin\delta)P_{n-2}^1(\sin\delta)]\cos\theta_o\sin\phi_o P_{n-2}^1\sin\phi_o\right\}$$

$$= -\frac{2(n-3)!}{(n-1)!}\left\{[P_{n-1}^2(\sin\delta)-P_{n-3}^2(\sin\delta)]\sin\theta_o\,\frac{\sin 2\phi_o}{2}\right.$$

$$\left.+[(n-2)P_{n-1}^1(\sin\delta)+(n-1)P_{n-3}^1(\sin\delta)]\cos\theta_o\sin\phi_o\right\}P_{n-2}^1\sin\phi_o$$

㉛

$$= [-\frac{1}{(n-1)(n-2)}\,P_{n-1}^2(\sin\delta)\sin\theta_o\sin 2\phi_o]P_{n-2}^1\sin\phi_o$$

㉜

$$+[-\frac{2}{n-1}\,P_{n-1}^1(\sin\delta)\cos\theta_o\sin\phi_o]P_{n-2}^1\sin\phi_o$$

㉝

$$+[-\frac{2}{n-2}\,P_{n-3}^1(\sin\delta)\cos\theta_o\sin\phi_o]P_{n-2}^1\sin\phi_o$$

where $P_{n-3}^2(\sin\delta)\equiv 0$ for $n\leq 4$ (B-33)

(18) $P_{n-2}^{2}\cos 2\phi_o$ (for m = 2)

$$-(2n-3)\left\{\frac{2(n-4)!}{n!}\,[P_1^1(\sin\delta)P_{n-2}^2(\sin\delta)]\sin\theta_o\cos\phi_o\cos 2\phi_o P_{n-2}^2\cos 2\phi_o\right.$$

$$\left.+\frac{2(n-4)!}{n!}\,[P_1^0(\sin\delta)P_{n-2}^2(\sin\delta)]\cos\theta_o\cos 2\phi_o P_{n-2}^2\cos 2\phi_o\right\}$$

$$= -\frac{2(n-4)!}{n!}\left\{[P_{n-1}^3(\sin\delta)-P_{n-3}^3(\sin\delta)]\sin\theta_o\,\frac{(\cos 3\phi_o+\cos\phi_o)}{2}\right.$$

$$\left.+[(n-3)P_{n-1}^2(\sin\delta)+(n-2)P_{n-3}^2(\sin\delta)]\cos\theta_o\cos 2\phi_o\right\}P_{n-2}^2\cos 2\phi_o$$

㉞

$$= [-\frac{1}{n(n-1)(n-2)(n-3)}\,P_{n-1}^3(\sin\delta)\sin\theta_o\cos 3\phi_o]P_{n-2}^2\cos 2\phi_o$$

㉟

$$+ \left[- \frac{1}{n(n-1)(n-2)(n-3)} P_{n-1}^{3}(\sin\delta)\sin\theta_o\cos\phi_o\right]P_{n-2}^{2}\cos 2\phi_s$$

㊱

$$+ \left[- \frac{2}{n(n-1)(n-2)} P_{n-1}^{2}(\sin\delta)\cos\theta_o\cos 2\phi_o\right]P_{n-2}^{2}\cos 2\phi_s$$

where $P_{n-3}^{2}(\sin\delta) = 0$ and $P_{n-3}^{3}(\sin\delta) = 0$ for $n \leq 4$ (B-34)

(19) $P_{n-2}^{2}\sin 2\phi_s$ (for $m = 2$)

$$-(2n-3)\left\{\frac{2(n-4)!}{n!}\left[P_1^1(\sin\delta)P_{n-2}^{2}(\sin\delta)\right]\sin\theta_o\cos\phi_o\sin 2\phi_o P_{n-2}^{2}\sin 2\phi_s\right.$$

$$\left.+ \frac{2(n-4)!}{n!}\left[P_1^0(\sin\delta)P_{n-2}^{2}(\sin\delta)\right]\cos\theta_o\sin 2\phi_o P_{n-2}^{2}\sin 2\phi_s\right\}$$

$$= - \frac{2(n-4)!}{n!}\left\{\left[P_{n-1}^{3}(\sin\delta) - P_{n-3}^{3}(\sin\delta)\right]\sin\theta_o \frac{(\sin 3\phi_o+\sin\phi_o)}{2}\right.$$

$$\left.+ \left[(n-3)P_{n-1}^{2}(\sin\delta) + (n-2)P_{n-3}^{2}(\sin\delta)\right]\cos\theta_o\sin 2\phi_o\right\} P_{n-2}^{2}\sin 2\phi_s$$

㊲

$$= \left[- \frac{1}{n(n-1)(n-2)(n-3)} P_{n-1}^{3}(\sin\delta)\sin\theta_o\sin 3\phi_o\right]P_{n-2}^{2}\sin 2\phi_s$$

㊳

$$+ \left[- \frac{1}{n(n-1)(n-2)(n-3)} P_{n-1}^{3}(\sin\delta)\sin\theta_o\sin\phi_o\right]P_{n-2}^{2}\sin 2\phi_s$$

㊴

$$+ \left[- \frac{2}{n(n-1)(n-2)} P_{n-1}^{2}(\sin\delta)\cos\theta_o\sin 2\phi_o\right]P_{n-2}^{2}\sin 2\phi_s$$

where $P_{n-3}^{2}(\sin\delta) = 0$ and $P_{n-3}^{3}(\sin\delta) = 0$ for $n \leq 4$ (B-35)

(20) P_{n-4}^{0} (for $m = 0$)

$$-(2n-7)\left\{\left[P_1^1(\sin\delta)P_{n-4}^{0}(\sin\delta)\right]\sin\theta_o\cos\phi_o P_{n-4}^{0}\right.$$

$$\left.+ \left[P_1^0(\sin\delta)P_{n-4}^{0}(\sin\delta)\right]\cos\theta_o P_{n-4}^{0}\right\}$$

$$= -\Big\{[P^1_{n-3}(\sin\delta) - P^1_{n-5}(\sin\delta)]\sin\theta_o\cos\phi_s$$

$$+ [(n-3)P^0_{n-3}(\sin\delta) + (n-4)P^0_{n-5}(\sin\delta)]\cos\theta_o\Big\}P^0_{n-4}$$

$$= [\overset{(40)}{-P^1_{n-3}(\sin\delta)\sin\theta_o\cos\phi_s}]P^0_{n-4} + [\overset{(41)}{-(n-3)P^0_{n-3}(\sin\delta)\cos\theta_o}]P^0_{n-4}$$

where $P^0_{n-5}(\sin\delta) = 0$ and $P^1_{n-5}(\sin\delta) = 0$ for $n \leq 4$ (B-36)

Next we want to cancel out, or convert, the labeled terms into the first terms in (B-13)-(B-17)

(21) adding for P^0_n

$$[\overset{①}{(n-1)P^0_{n-1}(\sin\delta)\cos\theta_o}]P^0_{n-2} + [\overset{㉕}{-(n-1)P^0_{n-1}(\sin\delta)\cos\theta_o}]P^0_{n-2} = 0$$

$$[\overset{⑥}{\tfrac{1}{n(n-1)}P^1_{n-1}(\sin\delta)\sin\theta_o\cos\phi_s}]P^2_n + [\overset{㉓}{-P^1_{n-1}(\sin\delta)\sin\theta_o\cos\phi_s}]P^0_{n-2}$$

$$= P^1_{n-1}(\sin\delta)\sin\theta_o\cos\phi_o[\frac{1}{n(n-1)}P^2_n - P^0_{n-2}]$$

$$= P^1_{n-1}(\sin\delta)\sin\theta_o\cos\phi_o[-P^0_n + \frac{1}{n(n-1)}P^2_{n-2}]$$ [see Appendix C, equation (C-4e)]

$$= [-P^1_{n-1}(\sin\delta)\sin\theta_o\cos\phi_s]P^0_n + [\overset{㊷}{\tfrac{1}{n(n-1)}P^1_{n-1}(\sin\delta)\sin\theta_o\cos\phi_s}]P^2_{n-2}$$

And

$$[\overset{⑧}{-\tfrac{1}{n(n-1)}P^1_{n-1}(\sin\delta)\sin\theta_o\cos\phi_o}]P^2_{n-2}$$

$$+ [\overset{㊷}{\tfrac{1}{n(n-1)}P^1_{n-1}(\sin\delta)\sin\theta_o\cos\phi_o}]P^2_{n-2} = 0$$

$$[\overset{⑯}{(n-3)P^0_{n-3}(\sin\delta)\cos\theta_o}]P^0_{n-4} + [\overset{㊶}{-(n-3)P^0_{n-3}(\sin\delta)\cos\theta_o}]P^0_{n-4} = 0$$

Thus we can add the following to P^0_o term

$$[-P^1_{n-1}(\sin\delta)\sin\theta_o\cos\phi_o] \tag{B-37}$$

Continuing, what follow are

$$\overset{⑮}{[(n-2)P^0_{n-3}(\sin\delta)\cos\theta_o]}P^0_{n-2} + \overset{㉖}{[-(n-2)P^0_{n-3}(\sin\delta)\cos\theta_o]}P^0_{n-2} = 0$$

$$\overset{㉔}{[P^1_{n-3}(\sin\delta)\sin\theta_o\cos\phi_o]}P^0_{n-2} + \overset{㊵}{[-P^1_{n-3}(\sin\delta)\sin\theta_o\cos\phi_o]}P^0_{n-4}$$

$$= P^1_{n-3}(\sin\delta)\sin\theta_o\cos\phi_o[P^0_{n-2} - P^0_{n-4}]$$

$$= P^1_{n-3}(\sin\delta)\sin\theta_o\cos\phi_o[-\frac{1}{(n-2)(n-3)}P^2_{n-2}] \quad \text{[see Appendix C, equation (C-4c)]}$$

$$= \overset{㊸}{[-\frac{1}{(n-2)(n-3)}P^1_{n-3}(\sin\delta)\sin\theta_o\cos\phi_o]}P^2_{n-2}$$

And

$$\overset{㉑}{[\frac{1}{(n-2)(n-3)}P^1_{n-3}(\sin\delta)\sin\theta_o\cos\phi_o]}P^2_{n-2}$$

$$+ \overset{㊸}{[-\frac{1}{(n-2)(n-3)}P^1_{n-3}(\sin\delta)\cos\theta_o\cos\phi_o]}P^2_{n-2} = 0$$

(22) adding for $P^1_n\cos\phi_o$

$$\overset{③}{[\frac{2}{n-1}P^1_{n-1}(\sin\delta)\cos\theta_o\cos\phi_o]}P^1_{n-2}\cos\phi_o$$

$$+ \overset{㉙}{[-\frac{2}{n-1}P^1_{n-1}(\sin\delta)\cos\theta_o\cos\phi_o]}P^1_{n-2}\cos\phi_o = 0$$

$$\overset{⑱}{[\frac{2}{n-2}P^1_{n-3}(\sin\delta)\cos\theta_o\cos\phi_o]}P^1_{n-2}\cos\phi_o$$

$$+ \overset{㉚}{[-\frac{2}{n-2}P^1_{n-3}(\sin\delta)\cos\theta_o\cos\phi_o]}P^1_{n-2}\cos\phi_o = 0$$

$$\overset{⑰}{[P^0_{n-3}(\sin\delta)\sin\theta_o]}P^1_{n-2}\cos\phi_o + \overset{②}{[-P^0_{n-1}(\sin\delta)\sin\theta_o]}P^1_{n-2}\cos\phi_s$$

$$= [P^0_{n-3}(\sin\delta) - P^0_{n-1}(\sin\delta)]\sin\theta_n P^1_{n-2}\cos\phi_s$$

$$= \overset{㊹}{[\frac{1}{(n-1)(n-2)} P^2_{n-1}(\sin\delta)\sin\theta_n]}P^1_{n-2}\cos\phi_s \qquad \text{[see Appendix C, equation (C-4b)]}$$

And

$$\overset{㊹}{[\frac{1}{(n-1)(n-2)} P^2_{n-1}(\sin\delta)\cos\phi_n]}P^1_{n-2}\cos\theta_n$$

$$+ \overset{㉗}{[-\frac{1}{(n-1)(n-2)} P^2_{n-1}(\sin\delta)\cos\theta_o]}P^1_{n-2}\cos\phi_s = 0$$

$$\overset{⑪}{[\frac{1}{(n+1)n(n-1)(n-2)} P^2_{n-1}(\sin\delta)\sin\theta_o\cos2\phi_n]}P^3_n\cos\phi_s$$

$$+ \overset{㉘}{[-\frac{1}{(n-1)(n-2)} P^2_{n-1}(\sin\delta)\sin\theta_n\cos2\phi_o]}P^1_{n-2}\cos\phi_s$$

$$= P^2_{n-1}(\sin\delta)\sin\theta_n\cos2\phi_o[\frac{1}{(n+1)n(n-1)(n-2)} P^3_n - \frac{1}{(n-1)(n-2)} P^1_{n-2}]\cos\phi_n$$

$$= P^2_{n-1}(\sin\delta)\sin\theta_o\cos2\phi_n[-\frac{1}{n(n+1)} P^1_n]\cos\phi_o \qquad \text{[see Appendix C, equation (C-4d)]}$$

$$= [-\frac{1}{n(n+1)} P^2_{n-1}(\sin\delta)\sin\theta_n\cos2\phi_o]P^1_n\cos\phi_s$$

Thus we can add the following to $P^1_n\cos\phi_s$ term

$$[-\frac{1}{n(n+1)} P^2_{n-1}(\sin\delta)\sin\theta_n\cos2\phi_n] \tag{S-38}$$

(23) adding for $P^1_n\sin\phi_s$

$$\overset{④}{[\frac{2}{n-1} P^1_{n-1}(\sin\delta)\cos\theta_o\sin\phi_o]}P^1_{n-2}\sin\phi_s$$

$$+ \overset{㉜}{[-\frac{2}{n-1} P^1_{n-1}(\sin\delta)\cos\theta_n\sin\phi_o]}P^1_{n-2}\sin\phi_s = 0$$

⑲

$$]\frac{2}{n-2} P^1_{n-3}(\sin\delta)\cos\theta_o \sin\phi_o]P^1_{n-2}\sin\phi_s$$

㉝

$$+ [-\frac{2}{n-2} P^1_{n-3}(\sin\delta)\cos\theta_o \sin\phi_o]P^1_{n-2}\sin\phi_s = 0$$

⑫

$$[\frac{1}{(n+1)n(n-1)(n-2)} P^2_{n-1}(\sin\delta)\sin\theta_o \sin 2\phi_o]P^3_n \sin\phi_s$$

㉛

$$+ [-\frac{1}{(n-1)(n-2)} P^2_{n-1}(\sin\delta)\sin\theta_o \sin 2\phi_o]P^1_{n-2}\sin\phi_s$$

$$= P^2_{n-1}(\sin\delta)\sin\theta_o \sin 2\phi_o [\frac{1}{(n+1)n(n-1)(n-2)} P^3_n - \frac{1}{(n-1)(n-2)} P^1_{n-2}]\sin\phi_s$$

$$= P^2_{n-1}(\sin\delta)\sin\theta_o \sin 2\phi_o [-\frac{1}{n(n+1)} P^1_n]\sin\phi_s$$ [see Appendix C, equation (C-4d)]

$$= [-\frac{1}{n(n+1)} P^2_{n-1}(\sin\delta)\sin\theta_o \sin 2\phi_o]P^1_n \sin\phi_s$$

Thus we can add the following to $P^1_n \sin\phi_s$ term

$$]-\frac{1}{n(n+1)} P^2_{n-1}(\sin\delta)\sin\theta_o \sin 2\phi_o] \qquad \text{(B-39)}$$

(24) adding for $P^2_n \cos 2\phi_s$

⑤

$$[\frac{2}{n(n-1)(n-2)} P^2_{n-1}(\sin\delta)\cos\theta_o \cos 2\phi_o]P^2_{n-2}\cos 2\phi_s$$

㊱

$$+ [-\frac{2}{n(n-1)(n-2)} P^2_{n-1}(\sin\delta)\cos\theta_o \cos 2\phi_o]P^2_{n-2}\cos 2\phi_s = 0$$

⑦

$$[-\frac{1}{n(n-1)} P^1_{n-1}(\sin\delta)\sin\theta_o \cos\phi_o]P^2_{n-2}\cos 2\phi_s$$

⑳

$$+ [\frac{1}{(n-2)(n-3)} P^1_{n-3}(\sin\delta)\sin\theta_o \cos\phi_o]P^2_{n-2}\cos 2\phi_s$$

$$= [-\frac{1}{n(n-1)} P^1_{n-1}(\sin\delta) + \frac{1}{(n-2)(n-3)} P^1_{n-3}(\sin\delta)]\sin\theta_s\cos\phi_s P^2_{n-2}\cos 2\phi_s$$

㊸

$$= [\frac{1}{n(n-1)(n-2)(n-3)} P^3_{n-1}(\sin\delta)\sin\theta_s\cos\phi_s]P^2_{n-2}\cos 2\phi_s \quad \text{[see Appendix C, equation (C-4e)]}$$

And

㊺

$$[\frac{1}{n(n-1)(n-2)(n-3)} P^3_{n-1}(\sin\delta)\sin\theta_s\cos\phi_s]P^2_{n-2}\cos 2\phi_s$$

㉟

$$+ [-\frac{1}{n(n-1)(n-2)(n-3)} P^3_{n-1}(\sin\delta)\sin\theta_s\cos\phi_s]P^2_{n-2}\cos 2\phi_s = 0$$

⑬

$$[\frac{1}{(n+2)(n+1)n(n-1)(n-2)(n-3)} P^3_{n-1}(\sin\delta)\sin\theta_s\cos 3\phi_s]P^4_n \cos 2\phi_s$$

㉞

$$+ [-\frac{1}{n(n-1)(n-2)(n-3)} P^3_{n-1}(\sin\delta)\sin\theta_s\cos 3\phi_s]P^2_{n-2} \cos 2\phi_s$$

$$= P^3_{n-1}(\sin\delta)\sin\theta_s\cos 3\phi_s[\frac{1}{(n+2)(n+1)n(n-1)(n-2)(n-3)} P^4_n$$

$$- \frac{1}{n(n-1)(n-2)(n-3)} P^2_{n-2}]\cos 2\phi_s$$

$$= P^3_{n-1}(\sin\delta)\sin\theta_s\cos 3\phi_s[-\frac{1}{(n+2)(n+1)n(n-1)} P^2_n]\cos 2\phi_s \quad \text{[see Appendix C, equation (C-4f)]}$$

$$= [-\frac{1}{(n+2)(n+1)n(n-1)} P^3_{n-1}(\sin\delta)\sin\theta_s\cos 3\phi_s]P^2_n\cos 2\phi_s$$

Thus we can add the following to $P^2_n\cos 2\phi_s$ term

$$[-\frac{1}{(n+2)(n+1)n(n-1)} P^3_{n-1}(\sin\delta)\sin\theta_s\cos 3\phi_s] \qquad (B-40)$$

(25) adding for $P^2_n\sin 2\phi_s$

⑨

$$[\frac{2}{n(n-1)(n-2)} P^2_{n-1}(\sin\delta)\cos\theta_s\sin 2\phi_s]P^2_{n-2}\sin 2\phi_s$$

㊴

$$+\left[-\frac{2}{n(n-1)(n-2)}P_{n-1}^{2}(\sin\delta)\cos\theta_o\sin2\phi_o\right]P_{n-2}^{2}\sin2\phi_s = 0$$

⑩

$$\left[-\frac{1}{n(n-1)}P_{n-1}^{1}(\sin\delta)\sin\theta_o\sin\phi_o\right]P_{n-2}^{2}\sin2\phi_s$$

㉒

$$+\left[\frac{1}{(n-2)(n-3)}P_{n-3}^{1}(\sin\delta)\sin\theta_o\sin\phi_o\right]P_{n-2}^{2}\sin2\phi_s$$

$$= \left[-\frac{1}{n(n-1)}P_{n-1}^{1}(\sin\delta) + \frac{1}{(n-2)(n-3)}P_{n-3}^{1}(\sin\delta)\right]\sin\theta_o\sin\phi_o P_{n-2}^{2}\sin2\phi_s$$

㊽

$$= \left[\frac{1}{n(n-1)(n-2)(n-3)}P_{n-1}^{3}(\sin\delta)\sin\theta_o\sin\phi_o\right]P_{n-2}^{2}\sin2\phi_s$$

[see Appendix
C, equation
(C-4e)]

And

㊻

$$\left[\frac{1}{n(n-1)(n-2)(n-3)}P_{n-1}^{3}(\sin\delta)\sin\theta_o\sin\phi_o\right]P_{n-2}^{2}\sin2\phi_o$$

㊳

$$+\left[-\frac{1}{n(n-1)(n-2)(n-3)}P_{n-1}^{3}(\sin\delta)\sin\theta_o\sin\phi_o\right]P_{n-2}^{2}\sin2\phi_s = 0$$

⑭

$$\left[\frac{1}{(n+2)(n+1)n(n-1)(n-2)(n-3)}P_{n-1}^{3}(\sin\delta)\sin\theta_o\sin3\phi_o\right]P_{n}^{4}\sin2\phi_s$$

㊲

$$+\left[-\frac{1}{n(n-1)(n-2)(n-3)}P_{n-1}^{3}(\sin\delta)\sin\theta_o\sin3\phi_o\right]P_{n-2}^{2}\sin2\phi_s$$

$$= P_{n-1}^{3}(\sin\delta)\sin\theta_o\sin3\phi_o\left[\frac{1}{(n+2)(n+1)n(n-1)(n-2)(n-3)}P_{n}^{4}\right.$$

$$\left. -\frac{1}{n(n-1)(n-2)(n-3)}P_{n-2}^{2}\right]\sin2\phi_s$$

$$= P_{n-1}^{3}(\sin\delta)\sin\theta_o\sin3\phi_o\left[-\frac{1}{(n+2)(n+1)n(n-1)}P_{n}^{2}\right]\sin2\phi_s$$

[see Appendix
C, equation
(C-4f)]

$$= \left[-\frac{1}{(n+2)(n+1)n(n-1)}P_{n-1}^{3}(\sin\delta)\sin\theta_o\sin3\phi_o\right]P_{n}^{2}\sin2\phi_s$$

Thus we can add the following to $P_n^2\sin2\phi_s$ term

$$\left[-\frac{1}{(n+2)(n+1)n(n-1)}P_{n-1}^{3}(\sin\delta)\sin\theta_o\sin3\phi_o\right] \qquad \text{(B-41)}$$

After performing the preceding steps from (B-13) to (B-41), now we can write the expression of magnetic potential for single dipole as

$$V = \frac{M}{r^2} \sum_{n=1}^{4} \left(\frac{r_o}{r}\right)^{n-1} \sum_{m=0}^{n} P_n^m(\cos\theta_s)(G_n^m \cos m\phi_s + H_n^m \sin m\phi_s) \qquad \text{(B-42)}$$

where

$$G_n^0 = nP_{n-1}^0(\sin\delta)\cos\theta_o - P_{n-1}^1(\sin\delta)\sin\theta_o\cos\phi_o \qquad \text{(B-42a)}$$

$$G_n^1 = P_{n-1}^0(\sin\delta)\sin\theta_o + \frac{2}{n} P_{n-1}^1(\sin\delta)\cos\theta_o\cos\phi_o$$

$$- \frac{1}{(n+1)n} P_{n-1}^2(\sin\delta)\sin\theta_o\cos 2\phi_o \qquad \text{(B-42b)}$$

$$H_n^1 = \frac{2}{n} P_{n-1}^1(\sin\delta)\cos\theta_o\sin\phi_o$$

$$- \frac{1}{(n+1)n} P_{n-1}^2(\sin\delta)\sin\theta_o\sin 2\phi_o \qquad \text{(B-42c)}$$

$$G_n^2 = \frac{1}{n(n-1)} P_{n-1}^1(\sin\delta)\sin\theta_o\cos\phi_o + \frac{2}{(n+1)(n(n-1))} P_{n-1}^2(\sin\delta)\cos\theta_o\cos 2\phi_o$$

$$- \frac{1}{(n+2)(n+1)n(n-1)} P_{n-1}^3(\sin\delta)\sin\theta_o\cos 3\phi_o \qquad \text{(B-42d)}$$

$$H_n^2 = \frac{1}{n(n-1)} P_{n-1}^1(\sin\delta)\sin\theta_o\sin\phi_o + \frac{2}{(n+1)(n(n-1))} P_{n-1}^2(\sin\delta)\cos\theta_o\sin 2\phi_o$$

$$- \frac{1}{(n+2)(n+1)n(n-1)} P_{n-1}^3(\sin\delta)\sin\theta_o\sin 3\phi_o \qquad \text{(B-42e)}$$

$$G_n^3 = \frac{1}{(n+1)n(n-1)(n-2)} P_{n-1}^2(\sin\delta)\sin\theta_o\cos 2\phi_o$$

$$+ \frac{2}{(n+2)(n+1)n(n-1)(n-2)} P_{n-1}^3(\sin\delta)\cos\theta_o\cos 3\phi_o \qquad \text{(B-42f)}$$

$$H_n^3 = \frac{1}{(n+1)n(n-1)(n+2)} P_{n-1}^2 (\sin\delta)\sin\theta_o \sin 2\phi_o$$

$$+ \frac{2}{(n+2)(n+1)n(n-1)(n-2)} P_{n-1}^3 (\sin\delta)\cos\theta_o \sin 3\phi_o \qquad \text{(B-42g)}$$

$$G_n^4 = \frac{1}{(n+2)(n+1)n(n-1)(n-2)(n-3)} P_{n-1}^3 (\sin\delta)\sin\theta_o \cos 3\phi_o \qquad \text{(B-42h)}$$

$$H_n^4 = \frac{1}{(n+2)(n+1)n(n-1)(n-2)(n-3)} P_{n-1}^3 (\sin\delta)\sin\theta_o \sin 3\phi_o \qquad \text{(B-42i)}$$

Since $P_n^m(\sin\delta) = 0$ for $n < m$, we can get the following expressions

For $n = 1$

$$G_1^0 = \cos\theta_o \qquad \text{(B-43a)}$$

$$G_1^1 = \sin\theta_o \qquad \text{(B-43b)}$$

$$H_1^1 = 0 \qquad \text{(B-43c)}$$

For $n = 2$

$$G_2^0 = 2P_1^0(\sin\delta)\cos\theta_o - P_1^1(\sin\delta)\sin\theta_o \cos\phi_o \qquad \text{(B-44a)}$$

$$G_2^1 = P_1^0(\sin\delta)\sin\theta_o + P_1^1(\sin\delta)\cos\theta_o \cos\phi_o \qquad \text{(B-44b)}$$

$$H_2^1 = P_1^1(\sin\delta)\cos\theta_o \sin\phi_o \qquad \text{(B-44c)}$$

$$G_2^2 = \frac{1}{2}P_1^1 (\sin\delta)\sin\theta_o \cos\phi_o \qquad \text{(B-44d)}$$

$$H_2^2 = \frac{1}{2}P_1^1 (\sin\delta)\sin\theta_o \sin\phi_o \qquad \text{(B-44e)}$$

For n = 3

$$G_3^0 = 3P_2^0(\sin\delta)\cos\theta_o - P_2^1(\sin\delta)\sin\theta_o\cos\phi_o \tag{B-45a}$$

$$G_3^1 = P_2^0(\sin\delta)\sin\theta_o + \frac{2}{3}P_2^1(\sin\delta)\cos\theta_o\cos\phi_o$$

$$- \frac{1}{12}P_2^2(\sin\delta)\sin\theta_o\cos2\phi_o \tag{B-45b}$$

$$H_3^1 = \frac{2}{3}P_2^1(\sin\delta)\cos\theta_o\sin\phi_o$$

$$- \frac{1}{12}P_2^2(\sin\delta)\sin\theta_o\sin2\phi_o \tag{B-45c}$$

$$G_3^2 = \frac{1}{6}P_2^1(\sin\delta)\sin\theta_o\cos\phi_o + \frac{1}{12}P_2^2(\sin\delta)\cos\theta_o\cos2\phi_o \tag{B-45d}$$

$$H_3^2 = \frac{1}{6}P_2^1(\sin\delta)\sin\theta_o\sin\phi_o + \frac{1}{12}P_2^2(\sin\delta)\cos\theta_o\sin2\phi_o \tag{B-45e}$$

$$G_3^3 = \frac{1}{24}P_2^2(\sin\delta)\sin\theta_o\cos2\phi_o \tag{B-45f}$$

$$H_3^3 = \frac{1}{24}P_2^2(\sin\delta)\sin\theta_o\sin2\phi_o \tag{B-45g}$$

For n = 4

$$G_4^0 = 4P_3^0(\sin\delta)\cos\theta_o - P_3^1(\sin\delta)\sin\theta_o\cos\phi_o \tag{B-46a}$$

$$G_4^1 = P_3^0(\sin\delta)\sin\theta_o + \frac{1}{2}P_3^1(\sin\delta)\cos\theta_o\cos\phi_o$$

$$- \frac{1}{20}P_3^2(\sin\delta)\sin\theta_o\cos2\phi_o \tag{B-46b}$$

$$H_4^1 = \frac{1}{2}P_3^1(\sin\delta)\cos\theta_o\sin\phi_o$$

$$- \frac{1}{20}P_3^2(\sin\delta)\sin\theta_o\sin2\phi_o \tag{B-46c}$$

$$G_4^2 = \frac{1}{12} P_3^1(\sin\theta)\sin\theta_o\cos\phi_o + \frac{1}{30} P_3^2(\sin\theta)\cos\theta_o\cos 2\phi_o$$

$$- \frac{1}{360} P_3^3(\sin\theta)\sin\theta_o\cos 3\phi_o \qquad \text{(B-46d)}$$

$$H_4^2 = \frac{1}{12} P_3^1(\sin\theta)\sin\theta_o\sin\phi_o + \frac{1}{30} P_3^2(\sin\theta)\cos\theta_o\sin 2\phi_o$$

$$- \frac{1}{360} P_3^3(\sin\theta)\sin\theta_o\sin 3\phi_o \qquad \text{(B-46e)}$$

$$G_4^3 = \frac{1}{120} P_3^2(\sin\theta)\sin\theta_o\cos 2\phi_o + \frac{1}{360} P_3^3(\sin\theta)\cos\theta_o\cos 3\phi_o \qquad \text{(B-46f)}$$

$$H_4^3 = \frac{1}{120} P_3^2(\sin\theta)\sin\theta_o\sin 2\phi_o + \frac{1}{360} P_3^3(\sin\theta)\cos\theta_o\sin 3\phi_o \qquad \text{(B-46g)}$$

$$G_4^4 = \frac{1}{720} P_3^3(\sin\theta)\sin\theta_o\cos 3\phi_o \qquad \text{(B-46h)}$$

$$H_4^4 = \frac{1}{720} P_3^3(\sin\theta)\sin\theta_o\sin 3\phi_o \qquad \text{(B-46i)}$$

The transformation from single dipole coordinate system to that of "System III longitude" is

$$r\hat{X}(\phi,\theta) = R_3(\lambda_o) r\hat{X}(\phi_s,\theta_s) \qquad \text{(B-47)}$$

where

r, θ_s, ϕ_s, and λ_o are the same as those in Appendix A,

θ is the colatitude of the point P in "System III longitude" system,

ϕ is the longitude of the point P as measured eastward from meridian $\lambda_{III}(1965) = 0°$,

$\hat{X}$ is the unit vector on radial vector $\vec{r}$ in the spherical coordinate system.

Thus, we obtain

$$r\hat{X}(\phi,\theta) = r\hat{X}(\phi_s - \lambda_o, \theta_s) \qquad \text{(B-48)}$$

This means

$$\theta_0 = \theta \qquad \text{(B-48a)}$$

$$\phi_0 = \phi + \lambda_0 \qquad \text{(B-48b)}$$

Substituting (B-48a) and (B-48b) into (B-42), we have

$$V = \frac{M}{r^2} \sum_{n=1}^{4} \left[\frac{r_0}{r}\right]^{n-1} \sum_{m=0}^{n} P_n^m(\cos\theta)[G_n^m \cos m(\phi+\lambda_0) + H_n^m \sin m(\phi+\lambda_0)]$$

$$= M \sum_{n=1}^{4} \frac{r_0^{n-1}}{r^{n+1}} \sum_{m=0}^{n} P_n^m(\cos\theta)$$

$$[(G_n^m \cos m\lambda_0 + H_n^m \sin m\lambda_0)\cos m\phi$$

$$+ (-G_n^m \sin m\lambda_0 + H_n^m \cos m\lambda_0)\sin m\phi] \qquad \text{(B-49)}$$

where G_0^m and H_n^m are listed in the expressions (B-43a)-(B-46i)

2. Expression of Magnetic Potential for Five-Dipole with Legendre Polynomials

The magnetic potential for 5 dipoles can be obtained by making the sum of equation (B-49) for all 5 dipoles, as follows

$$V = \sum_{i=1}^{5} V_i$$

$$= \sum_{i=1}^{5} M(i) \sum_{n=1}^{4} \frac{[r_0(i)]^{n-1}}{r^{n+1}} \sum_{m=0}^{n} P_n^m(\cos\theta)$$

$$\Big\{[G_n^m(i)\cos m\lambda_0(i) + H_n^m(i)\sin m\lambda_0(i)]\cos m\phi$$

$$+ [-G_n^m(i)\sin m\lambda_0(i) + H_n^m(i)\cos m\lambda_0(i)]\sin m\phi\Big\} \qquad \text{(B-50)}$$

where symbols of $G_n^m(i)$, $H_n^m(i)$ and the parameters for each dipole are the same as those for single dipole, just $G_n^m(i)$, $H_n^m(i)$, $\theta_o(i)$, $\phi_o(i)$, $\lambda_o(i)$, $r_o(i)$, $d(i)$, and $M(i)$ instead of G_n^m, H_n^m, θ_o, ϕ_o, λ_o, r_o, δ, and M, respectively.

3. Comparison of Magnetic Potentials for Five-Dipole and O_4 Model

From the O_4 model, Jupiter's magnetic potential is

$$V = a \sum_{n=1}^{3} \left(\frac{a}{r}\right)^{n+1} \sum_{m=0}^{n} (g_n^m \cos m\phi + h_n^m \sin m\phi)\overline{P_n^m}(\cos\theta) \qquad \text{(B-51)}$$

where

g_n^m and h_n^m are the Schmidt coefficients,

$\overline{P_n^m}(\cos\theta)$ is the associated Legendre polynomial with Schmidt normalization (see Appendix D)

With the substitution of $a = 1\ R_J$ into (B-51), magnetic potential of O_4 model becomes

$$V = \sum_{n=1}^{3} \left(\frac{1}{r}\right)^{n+1} \sum_{m=0}^{n} (g_n^m \cos m\phi + h_n^m \sin m\phi)\overline{P_n^m}(\cos\theta) \qquad \text{(B-52)}$$

By equating the coefficients of the Tesseral Harmonics of nth degree and mth order, we have 24 equations containing 24 adjustable parameters of 4 dipoles.

For the sake of simplicity, we denote G_n^m, H_n^m, θ_o, ϕ_o, λ_o, r_o, δ, and M instead of $G_n^m(i)$, $H_n^m(i)$, $\theta_o(i)$, $\phi_o(i)$, $\lambda_o(i)$, $r_o(i)$, $d(i)$, and $M(i)$, respectively, and designate $\sum_i$ instead of $\sum_{i=1}^{5}$

Following are 24 equations

$$\sum_i MG_1^0 = g_1^0 \qquad \text{(B-53a)}$$

$$\sum_i MG_1^1 \cos\lambda_o = g_1^1 \qquad \text{(B-53b)}$$

$$\sum_i MG_1^1(-\sin\lambda_o) = h_1^1 \qquad \text{(B-53c)}$$

$$\sum_i Mr_o G_2^0 = g_2^0 \qquad \text{(B-53d)}$$

$$\sum_i Mr_o(G_2^1\cos\lambda_o + H_2^1\sin\lambda_o) = \frac{1}{\sqrt{3}}\, g_2^1 \qquad \text{(B-53e)}$$

$$\sum_i Mr_o(-G_2^1\sin\lambda_o + H_2^1\cos\lambda_o) = \frac{1}{\sqrt{3}}\, h_2^1 \qquad \text{(B-53f)}$$

$$\sum_i Mr_o(G_2^2\cos 2\lambda_o + H_2^2\sin 2\lambda_o) = \frac{1}{2\sqrt{3}}\, g_2^2 \qquad \text{(B-53g)}$$

$$\sum_i Mr_o(-G_2^2\sin 2\lambda_o + H_2^2\cos 2\lambda_o) = \frac{1}{2\sqrt{3}}\, h_2^2 \qquad \text{(B-53h)}$$

$$\sum_i Mr_o^2 G_3^0 = g_3^0 \qquad \text{(B-53i)}$$

$$\sum_i Mr_o^2(G_3^1\cos\lambda_o + H_3^1\sin\lambda_o) = \frac{1}{\sqrt{6}}\, g_3^1 \qquad \text{(B-53j)}$$

$$\sum_i Mr_o^2(-G_3^1\sin\lambda_o + H_3^1\cos\lambda_o) = \frac{1}{\sqrt{6}}\, h_3^1 \qquad \text{(B-53k)}$$

$$\sum_i Mr_o^2(G_3^2\cos 2\lambda_o + H_3^2\sin 2\lambda_o) = \frac{1}{2\sqrt{15}}\, g_3^2 \qquad \text{(B-53l)}$$

$$\sum_i Mr_o^2(-G_3^2\sin 2\lambda_o + H_3^2\cos 2\lambda_o) = \frac{1}{2\sqrt{15}}\, h_3^2 \qquad \text{(B-53m)}$$

$$\sum_i Mr_o^2(G_3^3\cos 3\lambda_o + H_3^3\sin 3\lambda_o) = \frac{1}{6\sqrt{10}}\, g_3^3 \qquad \text{(B-53n)}$$

$$\sum_i Mr_n^2(-G_3^3\sin 3\lambda_n + H_3^3\cos 3\lambda_n) = \frac{1}{6\sqrt{10}}\,h_3^3 \qquad \text{(B-53o)}$$

$$\sum_i Mr_n^3 C_4^0 = 0 \qquad \text{(B-53p)}$$

$$\sum_i Mr_n^3(C_4^1\cos\lambda_n + H_4^1\sin\lambda_n) = 0 \qquad \text{(B-53q)}$$

$$\sum_i Mr_n^3(-G_4^1\sin\lambda_n + H_4^1\cos\lambda_n) = 0 \qquad \text{(B-53r)}$$

$$\sum_i Mr_n^3(G_4^2\cos 2\lambda_n + H_4^2\sin 2\lambda_n) = 0 \qquad \text{(B-53s)}$$

$$\sum_i Mr_n^3(-G_4^2\sin 2\lambda_n + H_4^2\cos 2\lambda_n) = 0 \qquad \text{(B-53t)}$$

$$\sum_i Mr_n^3(G_4^3\cos 3\lambda_n + H_4^3\sin 3\lambda_n) = 0 \qquad \text{(B-53u)}$$

$$\sum_i Mr_n^3(-G_4^3\sin 3\lambda_n + H_4^3\cos 3\lambda_n) = 0 \qquad \text{(B-53v)}$$

$$\sum_i Mr_n^3(G_4^4\cos 4\lambda_n + H_4^4\sin 4\lambda_n) = 0 \qquad \text{(B-53w)}$$

$$\sum_i Mr_n^3(-G_4^4\sin 4\lambda_n + H_4^4\cos 4\lambda_n) = 0 \qquad \text{(B-53x)}$$

APPENDIX C

RELATIONS AMONG THE ASSOCIATED LEGENDRE POLYNOMIALS

From recurrence relations, we have

$$(2\ell+1)(1-x^2)^{\frac{1}{2}}P_\ell^m = P_{\ell+1}^{m+1} - P_{\ell-1}^{m+1} \tag{C-1}$$

$$(2\ell+1)(1-x^2)^{\frac{1}{2}}P_\ell^m = (\ell+m)(\ell+m-1)P_{\ell-1}^{m-1} - (\ell-m+2)(\ell-m+1)P_{\ell+1}^{m-1} \tag{C-2}$$

where x is the argument of the associated Legendre polynomials, we have omitted it in the Legendre functions for the sake of convenience. Then we find

$$P_{\ell+1}^{m+1} - P_{\ell-1}^{m+1} = (\ell+m)(\ell+m-1)P_{\ell-1}^{m-1} - (\ell-m+2)(\ell-m+1)P_{\ell+1}^{m-1} \tag{C-3}$$

For $m = 1$, $n = \ell + 1$, equation (C-3) becomes

$$P_n^2 - P_{n-2}^2 = n(n-1)P_{n-2}^0 - n(n-1)P_n^0$$

that is

$$\frac{1}{n(n-1)} P_n^2 - P_{n-2}^0 = -P_n^0 + \frac{1}{n(n-1)} P_{n-2}^2 \tag{C-4a}$$

For $m = 1$, $n = \ell + 2$, equation (C-3) becomes

$$P_{n-1}^2 - P_{n-3}^2 = (n-1)(n-2)P_{n-3}^0 - (n-1)(n-2)P_{n-1}^0$$

that is

$$P^0_{n-3} - P^0_{n+1} = \frac{1}{(n-1)(n-2)} P^2_{n-1} - \frac{1}{(n+1)(n-2)} P^2_{n-3} \qquad \text{(C-4b)}$$

For $m = 1$, $n = \ell + 3$, equation (C-3) becomes

$$P^2_{n-2} - P^2_{n-4} = (n-2)(n-3)P^0_{n-4} - (n-2)(n-3)P^0_{n-2}$$

that is

$$P^0_{n-2} - P^0_{n-4} = - \frac{1}{(n-2)(n-3)} P^2_{n-2} + \frac{1}{(n-2)(n+3)} P^2_{n-4} \qquad \text{(C-4c)}$$

For $m = 2$, $n = \ell + 1$, equation (C-3) becomes

$$P^3_n + P^3_{n-2} = (n+1)nP^1_{n-2} - (n-1)(n-2)P^1_n$$

that is

$$\frac{1}{(n+1)n(n-1)(n-2)} P^3_n - \frac{1}{(n-1)(n+2)} P^1_{n-2} = - \frac{1}{n(n+1)} P^1_n$$

$$+ \frac{1}{(n+1)n(n-1)(n-2)} P^3_{n-2} \qquad \text{(C-4d)}$$

For $m = 2$, $n = \ell + 2$, equation (C-3) becomes

$$P^3_{n+1} - P^3_{n-3} = n(n-1)P^1_{n-3} - (n-2)(n-3)P^1_{n-1}$$

that is

$$- \frac{1}{n(n-1)} P^1_{n-1} + \frac{1}{(n-2)(n-3)} P^1_{n-3} = \frac{1}{n(n+1)(n-2)(n-3)} P^3_{n+1}$$

$$- \frac{1}{n(n+1)(n-2)(n-3)} P^3_{n-3} \qquad \text{(C-4e)}$$

For $m = 3$, $n = k + 1$, equation (C-3) becomes

$$P_n^4 - P_{n-2}^4 = (n+2)(n+1)P_{n-2}^2 - (n-2)(n-3)P_n^2$$

that is

$$\frac{1}{(n+2)(n+1)(n-2)(n-3)} P_n^4 - \frac{1}{(n-2)(n-3)} P_{n-2}^2 = - \frac{1}{(n+2)(n+1)} P_n^2$$

$$+ \frac{1}{(n+2)(n+1)(n-2)(n-3)} P_{n-2}^4 \qquad \text{(C-4f)}$$

APPENDIX D

MAGNETIC POTENTIAL AND MAGNETIC FIELD OF O_4 MODEL

Magnetic potential V of O_4 model is

$$V = a \sum_{n=1}^{3} \left(\frac{a}{r}\right)^{n+1} \sum_{m=0}^{n} (g_n^m \cos m\phi + h_n^m \sin m\phi)\overline{P_n^m}(\cos\theta) \qquad \text{(D-1)}$$

where the Schmidt-normalized Legendre polynomials with the argument x are

$$\overline{P_n^0}(x) = P_n(x) \qquad \text{(D-1a)}$$

$$\overline{P_n^m}(x) = \left[\frac{2(n-m)!}{(n+m)!}\right]^{\frac{1}{2}} (1-x^2)^{\frac{m}{2}} \frac{d^m \overline{P_n}(x)}{dx^m} \qquad \text{for } 1 \le m \le n \qquad \text{(D-1b)}$$

and

$$P_1(x) = x = \cos\theta \qquad dP_1(x)/dx = 1 \qquad d^2P_2(x)/dx = 3$$

$$P_2(x) = \frac{1}{2}\,(3x^2-1) \qquad dP_2(x)/dx = 3x \qquad d^2P_3(x)/dx^2 = 15x$$

$$P_3(x) = \frac{1}{2}\,(5x^3-3x) \qquad dP_3(x)/dx = \frac{3}{2}(5x^2-1) \qquad d^3P_3(x)/dx^3 = 15$$

$$\overline{P_1^0}(x) = x \qquad d\overline{P_1^0}(x)/dx = 1$$

$$\overline{P_1^1}(x) = (1-x^2)^{\frac{1}{2}} \qquad d\overline{P_1^1}(x)/dx = -\frac{x}{(1-x^2)^{1/2}}$$

$$\overline{P_2^0}(x) = \frac{1}{2}\,(3x^2-1) \qquad d\overline{P_2^0}(x)/dx = 3x$$

$$\overline{P_2^1}(x) = [3(1-x^2)]^{\frac{1}{2}}x \qquad d\overline{P_2^1}(x)dx = \left[\frac{3}{1-x^2}\right]^{\frac{1}{2}}(1-2x^2)$$

$$\overline{P_2^2}(x) = (\tfrac{3}{4})^{\frac{1}{2}}(1-x^2) \qquad d\overline{P_2^2}(x)/dx = -3^{\frac{1}{2}}x$$

$$\overline{P_3^0}(x) = \tfrac{1}{2}\ (5x^3-3x) \qquad d\overline{P_3^0}(x)/dx = \tfrac{3}{2}\ (5x^2-1)$$

$$\overline{P_3^1}(x) = [\tfrac{3}{8}\ (1-x^2)]^{\frac{1}{2}}(5x^2-1) \qquad d\overline{P_3^1}(x)/dx = \frac{(11x-15x^3)}{[\frac{8}{3}\ (1-x^2)]^{1/2}}$$

$$\overline{P_3^2}(x) = (\tfrac{15}{4})^{\frac{1}{2}}(1-x^2)x \qquad d\overline{P_3^2}(x)/dx = (\tfrac{15}{4})^{\frac{1}{2}}(1-3x^2)$$

$$\overline{P_3^3}(x) = (\tfrac{5}{8})^{\frac{1}{2}}(1-x)^{\frac{3}{2}} \qquad d\overline{P_3^3}(x)/dx = -[\tfrac{45}{8}\ (1-x^2)]^{\frac{1}{2}}x$$

The magnetic field $\vec{B}$ can be obtained from

$$\vec{B} = -\nabla V \tag{D-2}$$

The components of magnetic field $\vec{B}$ in spherical coordinate system are

$$B_r = -\frac{\partial V}{\partial r} = \sum_{n=1}^{3}\ (n+1)(\frac{a}{r})^{n+2} \sum_{m=0}^{n} (g_n^m \cos m\phi + h_n^m \sin m\phi)\overline{P_n^m}(\cos\theta) \tag{D-2a}$$

$$B_\theta = -\frac{1}{r}\frac{\partial V}{\partial \theta} = (\sin\theta) \sum_{n=1}^{3} (\frac{a}{r})^{n+2} \sum_{m=0}^{n} (g_n^m \cos m\phi + h_n^m \sin m\phi) \frac{d\overline{P_n^m}(\theta)}{d\theta} \tag{D-2b}$$

$$B_\phi = -\frac{1}{r\sin\theta}\frac{\partial V}{\partial \phi} = \frac{1}{\sin\theta}\sum_{n=1}^{3} (\frac{a}{r})^{n+2} \sum_{m=0}^{n} m$$

$$(g_n^m \sin m\phi - h_n^m \cos m\phi)\overline{P_n^m}(\cos\theta) \tag{D-2c}$$

where

$\phi = -\lambda_{III}(1965)$,

λ_{III} is the System III longitude

The Jupiter's surface is given simply by

$$\frac{r}{a} = \left(1 + \frac{400}{71372}\right)(1 - \cos^2\theta) \qquad \text{(D-3)}$$

where

$a = 1R_J$,

$\varepsilon = 0.065$ (flattening rate)

Fifteen coefficients of the field for g_n^m and h_n^m were given by Acuña and Ness (1976), as follows

$g_1^0 = 4.216$

$g_1^1 = -0.664$ $\qquad$ $h_1^1 = 0.264$

$g_2^0 = -0.203$

$g_2^1 = -0.735$ $\qquad$ $h_2^1 = -0.469$

$g_2^2 = 0.513$ $\qquad$ $h_2^2 = 0.088$

$g_3^0 = -0.233$

$g_3^1 = -0.076$ $\qquad$ $h_3^1 = -0.580$

$g_3^2 = 0.168$ $\qquad$ $h_3^2 = 0.487$

$g_3^3 = -0.231$ $\qquad$ $h_3^3 = -0.294$ $\qquad$ (D-4)

The relations between the Schmidt-normalized Legendre polynomials and the associated Legendre polynomials are

$$\overline{P_1^0}(x) = P_1^0(x) = \cos\theta \qquad \text{(D-5a)}$$

$$\overline{P_1^1}(x) = P_1^1(x) = \sin\theta \tag{D-5b}$$

$$\overline{P_2^0}(x) = P_2^0(x) = \frac{1}{4}\,(3\cos 2\theta + 1) \tag{D-5c}$$

$$\overline{P_2^1}(x) = \frac{1}{\sqrt{3}}\,P_2^1(x) = \frac{\sqrt{3}}{2}\,\sin 2\theta \tag{D-5d}$$

$$\overline{P_2^2}(x) = \frac{1}{2\sqrt{3}}\,P_2^2(x) = \frac{\sqrt{3}}{4}\,(1 - \cos 2\theta) \tag{D-5e}$$

$$\overline{P_3^0}(x) = P_3^0(x) = \frac{1}{8}\,(5\cos 3\theta + 3\cos\theta) \tag{D-5f}$$

$$\overline{P_3^1}(x) = \frac{1}{\sqrt{6}}\,P_3^1(x) = \sqrt{\frac{3}{2}} \cdot \frac{1}{8}\,(\sin\theta + 5\sin 3\theta) \tag{D-5g}$$

$$\overline{P_3^2}(x) = \frac{1}{2\sqrt{15}}\,P_3^2(x) = \frac{\sqrt{15}}{8}\,(\cos\theta - \cos 3\theta) \tag{D-5h}$$

$$\overline{P_3^3}(x) = \frac{1}{8\sqrt{10}}\,P_3^3(x) = \sqrt{\frac{5}{2}} \cdot \frac{1}{8}\,(3\sin\theta - \sin 3\theta) \tag{D-5i}$$

The components B_r, B_θ, and B_ϕ are

$$B_r = 2\left(\frac{a}{r}\right)^3 T_{r1} + 3\left(\frac{a}{r}\right)^4 T_{r2} + 4\left(\frac{a}{r}\right)^5 T_{r3} \tag{D-6a}$$

$$B_\theta = \left(\frac{a}{r}\right)^3 T_{\theta 1} + \left(\frac{a}{r}\right)^4 T_{\theta 2} + \left(\frac{a}{r}\right)^5 T_{\theta 3} \tag{D-6b}$$

$$B_\phi = \left(\frac{a}{r}\right)^3 T_{\phi 1} + \left(\frac{a}{r}\right)^4 T_{\phi 2} + \left(\frac{a}{r}\right)^5 T_{\phi 3} \tag{D-6c}$$

where

$$T_{r1} = \overline{P_1^0}\,g_1^0 + \overline{P_1^1}\,GH_{11}$$

$$T_{r2} = \overline{P_2^0}\,g_2^0 + \overline{P_2^1}\,GH_{21} + \overline{P_2^2}\,GH_{22}$$

$$T_{r3} = \overline{P_3^0} g_3^0 + \overline{P_3^1} GH_{31} + \overline{P_3^2} GH_{32} + \overline{P_3^3} GH_{33}$$

$$T_{\theta 1} = \overline{P_1^1} g_1^0 - \overline{P_1^0} GH_{11}$$

$$T_{\theta 2} = \sqrt{3}\, \overline{P_2^1}\, g_2^0 - \sqrt{\frac{1}{3}}\, (4\overline{P_2^0} - 1) GH_{21} - \overline{P_2^1} GH_{22}$$

$$T_{\theta 3} = \sqrt{6}\, \overline{P_3^1} g_3^0 - \sqrt{\frac{3}{2}}\, (3\overline{P_3^0} - \overline{P_1^0}) GH_{31}$$

$$- \sqrt{\frac{3}{5}}\, (\sqrt{6}\, \overline{P_3^1} - \overline{P_1^1}) GH_{32} - \sqrt{\frac{3}{2}}\, \overline{P_3^2} GH_{33}$$

$$T_{\phi 1} = \overline{GH_{11}}$$

$$T_{\phi 2} = \sqrt{3}\, \overline{P_1^0}\, \overline{GH_{21}} + \sqrt{3}\, \overline{P_1^1}\, \overline{GH_{22}}$$

$$T_{\phi 3} = \sqrt{\frac{1}{6}}\, (5\overline{P_2^0} + 1) \overline{GH_{31}} + \sqrt{5}\, \overline{P_2^1}\, \overline{GH_{32}} + \sqrt{\frac{15}{2}}\, \overline{P_2^2}\, \overline{GH_{33}}$$

and

$$GH_{11} = g_1^1 \cos\phi + h_1^1 \sin\phi \qquad \overline{GH_{11}} = g_1^1 \sin\phi - h_1^1 \cos\phi$$

$$GH_{21} = g_2^1 \cos\phi + h_2^1 \sin\phi \qquad \overline{GH_{21}} = g_2^1 \sin\phi - h_2^1 \cos\phi$$

$$GH_{22} = g_2^2 \cos 2\phi + h_2^2 \sin 2\phi \qquad \overline{GH_{22}} = g_2^2 \sin 2\phi - h_2^2 \cos 2\phi$$

$$GH_{31} = g_3^1 \cos\phi + h_3^1 \sin\phi \qquad \overline{GH_{31}} = g_3^1 \sin\phi - h_3^1 \cos\phi$$

$$GH_{32} = g_3^2 \cos 2\phi + h_3^2 \sin 2\phi \qquad \overline{GH_{32}} = g_3^2 \sin 2\phi - h_3^2 \cos 2\phi$$

$$GH_{33} = g_3^3 \cos 3\phi + h_3^3 \sin 3\phi \qquad \overline{GH_{33}} = g_3^3 \sin 3\phi - h_3^3 \cos 3\phi$$

APPENDIX E

SIGN TREATMENT FOR PARAMETERS OF FIVE-DIPOLE IN THE COMPUTATION

During the computation of solving 24 equations given in (B-53a)-(B-53x) of Appendix B, which contain 24 parameters of 4 dipoles, we have the following sign treatment in order to get the significant parameters

(1) if replacing $-r_o$ by $+r_o$, we have to change ϕ_o into $\phi + 180°$, δ into $-\delta$;

(2) if replacing δ by $180° - \delta$, we have to change ϕ_o into $\phi + 180°$,

(3) if replacing θ_o by $180° - \theta_o$, we have to change M into -M, ϕ_o into $\phi_o + 180°$, and λ_o into $\lambda_o + 180°$

APPENDIX F

EQUATIONS OF MAGNETIC FIELD LINE FOR SINGLE DIPOLE

In Figure A-1, we can find that the magnetic field $\vec{B}$ of single dipole in plane X*O'Z* is

$$\vec{B} = \frac{3\bar{r}_e(\bar{r}_e \vec{M}) - \vec{M}}{r_e^3} \qquad \text{(F-1)}$$

The components B_r, B_θ, and B_ϕ of the magnetic field $\vec{B}$ in the directions $\bar{r}_e$, $\bar{\theta}^*$, and $\bar{\phi}^*$ are

$$B_r = \frac{3M\cos\theta^* - M\cos\theta^*}{r_e^3} = \frac{2M\cos\theta^*}{r_e^3} \qquad \text{(F-1a)}$$

$$B_\theta = \frac{0 - M(-\sin\theta^*)}{r_e^3} = \frac{M\sin\theta^*}{r_e^3} \qquad \text{(F-1b)}$$

$$B_\phi = 0 \qquad \text{(F-1c)}$$

Thus, the magnetic field strength B can be written as

$$B = (B_r^2 + B_\theta^2 + B_\phi^2)^{1/2} = \frac{M}{r_e^3}\sqrt{4 - 3\sin^2\theta^*} \qquad \text{(F-2)}$$

The equations of magnetic field line in plane X*O'Z* are given by

$$r_e = L\sin^2\theta^* \qquad \text{(F-3a)}$$

$$\phi^* = \text{constant} \qquad \text{(F-3b)}$$

$$B = \frac{M}{r_e^3}\sqrt{4 - 3\sin^2\theta^*} \tag{F-3c}$$

where L denotes the major axis of shell with certain number. The radial distance r can be found in (A-8a)

$$r = r_e/[1 - 2(\frac{r_e}{r})x + (\frac{r_e}{r})^2]^{\frac{1}{2}} \tag{F-4}$$

where x is defined in (A-22). Substituting (F-3a) and (A-8b) into (F-4), we can get

$$r = L\frac{[(D^2+E^2) - 2(\frac{r_e}{r})(A\cdot D+B\cdot E) + (\frac{r_e}{r})^2(A^2+B^2)]}{[1 - 2(\frac{r_e}{r})x + (\frac{r_e}{r})^2]^{3/2}} \tag{F-5}$$

where A, B, D, and E are given in (A-2a)-(A-4b)

For the sub-Io position, we use

$$\phi = \phi_{Io} \tag{F-6a}$$

$$\theta = 90° \tag{F-6b}$$

$$r = a_{Io} \tag{F-6c}$$

where

ϕ_{Io} is the longitude of Io as measured eastward from X-axis,

a_{Io} is the distance of Io from Jupiter.

With the substitution of $\phi = \phi_{Io}$, $\theta = 90°$, $r = a_{Io}$, from (F-5) we can obtain

$$L = \frac{a_{Io}\left\{1 - 2(\frac{r_e}{a_{Io}})[\cos\delta\cos(\phi_{Io}-\phi_o)] + (\frac{r_e}{a_{Io}})^2\right\}^{3/2}}{(\sin^2\phi_{Io}+\cos^2\theta_o\cos^2\phi_{Io}) - 2(\frac{r_e}{a_{Io}})[A(-\cos\theta_o\cos\phi_{Io})+B\sin\phi_{Io}] + (\frac{r_e}{a_{Io}})^2(A^2+B^2)} \tag{F-7}$$

Applying (A-8a) and (A-8c) to (F-3a) gives

$$\tan\phi^* = \frac{\sin\phi^*}{\cos\phi^*} = \frac{r\, E - r_o\, B}{-r\, D + r_o\, A} = \frac{E - \frac{r_o}{r}\, B}{-D + \frac{r_o}{r}\cdot A} = \text{constant} \tag{F-8}$$

Thus, for the Io flux tube, substitution of (F-6a)-(F-6c) into (F-8) leads us to

$$\frac{\sin\phi_{Io} - \frac{r_o}{a_{Io}}\cdot B}{\cos\theta_o \cos\phi_{Io} + \frac{r_o}{a_{Io}}\cdot A} = \frac{E - \frac{r_o}{r}\, B}{-D + \frac{r_o}{r}\, A} \tag{F-9}$$

Therefore, the expressions (F-3a)-(F-3c) in X*Y*Z* system can be converted into the following ones in XYZ system

$$r = L\, \frac{[(D^2+E^2) - 2(\frac{r_o}{r})(A\cdot D+B\cdot E) + (\frac{r_o}{r})^2(A^2+B^2)]}{[1 - 2(\frac{r_o}{r})x + (\frac{r_o}{r})^2]^{3/2}} \tag{F-10a}$$

$$\frac{\sin\phi_{Io} - \frac{r_o}{a_{Io}}\cdot B}{\cos\theta_o \cos\phi_{Io} + \frac{r_o}{a_{Io}}\cdot A} = \frac{E - \frac{r_o}{r}\cdot B}{-D + \frac{r_o}{r}\, A} \tag{F-10b}$$

$$B = \frac{M}{\left\{r[1 - 2(\frac{r_o}{r})x + (\frac{r_o}{r})^2]^{1/2}\right\}^3}$$

$$\sqrt{4 - 3\,\frac{[(D^2+E^2) - 2(\frac{r_o}{r})(A\cdot D+B\cdot E) + (\frac{r_o}{r})^2(A^2+B^2)]}{1 - 2(\frac{r_o}{r})x + (\frac{r_o}{r})^2}} \tag{F-10c}$$

These equations can be used for solving the spherical coordinates (r, θ, ϕ) of a point with a certain magnetic field strength, which is located on the Io flux tube, so that the magnetic field for single dipole is reasonably considered as the first approximation of Jupiter's magnetic field

APPENDIX G

ISOCONTOUR OF MAGNETIC FIELD STRENGTH

1. Evaluation of Spherical Coordinates (r, θ_s, ϕ_s) of Isocontour for Single Dipole

For the first approximation, with ignoring the offset r_o of single dipole, the equations (F-7), (F-10a), (F-10b), and (F-10c) become

$$L = \frac{e_{Io}}{\sin^2\phi_{Io} + \cos^2\theta_o \cos^2\phi_{Io}} \tag{G-1}$$

$$r = L(D^2 + E^2) \tag{G-1a}$$

$$-D\sin\phi_{Io} = E\cos\theta_o \cos\phi_{Io} \tag{G-1b}$$

$$B = \frac{M}{r^3}\sqrt{4 - 3(D^2+E^2)} \tag{G-1c}$$

Combination of (G-1a) and (G-1c) yields

$$\left(\frac{BL^3}{M}\right)^2 (D^2+E^2)^6 + 3(D^2+E^2) - 4 = 0 \tag{G-2}$$

The solution of equation (G-2) is the function of parameters θ_o, M, B of single dipole, orbital distance e_{Io} and sub-Io longitude ϕ_{Io}, named by

$$D^2 + E^2 = S \tag{G-3}$$

(1) for $\phi_{Io} = 0°$, (G-1b) leads to $E = 0$, back to (A-4b), it is easy to get

$$\theta_s = 0° \qquad \text{(G-4a)}$$

while $\theta_o = 90°$, (A-4a) gives $D = -\cos\theta_o < 0$, so, we only can take the negative root of S for D. That is

$$D = -\sqrt{S} \qquad \text{(G-4b)}$$

while $\theta_o \neq 90°$, regulation for sign of D is still valid, (A-4a) gives

$$D = \sin(\theta_o - \theta_s) = -\sqrt{S}$$

then

$$\theta_s = \sin^{-1}\sqrt{S} - \theta_o \qquad \text{(G-4c)}$$

(2) for $\phi_{Io} \neq 0°$, (G-1b) leads to

$$D = -\frac{\cos\theta_o \cos\phi_{Io}}{\sin\phi_{Io}} E \qquad \text{(G-5)}$$

Substituting (G-5) into (G-3), we get

$$E = \sqrt{\frac{S\sin^2\phi_{Io}}{\sin^2\phi_{Io} + \cos^2\theta_o \cos^2\phi_{Io}}}$$

There are two cases

$$\text{if } \sin\phi_{Io} > 0, \text{ then } E = \sqrt{\frac{S}{\sin^2\phi_{Io} + \cos^2\theta_o \cos^2\phi_{Io}}}\,\sin\phi_{Io} \qquad \text{(G-6a)}$$

$$\text{if } \sin\phi_{Io} < 0, \text{ then } E = -\sqrt{\frac{S}{\sin^2\phi_{Io} + \cos^2\theta_o \cos^2\phi_{Io}}}\,\sin\phi_{Io} \qquad \text{(G-6b)}$$

From (A-5), we have

$$F = \sqrt{1 - (D^2+E^2)} \qquad (G\text{-}7)$$

For Jovian northern hemisphere, if $r \leq a_{Io}$, there exists

$$\cos\theta_s \cos\theta_o + \sin\theta_s \sin\theta_o \cos\phi_s \geq 0 \qquad (G\text{-}8)$$

From (A-4a), (A-4c), and (G-7), there is

$$\cos\theta_s = D\sin\theta_o + F\cos\theta_o \qquad (G\text{-}8a)$$

then

$$\sin\theta_s = \sqrt{1 - \cos^2\theta_s} \qquad (G\text{-}8b)$$

From (A-4b), we get

$$\sin\phi_s = \frac{E}{\sin\theta_s} \qquad (G\text{-}8c)$$

From (A-4a), (A-4c), and (G-7) again, there is

$$\cos\phi_s = \frac{-D\cos\theta_o + F\sin\theta_o}{\sin\theta_s} \qquad (G\text{-}8d)$$

Same steps as before, for Jovian southern hemisphere, if $r \leq a_{Io}$, there exists

$$\cos\theta_s \cos\theta_o + \sin\theta_s \sin\theta_o \cos\phi_s \leq 0 \qquad (G\text{-}9)$$

then

$$\cos\theta_s = D\sin\theta_o - F\cos\theta_o \qquad (G\text{-}9a)$$

$$\sin\theta_s = \sqrt{1 - \cos^2\theta_s} \qquad (G\text{-}9b)$$

$$\sin\phi_s = \frac{E}{\sin\theta_s} \tag{G-9c}$$

$$\cos\phi_s = \frac{-D\cos\theta_s - F\sin\theta_s}{\sin\theta_s} \tag{G-9d}$$

Thus, in both cases, θ_s and ϕ_s are solvable, and the radial distance is

$$r = L(D^2+E^2) = L\cdot S \tag{G-10}$$

Therefore, the spherical coordinates $r^{(1)}$, $\theta_s^{(1)}$, and $\phi_s^{(1)}$ are complete for the first approximation of single dipole.

Considering the offset r_o of single dipole, we can solve the equations (F-10a), (F-10b), and (F-10c) by using initial solutions $r^{(1)}$, $\theta_s^{(1)}$, and $\phi_s^{(1)}$ obtained from the first approximation; then, we can get the spherical coordinates $r^{(2)}$, $\theta_s^{(2)}$, and $\phi_s^{(2)}$ for the second approximation.

2. Computation of Spherical Coordinates (r, θ, ϕ) of Isocontour for Five-Dipole

(1) Magnetic field strength and its components for five-dipole

From (A-21), the magnetic potential V for five-dipole can be evaluated by making the sum of single dipole from i = 1 to i = 5, that is

$$V = \sum_i \frac{M}{r^2} \frac{(F - \frac{r_o}{r}\cdot C)}{[1 - 2(\frac{r_o}{r})x + (\frac{r_o}{r})^2]^{3/2}} \tag{G-11}$$

where we have omitted the subscript i for r_o, M, and parameters contained in terms x, F, and C, from (B-48a) and (B-48b), for each dipole, we have

$$\theta_s = \text{[illegible]} \qquad \text{(G-11a)}$$

$$\phi_s = \phi + \lambda_o \qquad \text{(G-11b)}$$

where we have omitted the subscript i for λ_o too. For the purpose of simplicity, we assume

$$K(r) = 1 - 2\left(\frac{r_o}{r}\right)x + \left(\frac{r_o}{r}\right)^2 \qquad \text{(G-12)}$$

The components of magnetic field strength B are

$$B_r = \sum_i \left(-\frac{\partial V_i}{\partial r}\right) = -\sum_i V_i \frac{\partial \ln V_i}{\partial r}$$

$$= \sum_i \frac{V_i}{r}\left[2 - \frac{\frac{r_o}{r}\,C}{F - \frac{r_o}{r}\,C} + 3\,\frac{\frac{r_o}{r}\cdot x - \left(\frac{r_o}{r}\right)^2}{K(r)}\right] \qquad \text{(G-13)}$$

$$B_\theta = \sum_i \left(-\frac{\partial V_i}{r\partial\theta}\right) = -\sum_i V_i \frac{\partial \ln V_i}{r\partial\theta}$$

$$= \sum_i \frac{V_i}{r}\left[\frac{-U}{F - \frac{r_o}{r}\,C} - 3\,\frac{\frac{r_o}{r}\cdot y}{K(r)}\right] \qquad \text{(G-14)}$$

where

$$U = -\sin\theta\cos\theta_o + \cos\theta\sin\theta_o\cos\phi_s \qquad \text{(G-14a)}$$

$$y = -\sin\theta\sin\theta + \cos\theta\cos\theta\cos(\phi_s - \phi_o) \qquad \text{(G-14b)}$$

$$B_\phi = \sum_i \left(-\frac{\partial V_i}{r\sin\theta\partial\phi}\right) = -\sum_i V_i \frac{\partial \ln V_i}{r\sin\theta\partial\phi}$$

$$= \sum_i \frac{V_i}{r}\left[\frac{-W}{F - \frac{r_o}{r}\cdot C} - 3\,\frac{\frac{r_o}{r}\,z}{K(r)}\right] \qquad \text{(G-15)}$$

where

$$W = -\sin\theta_s \sin\phi_s \qquad \text{(G-15a)}$$

$$z = -\cos\delta\sin(\phi_s - \phi_o) \qquad \text{(G-15b)}$$

Even in the Jovian near field, we still can neglect the $(\frac{r_o}{r})^2$ terms in components B_r, B_θ, B_ϕ, and their subsequent derivatives without appreciable loss of accuracy. Thus, substituting magnetic potential V_i into (G-13)-(G-15), we can rewrite them as

$$B_r = \sum_i \frac{M}{r^3}\left[\frac{2F - \frac{r_o}{r}(3C + F\cdot x)}{K(r)^{5/2}}\right] \qquad \text{(G-16)}$$

$$B_\theta = \sum_i \frac{M}{r^3}\left[\frac{-U + \frac{r_o}{r}(2U\,x - 3F\,y)}{K(r)^{5/2}}\right] \qquad \text{(G-17)}$$

$$B_\phi = \sum_i \frac{M}{r^3}\left[\frac{-W + \frac{r_o}{r}(2W\,x - 3F\,z)}{K(r)^{5/2}}\right] \qquad \text{(G-18)}$$

(2) Taylor expansion of magnetic field strength B for five-dipole

If considering the second approximation $r^{(2)}$, $\theta_s^{(2)}$, $\phi_s^{(2)}$ as the initial solutions for contour of magnetic field strength B, then we can expand B at $(r^{(2)}, \theta_s^{(2)}, \phi_s^{(2)})$ in Taylor series with the first order derivatives, as follows

$$B(\text{constant}) = B(r^{(2)},\theta_s^{(2)},\phi_s^{(2)}) + \frac{\partial B}{\partial r}(r-r^{(2)})$$

$$+ \frac{\partial B}{\partial \theta}(\theta-\theta_s^{(2)}) + \frac{\partial B}{\partial \phi}(\phi-\phi_s^{(2)}) \tag{G-19}$$

and equation for magnetic field line is

$$\frac{B_r}{dr} = \frac{B_\theta}{rd\theta} = \frac{B_\phi}{r\sin\theta d\phi} \tag{G-20}$$

Thus, we get the following approximation

$$r-r^{(2)} \cong dr = \frac{B_r}{B_\theta} rd\theta \cong \frac{B_r}{B_\theta} r^{(2)}(\theta-\theta_s^{(2)}) \tag{G-21a}$$

$$\phi-\phi_s^{(2)} \cong d\phi = \frac{B_\phi}{\sin\theta B_\theta} d\theta \cong \frac{B_\phi}{\sin\theta_s^{(2)} B_\theta}(\theta-\theta_s^{(2)}) \tag{G-21b}$$

Substituting (G-21a) and (G-21b) into (G-19), we obtain

$$\Delta\theta = \theta-\theta_s^{(2)} = \left.\frac{B-B_{(r,\theta,\phi)}}{r\left(\frac{\partial B}{\partial r}\frac{B_r}{B_\theta} + \frac{\partial B}{r\partial\theta} + \frac{\partial B}{r\sin\theta\partial\phi}\cdot\frac{B_\phi}{B_\theta}\right)}\right|_{\substack{r = r^{(2)} \\ \theta = \theta_s^{(2)} \\ \phi = \phi_s^{(2)}}} \tag{G-22}$$

this implies that

$$\theta = \theta_s^{(2)} + \Delta\theta \tag{G-22a}$$

$$r = r_s^{(2)} + \frac{B_r}{B_\theta} r_s^{(2)} \cdot\Delta\theta \tag{G-22b}$$

$$\phi = \phi_s^{(2)} + \frac{B_\phi}{\sin\theta_s^{(2)} B_\theta} \cdot\Delta\theta \tag{G-22c}$$

Using iteration of (G-22), we can finally get the spherical coordinates (r, θ, ϕ) of contour of magnetic field strength for five-dipole.

(3) Derivatives of magnetic field strength and its components

$$\frac{\partial B}{\partial r} = \frac{1}{B}\left(B_r \frac{\partial B_r}{\partial r} + B_\theta \frac{\partial B_\theta}{\partial r} + B_\phi \frac{\partial B_\phi}{\partial r}\right) \tag{G-23a}$$

$$\frac{\partial B}{r\partial\theta} = \frac{1}{B}\left(B_r \frac{\partial B_r}{r\partial\theta} + B_\theta \frac{\partial B_\theta}{r\partial\theta} + B_\phi \frac{\partial B_\phi}{r\partial\theta}\right) \tag{G-23b}$$

$$\frac{\partial B}{r\sin\theta\partial\phi} = \frac{1}{B}\left(B_r \frac{\partial B_r}{r\sin\theta\partial\phi} + B_\theta \frac{\partial B_\theta}{r\sin\theta\partial\phi} + B_\phi \frac{\partial B_\phi}{r\sin\theta\partial\phi}\right) \tag{G-23c}$$

and

$$\frac{\partial B_r}{\partial r} = -3 \sum_i \left[\frac{B_r}{r} - \frac{M}{r^4}\left(\frac{r_0}{r}\right) \frac{(C - 3F \cdot x)}{K(r)^{7/2}}\right] \tag{G-24a}$$

$$\frac{\partial B_\theta}{\partial r} = -3 \sum_i \left[\frac{B_\theta}{r} - \frac{M}{r^4}\left(\frac{r_0}{r}\right) \frac{(U \cdot x + F \cdot y)}{K(r)^{7/2}}\right] \tag{G-24b}$$

$$\frac{\partial B_\phi}{\partial r} = -3 \sum_i \left[\frac{B_\phi}{r} - \frac{M}{r^4}\left(\frac{r_0}{r}\right) \frac{(W \cdot x + F \cdot z)}{K(r)^{7/2}}\right] \tag{G-24c}$$

$$\frac{\partial B_r}{\partial \theta} = \sum_i \frac{M}{r^3} \left[\frac{2U - \frac{r_0}{r}(5U \cdot x - 9F \cdot y)}{K(r)^{7/2}}\right] \tag{G-25a}$$

$$\frac{\partial B_\theta}{\partial \theta} = \sum_i \frac{M}{r^3} \left[\frac{F - \frac{r_0}{r}(6U \cdot y + F \cdot x)}{K(r)^{7/2}}\right] \tag{G-25b}$$

$$\frac{\partial B_\phi}{\partial \theta} = \sum_i \frac{M}{r^3} \left[\frac{-3\frac{r_0}{r}(U \cdot z + W \cdot y)}{K(r)^{7/2}}\right] \tag{G-25c}$$

$$\frac{\partial B_r}{\partial \phi} = \sum_i \frac{M}{r^3} \sin\theta \left[\frac{2W - \frac{r_s}{r}(5W\,x - 9F\cdot r)}{K(r)^{7/2}}\right] \qquad \text{(G-26a)}$$

$$\frac{\partial B_\theta}{\partial \phi} = \sum_i \frac{M}{r^3} \left[\frac{-W\cos\theta + \frac{r_s}{r}(4W\cdot x - 3F\cdot z)\cos\theta - 3\frac{r_s}{r}(U\cdot x + W\,y)\sin\theta}{K(r)^{7/2}}\right] \qquad \text{(G-26b)}$$

$$\frac{\partial B_\phi}{\partial \phi} = \sum_i \frac{M}{r^3} \left[\frac{-T + \frac{r_s}{r}(4T\cdot x - 3F\,z - 6W\cdot s\sin\theta)}{K(r)^{7/2}}\right] \qquad \text{(G-26c)}$$

where

$$T = -\sin\theta_s\cos\phi_s$$

$$W = -\cos\theta\cos(\phi_s - \phi_o)$$

Following are the differential relations among F, U, W, T, and x, y, z, s

$$\frac{\partial F}{\partial \theta} = U \qquad \frac{\partial x}{\partial \theta} = y$$

$$\frac{\partial F}{\partial \phi} = W\sin\theta \qquad \frac{\partial x}{\partial \phi} = z\sin\theta$$

$$\frac{\partial^2 F}{\partial \theta^2} = -F \qquad \frac{\partial^2 x}{\partial \theta^2} = -x$$

$$\frac{\partial^2 F}{\partial \theta \partial \phi} = W\cos\theta \qquad \frac{\partial^2 x}{\partial \theta \partial \phi} = z\cos\theta$$

$$\frac{\partial^2 F}{\partial \phi^2} = T\sin\theta \qquad \frac{\partial^2 x}{\partial \phi^2} = s\sin\theta$$

APPENDIX H

DERIVATION FOR DRIFT RATE OF S BURST

Directional derivative of magnetic field strength B along the magnetic field line is

$$\frac{dB}{ds} = \nabla B \cdot \frac{\vec{B}}{B} \tag{H-1}$$

and

$$\nabla B = \frac{\nabla(B^2)}{2B} = \frac{\nabla(\vec{B}\cdot\vec{B})}{2B} \tag{H-2}$$

From (A-16), magnetic field of five-dipole can be represented by

$$\vec{B} = \sum_i \frac{3\hat{r}_s(\hat{r}_s\cdot\vec{M}_i) - \vec{M}_i}{r_s^3} \tag{H-3}$$

where

$\vec{M}_i$ denotes the magnetic moment vector of ith dipole,

r_s denotes the radial distance from the center of ith dipole to the given point P.

Since the offset r_o of each dipole is very small compared with the Jovicentric radial distance r, we can assume that the radial distance r_s from each dipole is equal to r. This establishes that

$$\vec{B} = \frac{1}{r^3}\,[3\hat{r}(\hat{r}\cdot\sum_i \vec{M}_i) - (\sum_i \vec{M}_i)] \tag{H-4a}$$

and

$$\vec{B}\cdot\vec{B} = \frac{1}{r^6}\,[3(\hat{r}\cdot\sum_i \vec{M}_i) + (\sum_i \vec{M}_i)^2] \qquad \text{(H-4b)}$$

Furthermore, from (A-20), magnetic potential V can be simplified to

$$V = \sum_i \frac{\hat{r}\cdot\vec{M}_i}{r^2} = \frac{\hat{r}}{r^2}\cdot(\sum_i \vec{M}_i) \qquad \text{(H-5)}$$

With the help of (H-5), (H-4b) can be written as

$$\vec{B}\cdot\vec{B} = \frac{1}{r^6}\,[3V^2r^4 + (\sum_i \vec{M}_i)^2] = \frac{3V^2}{r^2} + \frac{(\sum_i \vec{M}_i)^2}{r^6} \qquad \text{(H-6)}$$

Tracing back to the equations of equating magnetic scalar potentials in (B-53a)-(B-53c), we have the following relations

$$\sum_i M_i\cos\theta_o = g_1^0 = M_1\cos\theta_o \qquad \text{for z component} \qquad \text{(H-7a)}$$

$$\sum_i M_i\sin\theta_o\cos\lambda_o = g_1^1 = M_1\sin\theta_o\cos\lambda_o \qquad \text{for longitudinal component} \qquad \text{(H-7b)}$$

$$\sum_i M_i\sin\theta_o(-\sin\lambda_o) = h_1^1 = M_1\sin\theta_o(-\sin\lambda_o) \qquad \text{for azimuthal component} \qquad \text{(H-7c)}$$

where we denote θ_o and λ_o instead of $\theta_o(i)$ and $\lambda_o(i)$ for each dipole on left-hand side, denote same θ_o and λ_o instead of $\theta_o(1)$ and $\lambda_o(1)$ for "main dipole" on right-hand side for the sake of convenience.

Equations (H-7a)-(H-7c) indicate the equivalent relation

$$\sum_i \vec{M}_i = \vec{M}_1 \qquad \text{(H-8)}$$

where $\vec{M}_1$ is the magnetic moment vector of "main dipole." As a result, (M-4a), (M-4b), and (M-5) become

$$\vec{B} = \frac{3\hat{r}(\hat{r}\ \vec{M}_1)}{r^3} - \frac{\vec{M}_1}{r^3} \qquad \text{(M-9a)}$$

$$\vec{B}\cdot\vec{B} = \frac{3V^2}{r^2} + \frac{(M_1)^2}{r^6} \qquad \text{(M-9b)}$$

$$V = \frac{\hat{r}\cdot\vec{M}_1}{r^2} \qquad \text{(M-9c)}$$

Substituting (M-9b) into (M-2), for the term $\nabla(\vec{B}\ \vec{B})$ we get

$$\nabla(\vec{B}\cdot\vec{B}) = \frac{6V\nabla V}{r^2} + 3V^2\nabla(\frac{1}{r^2}) + (M_1)^2\nabla(\frac{1}{r^6})$$

$$= -\frac{6V\vec{B}}{r^2} - \frac{6V^2\hat{r}}{r^3} - \frac{6(M_1)^2\hat{r}}{r^7} \qquad \text{(M-10)}$$

Given (M-2), (M-9a), (M-9b), and (M-9c), the directional derivative in (M-1) is

$$\frac{dB}{ds} = \frac{1}{2B^2}\ [\nabla(\vec{B}\ \vec{B})]\cdot\vec{B}$$

$$= \frac{1}{2B^2} \times 6\left\{\frac{B^2V}{r^2} + [\frac{V^2}{r^3} + \frac{(M_1)^2}{r^7}]\hat{r}\cdot[\frac{3\hat{r}(r\ \vec{M}_1) - \vec{M}_1}{r^3}]\right\}$$

$$= -\frac{3V}{r^2} - \frac{6}{B^2}\left[\frac{V^2}{r^6} + \frac{(M_1)^2}{r^{10}}\right] \quad (r\ \vec{M}_1)$$

$$= -\frac{3V}{r^2} - \frac{6}{B^2}\left[\frac{V^2}{r^6} + \frac{(M_1)^2}{r^{10}}\right] \quad \nabla r^2$$

$$= -\frac{3V}{r^2} - \frac{6V^3}{B^2 r^4} - \frac{6V}{B^2 r^8} \cdot (M_1)^2$$

$$= -\frac{3V}{r^2} - \frac{6V^3}{B^2 r^4} - \frac{6V}{B^2 r^8} \left(B^2 - \frac{3V^2}{r^2}\right) r^6$$

$$= -\frac{9V}{r^2} + \frac{12V^3}{B^2 r^4} \qquad \text{(H-11)}$$

From (H-9b), magnetic potential V can be written as

$$V = \sum_i V_i = \frac{r}{\sqrt{3}} \sqrt{B^2 - \frac{(M_1)^2}{r^6}} \qquad \text{(H-12)}$$

Substituting (H-12) into (H-11), we finally arrive at

$$\frac{dB}{ds} = -\frac{9}{\sqrt{3}r} \sqrt{B^2 - \frac{(M_1)^2}{r^6}} + \frac{4}{\sqrt{3}B^2 r} \left[B^2 - \frac{(M_1)^2}{r^6}\right]^{3/2} \qquad \text{(H-13)}$$

Known $\frac{dB}{ds}$, the drift rate of S burst can be immediately obtained from

$$\frac{df_c}{dt} = 2.8 \frac{dB}{ds} V_{||} \qquad \text{(H-14)}$$

where $V_{||}$ is the velocity of electron parallel to the magnetic field $\vec{B}$, f_c is the electron cyclotron frequency;

APPENDIX I

D_E LIMITS AND BOUNDARIES OF IO PHASE AND CML FOR SOURCES A AND B

The upper and lower limits of declination of Earth (D_E) during the period from 1960 to June 1966 as found from Table III-3 are as follows:

(1) Io-A source

$D_E = -0.62°$ on July 18, 1961

$D_E = +3.00°$ on Sept. 10, 1963

The emission events for D_E value of $-0.66°$ on Aug. 12, 1961, and Oct. 31, 1961, are not available because they were not observed within the frequency range 35-36 MHz on these days.

(2) Io-B source

$D_E = -0.72°$ on May 11, 1961, and on Sept. 28, 1961.

The emission events for D_E value of $-1.32°$ on Feb. 13, 1961, are not available for the same reasons mentioned above.

The boundaries of Io phase and CML during the above period are as follows:

For the Io-B source, the maximum of γ_{Io} is 107.3° (upper cutoff), corresponding to a range of CML values from 102.7° to 190.4°. For the same source, the minimum of γ_{Io} is 77.1° (lower cutoff), corresponding to CML values from 100.1° to 186.3°.

REFERENCES

Acuña, M.H., Behannon, K.W., and Connerney, J.E.P. 1983, in *Physics of the Jovian Magnetosphere*, ed. A.J. Dessler [Cambridge: Cambridge University Press], p. 4.

Acuña, M.H., and Ness, N.F. 1976, *J. Geophys. Res.*, 81, 2917.

Alexander, J.K. 1975, *Astrophys. J.*, 195, 227.

Bagenal, F. 1983, *J. Geophys. Res.*, 88, 3013.

Bigg, E.K. 1964, *Nature*, 203, 1008.

Burke, B.F., and Franklin, K.L. 1955, *J. Geophys. Res.*, 60, 213.

Carr, T.D., and Desch, M.D. 1976, in *Jupiter*, ed. T. Gehrels [Tucson: University of Arizona Press], p. 693.

Carr, T.D., Desch, M.D., and Alexander, J.K. 1983, in *Physics of the Jovian Magnetosphere*, ed. A.J. Dessler [Cambridge: Cambridge University Press], p. 226.

Davis, L., Jr., Jones, D.E., and Smith, E.J. 1975, Presented at AGU Fall Meeting, San Francisco, California.

Drell, S.D., Foley, H.M., and Ruderman, M.A. 1965, *J. Geophys. Res.*, 70, 3131.

Dulk, G.A. 1965, Ph.D. dissertation, University of Colorado, Boulder, Colorado.

Dulk, G.A. 1967, *Icarus*, 7, 173.

Flagg, R.S., and Desch, M.D. 1979, *J. Geophys. Res.*, 84, 4238.

Franklin, K.L., and Burke, B.F. 1956, *Astron. J.*, 61, 177.

Garnavich, P.M. 1983, M.S. thesis, Massachusetts Institute of Technology, Cambridge, Massachusetts.

Goldreich, P., and Lynden-Bell, D. 1969, *Astrophys. J.*, 156, 59.

Goldstein, M.L., and Goertz, C.K. 1983, in *Physics of the Jovian Magnetosphere*, ed. A.J. Dessler [Cambridge: Cambridge University Press], p. 317.

Goldstein, M.L., Sharma, R.R., Ben-Ari, M., Eviatar, A., and Papadopoulos, K. 1983, J. Geophys. Res., 88, 792

Goldstein, M.L., and Thieman, J.R. 1981, J. Geophys. Res., 86, 8569.

Gulkis, S., and Carr, T.D. 1966, Science, 154, 257.

Gurnett, D.A., and Goertz, C.K. 1981, J. Geophys. Res., 86, 717.

Harris, E.G. 1969, in Physics of Hot Plasma ed. B.J. Rye and J.C. Taylor (Edinburgh: Oliver and Boyd), p. 145.

Hashimoto, K., and Goldstein, M.L. 1983, J. Geophys. Res., 88, 2010.

Maeda, K., and Carr, T.D. 1984, Nature, 308, 168.

Maeda, K., and Carr, T.D. 1985, Paper in preparation.

McClain, E.F., and Sloanaker, R.M. 1959, Proceedings IAU Symposium No. 9—URSI Symposium No. 1, ed. R. Bracewell (Stanford: Stanford University Press), p. 61

Piddington, J.H. 1967, University of Iowa Report, p. 87

Sloanaker, R.M. 1959, Astron. J., 64, 346.

Thieman, J.R. 1977, Ph.D. dissertation, University of Florida, Gainesville, Florida.

Thieman, J.R., and Smith, A.G. 1979, J. Geophys. Res., 84, 2862.

Warwick, J.W. 1961, Ann. N.Y. Acad. Sci., 95, 39.

Warwick, J.W. 1964, Ann. Rev. Astron. Astrophys., 2, 1

Warwick, J.W., Dulk, G.A., and Riddle, A.C. 1975, Jupiter Radio Emission: January 1960–March 1975 (Radio Astronomy Observatory Report), University of Colorado, Boulder, Colorado.

Wilson, R.G., Warwick, J.W., and Libby, W.F. 1968, Nature, 220, 1215.

BIOGRAPHICAL SKETCH

Wan-xiao Wang was born on January 2, 1946, in Ninghai, Chekiang, China. He studied optics at Chekiang University, Hangchow, Chekiang, the degree equivalent to Bachelor of Science was conferred in July 1968.

He married Ne-na Tiao in July 1970, and they now have two sons, Xiao-hui and Han-hui.

He began his graduate studies at the Graduate School, the University of Science and Technology of China, in October 1978, pursuing research in radio astronomy. In January 1981, he came to the Department of Astronomy of the University of Florida. From June 1982 on, he spent more than two years in the processing and the analysis of Jupiter data obtained from Voyager 1 and Voyager 2, in constructing 5-dipole model—an alternative representation of Jovian O_4 magnetic field, and in applying this model to Jupiter's decametric emission. In addition, he is working on the theory and experimentation for the electromagnetic scattering at the Space Astronomy Laboratory, the University of Florida. The degree of Master of Science was conferred in December 1982 and the degree of Doctor of Philosophy was awarded in May 1985, both by the University of Florida.

I certify that I have read this study and that in my opinion it conforms to acceptable standards of scholarly presentation and is fully adequate, in scope and quality, as a dissertation for the degree of Doctor of Philosophy.

Thomas D. Carr

Thomas D. Carr, Chairman
Professor of Astronomy

I certify that I have read this study and that in my opinion it conforms to acceptable standards of scholarly presentation and is fully adequate, in scope and quality, as a dissertation for the degree of Doctor of Philosophy.

G R Lebo

George R. Lebo, Cochairman
Associate Professor of Astronomy

I certify that I have read this study and that in my opinion it conforms to acceptable standards of scholarly presentation and is fully adequate, in scope and quality, as a dissertation for the degree of Doctor of Philosophy.

Alex G Smith

Alex G. Smith
Professor of Astronomy

I certify that I have read this study and that in my opinion it conforms to acceptable standards of scholarly presentation and is fully adequate, in scope and quality, as a dissertation for the degree of Doctor of Philosophy.

Kwan-yu Chen

Kwan-yu Chen
Professor of Astronomy

I certify that I have read this study and that in my opinion it conforms to acceptable standards of scholarly presentation and is fully adequate, in scope and quality, as a dissertation for the degree of Doctor of Philosophy.

Thomas L. Bailey

Thomas L. Bailey
Professor of Physics

I certify that I have read this study and that in my opinion it conforms to acceptable standards of scholarly presentation and is fully adequate, in scope and quality, as a dissertation for the degree of Doctor of Philosophy.

Heinrich K. Eichhorn
Professor of Astronomy

This dissertation was submitted to the Graduate Faculty of the Department of Astronomy in the College of Liberal Arts and Sciences and to the Graduate School and was accepted as partial fulfillment of the requirements for the degree of Doctor of Philosophy.

May 1985

Dean, Graduate School